GCA TECHNICAL REPORT NO. 65-11-N

51 copies

STUDY OF EARTH'S ATMOSPHERE

R. MINZNER

GCA CORPORATION
Bedford, Massachusetts

FINAL REPORT

CONTRACT NO. NASw-976

PREPARED FOR

NATIONAL AERONAUTICS AND SPACE ADMINISTRATION

HEADQUARTERS

WASHINGTON, D. C.

APRIL 1965

GCA Technical Report No. 65-11-N

STUDY OF EARTH'S ATMOSPHERE

Raymond A. Minzner

FINAL REPORT

Contract No. NASw-976

April 1965

GCA CORPORATION
GCA TECHNOLOGY DIVISION
Bedford, Massachusetts

Prepared for

NATIONAL AERONAUTICS AND SPACE ADMINISTRATION
Headquarters
Washington 25, D. C.

TABLE OF CONTENTS

STUDY OF EARTH'S ATMOSPHERE

By Raymond A. Minzner

INTRODUCTION

This summary report presents the results of scientific investigations accomplished under NASA Contract No. NASw-976. A variety of scientific problems relative to Studies of the Earth's Atmosphere were investigated and these resulted in the generation of (1) two scientific reports, (2) a number of unpublished reports, and (3) one published journal article.

1. PUBLISHED GCA TECHNICAL REPORTS

   Temperature Determination of Planetary Atmospheres (R. A. Minzner, G. O. Sauermann, and L. R. Peterson) GCA Tech. Rpt. No. 64-9-N.

   Low Mesopause Temperatures over Eglin Test Range Deduced from Density Data (R. A. Minzner, G. O. Sauermann, and G. A. Faucher) GCA Tech. Rpt. No. 65-1-N.

2. UNPUBLISHED TECHNICAL REPORTS

   Atmospheric-Structure Data.

   Planetary Atmospheres Generated from Solar Radiation and Absorption Considerations.

   Analytical Investigation of the Existence of Successive Isopycnic Layers.

   Temperature Determination from Diffusion Data.

   Proposed Transition Model Atmospheres and Problems Associated with Their Generation.

3. TECHNICAL PAPERS WHICH HAVE BEEN PUBLISHED BY (OR HAVE BEEN SUBMITTED TO) ACCREDITED SCIENTIFIC JOURNALS

Title	Journal
Low Mesopause Temperatures over Eglin Test Range Deduced from Density Data (R. A. Minzner, G. O. Sauermann, and G. A. Faucher).	J. Geophys. Res. Feb. 1965
Temperature Determination of Planetary Atmospheres (R. A. Minzner, G. O. Sauermann, and L. R. Peterson).	J. Geophys. Res. (to be published)

For the purpose of the present publication, only the abstracts are given of the previously published GCA Corporation technical reports, and these are presented in the appendix. The details are available in the original reports for the interested reader. The one published journal article is quite short and is reproduced in its entirety in the appendix.

The previously unpublished work constitutes the main body of this report and is presented in considerable detail and scope but not necessarily with the degree of completeness which would be presented in individual scientific reports. Since each work forms a separate topic and can be adapted for publication in individual scientific reports, each is presented as an entity. The references, equations, and figures and tables are numbered serially within each work. In this format the highlights of the work accomplished under Contract NASw-976 can be presented in a clear concise manner and with sufficient detail to indicate the areas remaining for further investigation. Some of this material has previously appeared in the form of Quarterly Reports.

ATMOSPHERIC STRUCTURE DATA

Introduction

The initial analysis of the atmospheric structure includes data from observations between 30 and 200 km as obtained from 32 recent rocket flights from 1961 to 1964. No satellite data were considered. The prime purpose of this discussion is to provide the tools and parameters useful in the analysis and interpretation of the density data.

Clearly, the systematic fluctuations in atmospheric structure are likely to be complicated functions of many effects. Generally these variations are functions of at least some of the following variables: (1) solar activity, (2) latitude, (3) time of day, (4) time of year (as measured by the declination angle for example), (5) angular distance from the observation point to the subsolar point (shortened to subsolar angle), and (6) prevailing atmospheric convection currents. Obviously these variables are not all independent. For a statistical analysis one would like to use variables that are not strongly correlated to describe the structure variations, and it is in this light that one might try to choose which variables to use.

Certainly, one independent variable is solar activity; consequently, it is of prime interest. In treating (2) through (6) it might be assumed that the atmospheric currents are independent of longitude and can be lumped with latitude variation. In addition, the subsolar angle varies in the same way that time of day varies and depends to some extent on the declination angle. Thus a reasonable set of variables might be solar activity, latitude, time of day, and declination angle.

Possible smaller sets may also be considered; in fact, it would be desirable to make the set small enough so that the analysis can be represented by only a few simple graphs. It is useful, therefore, to consider the variable given as the angular distance to the subsolar point. This parameter is itself a function of latitude, time of day, and declination angle and could in some cases be substituted for these variables. For example, one might find it useful to plot the density as a function of solar activity and subsolar angle.

With the exception of the convection currents, all the other parameters suggested have been collected for each of 32 recent flights (see Table 1). Columns (1) through (8) give the vital statistics of the launch itself as well as the measurement technique, altitude range of data, and the principal investigator. The solar activity is expressed in terms of the 10.7 cm flux (10^{-22} joules $\cdot$ m^{-2} $\cdot$ sec^{-1} $\cdot$ $(cps)^{-1}$) as tabulated in Reference 1, with the values on the day preceeding the flight and the day of the flight appearing in Column (9). Column (10) gives the declination angle of the sun on the day of the flight. Columns (10) through (13) list the parameters necessary for the calculation of the subsolar angle α. The discussion of the subsolar angle and its calculation appearing below is an expansion of work previously done by Peterson [2]*.

*Numbers in [ ] throughout text indicate reference numbers.

TABLE 1

Rocket Designation	Date	Standard Time	Site	Coordinates	Technique	Altitude Range (km)	Principal Investigator	10.7 cm Solar Flux		Declination Angle β (degrees)	Local Mean Time (hours)	Local Apparent Time (hours)	Sub-Solar Angle χ (degrees)	Reference
NASA-10.50	6/6/61	16:48 EST	Wallops	37°50'N 75°29'W	1 m sphere	33-110	Peterson	86	88	+22.7	16.78	16.81	62.6°	7
	Double Experiment		Wallops	37°50'N 75°29'W	7" sphere	56-92	Peterson	86	88	+22.7	16.78	16.81	62.6°	7
NASA-10.91 UA	5/18/62	13:02 EST	Wallops	37°50'N 75°29'W	quad. mass spectrometer	108-135	Schaefer	93	95	+19.6	13.01	13.07	23.0°	2
NASA-14.19 UA	6/6/62	18:40 EST	Wallops	37°50'N 75°29'W	pitot tube	60-100	Horvath	85	87	+22.7	18.64	18.67	83.7°	6
NASA-10.43	6/6/62	19:10 EST	Wallops	37°50'N 75°29'W	1 m sphere	30-110	Peterson	85	87	+22.7	19.14	19.17	89.0°	7
NASA-14.20	12/1/62	15:34 EST	Wallops	37°50'N 75°29'W	1 m sphere	52-90	Horvath	77	77	-21.8	15.54	15.72	79.4°	6
AB-3.345	2/13/63	18:30 CST	Eglin	30°24'N 86°43'W	2.74 m sphere	95-155	Faucher	74	74	-13.3	18.72	18.48	102.8°	4
PMR-2	3/29/63	14:57 M	Kwajalein	09°24'N 167°44'E	0.66 m sphere	65-120	Peterson	73	75	+ 3.1	14.13	14.04	31.1°	3
NC-3.115F	6/6/63	07:30 MST	White Sands	32°24'N 106°21'W	magn. mass spectrometer	100-200	Nier	78	77	+22.6	07.41	07.44	61.1°	1
PMR-3	6/18/63	15:28 M	Kwajalein	09°24'N 167°44'E	0.66 m sphere	73-120	Peterson	86	82	+23.4	14.65	14.64	40.3°	3
PMR-4	6/20/63	15:00 M	Kwajalein	09°24'N 167°44'E	0.66 m sphere	33-110	Peterson	79	75	+23.4	14.18	14.16	34.0°	3
NASA-10.75	8/2/63	18:33 EST	Wallops	37°50'N 75°29'W	0.66 m sphere	89-102	Peterson	87	87	+17.8	18.53	18.43	84.1°	7
ERDA-001	11/4/63	03:00 MST	White Sands	32°24'N 106°21'W	7" sphere	35-112	Champion	83	83	-15.2	02.91	03.19	133.4°	5
ERDA-002	11/4/63	17:00 MST	White Sands	32°24'N 106°21'W	7" sphere	33-110	Champion	83	83	-15.4	16.91	17.19	88.3°	5
PMR-7	11/10/63	04:26 M	Kwajalein	09°24'N 167°44'E	0.66 m sphere	37-120	Peterson	76	75	-16.8	03.62	03.89	122.9°	3
PMR-8	11/15/63	02:58 M	Kwajalein	09°24'N 167°44'E	0.66 m sphere	64-120	Peterson	78	81	-18.2	02.15	02.41	143.1°	3
NASA-10.131	11/26/63	13:44 EST	Wallops	37°50'N 75°29'W	0.66 m sphere	32-114	Peterson	82	82	-20.9	13.71	13.92	64.7°	7
NASA-10.55 UA	12/7/63	08:11 EST	Wallops	37°50'N 75°29'W	0.66 m sphere	58-88	Peterson	76	77	-22.6	08.16	08.30	79.8°	7
	Double Experiment		Wallops	37°50'N 75°29'W	grenade	53-78	Nordberg	76	77	-22.6	08.16	08.30	79.8°	8
NASA-14.21 UA	12/7/63	08:34 EST	Wallops	37°50'N 75°29'W	pitot tube	49-82	Horvath	76	77	-22.6	08.54	08.68	76.4°	6
PMR-11	1/24/64	06:25 M	Kwajalein	09°24'N 167°44'E	0.66 m sphere	33-98	Peterson	75	74	-19.5	05.60	05.40	101.6°	3
NASA-14.22 UA	2/4/64	01:35 GMT	Ascension Is.	07°59'S 14°25'W	pitot tube	35-106	Horvath	71	71	-16.6	00.62	00.39	154.8°	6
ERDA-004	2/18/64	14.50 MST	White Sands	32°24'N 106°21'W	7" sphere	41-110	Champion	74	76	-11.7	14.74	14.51	56.9°	5
ERDA-005	2/19/64	14:30 MST	White Sands	32°24'N 106°21'W	7" sphere	30-115	Champion	76	76	-11.5	14.41	14.18	53.6°	5
PMR-12	3/14/64	06:20 M	Kwajalein	09°24'N 167°44'E	0.66 m sphere	32-120	Peterson	78	79	- 2.7	05.52	05.36	99.9°	3
NASA-14.23 UA	4/15/64	01:22 GMT	Ascension Is.	07°59'S 14°25'W	pitot tube	32-100	Horvath	72	71	+ 9.7	00.41	00.41	173.6°	6
NASA-14.24 UA	4/15/64	15:56 GMT	Ascension Is.	07°59'S 14°25'W	pitot tube	32-97	Horvath	72	71	+ 9.9	14.97	14.97	47.8	6
Sparcasphere-1	5/6/64	18:31 PST	Pt. Mugu	33°15'N 119°30'W	0.66 m sphere	98-110	Peterson	72	71	+16.8	18.58	18.64	88.3°	7
PMR-13	5/12/64	23:25 M	Kwajalein	09°24'N 167°44'E	0.66 m sphere	37-120	Peterson	70	69.4	+18.2	22.60	22.66	145.0°	3
PMR-14	6/17/64	13:01 M	Kwajalein	09°24'N 167°44'E	0.66 m sphere	32-120	Peterson	70.6	71.1	+23.4	12.20	12.19	14.2°	3
PMR-15	6/18/64	14:19 M	Kwajalein	09°24'N 167°44'E	0.66 m sphere	34-120	Peterson	71.1	71.7	+23.4	13.50	13.48	25.4°	3
PMR-16	6/19/64	04:30 M	Kwajalein	09°24'N 167°44'E	0.66 m sphere	32-120	Peterson	71.7	70.1	+23.4	03.68	03.66	117.1°	3
NASA-10.153	11/17/64	16:10 EST	Wallops	37°50'N 75°20'W	0.66 m sphere	53-117	Peterson	71.9	75.5	-19.2	16.14	16.39	84.0°	7
Sparcasphere-4	12/17/64	11:54 PST	Pt. Mugu	33°15'N 119°30'W	0.66 m sphere	33-109	Peterson	79.9	79.6	-23.4	11.96	12.02	57.5°	7

REFERENCES FOR TABLE 1

1. Nier, A. O., J. H. Hoffman, C. Y. Johnson and J. C. Holmes, "Neutral Composition of the Atmosphere in the 100 to 200 kilometer Range," J. Geophys. Res., 69, 979 (1963).

2. Schaefer, E. J. and M. H. Nichols, "Upper Air Neutral Composition Measurements by a Mass Spectrometer," J. Geophys. Res., 69, 4649 (1964).

3. Peterson, J. W., W. H. Hansen, K. D. McWatters and G. Bonfanti, "Atmospheric Measurements over Kwajalein using Falling Spheres," Univ. Michigan, College of Engineering, Final Tech. Rpt., ORA Project 05436 (Jan. 1965). (Also Reference 7.)

4. Minzner, R. A., G. O. Sauermann and G. A. Faucher, "Low Mesopause Temperatures over Eglin Test Range Deduced from Density Data," J. Geophys. Res., 70, 739 (1965).

5. Champion, K. S. W. and A. C. Faire, "Falling Sphere Measurements of Atmospheric Density, Temperature and Pressure up to 115 km," AFCRL-64-554, Environmental Res. Pap. No. 34 (1964).

6. Horvath, J. J., Private Communication (1965).

7. Peterson, J. W., Private Communication (1965).

8. Smith, H., L. Katchen, P. Socher, P. Swartz and S. Theon, "Temperature, Pressure, Density, and Wind Measurements with the Rocket Grenade Experiment 1960-1963," NASA Technical Report R-211, Washington, D.C. (Oct. 1964).

The units employed in expressing the 10.7 cm flux are somewhat different from those employed by some photochemists. Consequently a short discussion of the conversion of units of solar flux is also given.

The Angular Distance from the Subsolar Point

The subsolar point is that point on the surface of the earth through which at any instant would pass the line connecting the center of the earth and the center position of the sun at that instant. The angular distance between this point and the observer's location, as measured from the center of the earth, is known as α, the angular distance from the subsolar point. It has a maximum range of values of 0 to $+180^{o}$.

This variable may be of use in examining upper atmospheric parameters, although its direct effects are likely to be small in the very high altitude regions because of the low air density. There may, however, be substantial indirect effects because variations in the high atmosphere are strongly dependent on variations in the lower thermosphere, and the lower thermosphere is almost certainly a function of the sun's angle with respect to the zenith.

In order to obtain a simple but satisfactory approximate formula for calculating the angular distance of the sun from zenith, we assume a rotating spherical earth which is traveling in a circular orbit about the sun and whose spin angular momentum vector makes a constant angle γ with respect to the orbital angular momentum vector. One can use the spherical coordinates shown below (Figure 1) throughout the analysis.

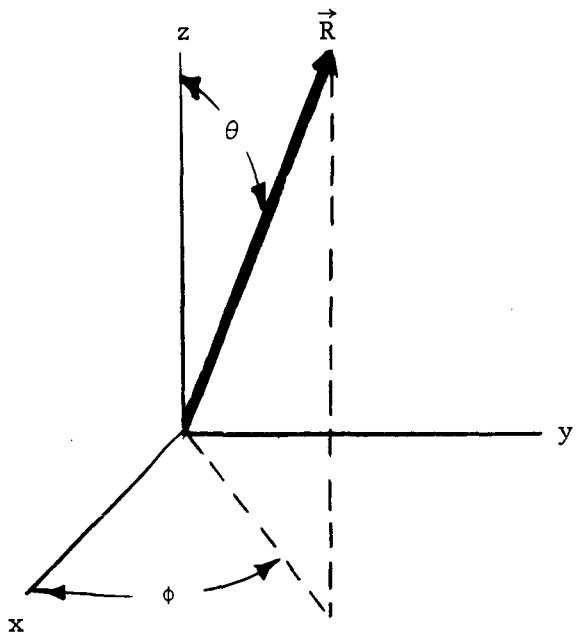

Figure 1

$$x = R \sin\theta \cos\phi$$
$$y = R \sin\theta \sin\phi \qquad (1)$$
$$z = R \cos\theta$$

For convenience the earth is defined as a unit sphere rotating about the z axis with the sun's hour circle in the x-z plane, i.e., the plane defined by the earth's axis and the sun is contained by the x-z plane. Also, two vectors $\vec{A}$ and $\vec{B}$, as shown in Figure 2, are defined. The vector $\vec{A}$ points directly at the sun which is assumed to be at some angle $\theta_A = 90^o - \beta$ in the x-z plane, the angle β being the declination angle discussed later in the development. The vector $\vec{B}$ locates the point of observation fixed with respect to earth and is therefore rotating about the z axis describing a cone. The cone angle is $\theta_B = 90^o - \theta_L$ and the rotation angle is ϕ_B defined such that $\phi_B = 0$ at apparent noon and $\phi_B = (t_n/24)\ 360^o$ at any later time t_n (in hours past apparent noon). The angle θ_L is the latitude of the point of observation. The angle α between vectors $\vec{A}$ and $\vec{B}$ is obviously the angular distance between the subsolar point and the zenith of the observation point.

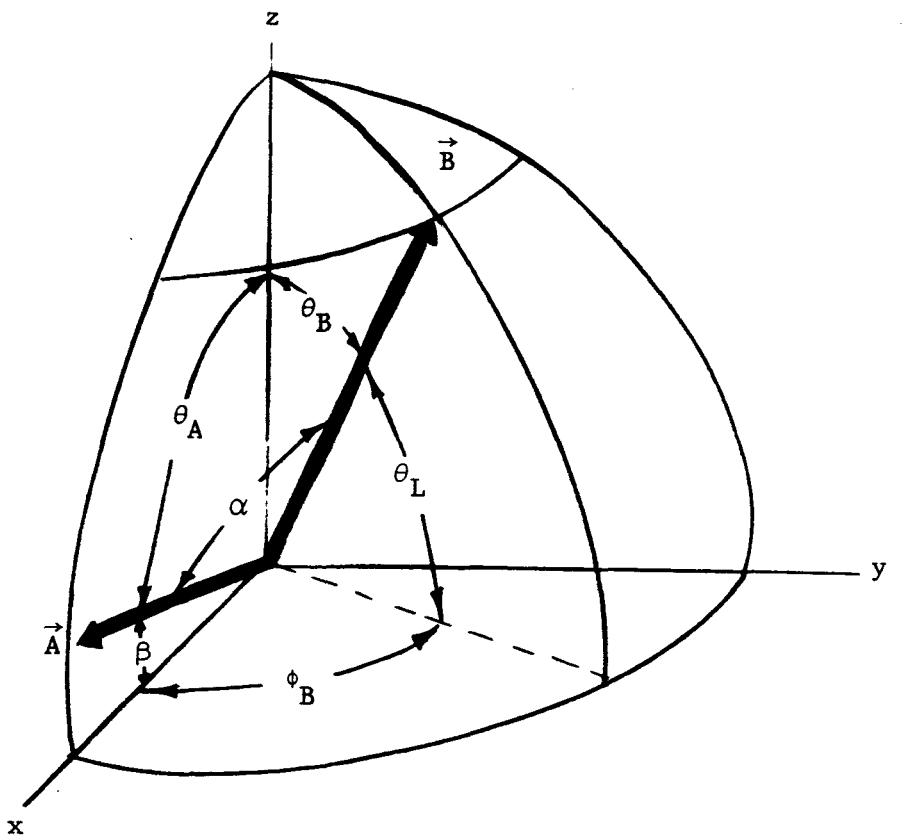

Figure 2

The angle α is very easy to obtain from the dot product of $\vec{A}$ and $\vec{B}$. Since $|\vec{A}| = |\vec{B}| = 1$, one has the expression

$$\cos \alpha = \frac{\vec{A} \cdot \vec{B}}{|A|\,|B|} = \vec{A} \cdot \vec{B} \ . \tag{2}$$

In terms of the unit basis vectors $\hat{i}$, $\hat{j}$, $\hat{k}$ of a rectangular coordinate system the unit vectors $\vec{A}$ and $\vec{B}$ may be written as

$$\vec{A} = \hat{i} \sin \theta_A + \hat{k} \cos \theta_A \ ,$$

$$\vec{B} = \hat{i} \sin \theta_B \cos \phi_B + \hat{j} \sin \theta_B \sin \phi_B + \hat{k} \cos \theta_B \ .$$

After transforming the angles by use of the relations $\theta_B = 90^o - \theta_L$ and $\theta_A = 90^o - \beta$ one obtains

$$\cos \alpha = \sin \theta_L \sin \beta + \cos \theta_L \cos \beta \cos \phi_B \ , \tag{3}$$

where θ_L = latitude of the observation point
β = declination angle of the sun
$\phi_B = (15\ t_n)^o$ with t_n in hours past apparent noon.

The declination angle β can be found accurately from a nautical almanac or approximately from an equation resulting from the assumption of a circular orbit around the sun. The approximate equation arising out of one of the basic formulas of spherical trigonometry is

$$\tan \beta = \tan \gamma \sin \left[(N\text{-}80) \frac{360}{365} \right] \ , \tag{4}$$

where β = declination angle $(-\gamma < \beta < \gamma)$
γ = inclination of earth's axis with respect to the orbital angular momentum vector $(\tan \gamma = .4336)$
N = number of days past December 31.

According to this simple equation the declination angle becomes positive at N = 80, corresponding to the March 21 equinox, and turns negative again at N = 263, corresponding to September 20. The fall equinox is normally on September 22 but this two-day discrepancy is not serious.

Time is ordinarily recorded with the reference point at midnight rather than at noon. If the sign of cos (15 t_n) is changed from + to - and the time t_n is redefined as t, the time in hours past "apparent" midnight, (i.e., local apparent time), then Equation (3) becomes

$$\cos \alpha = \sin \theta_L \sin \beta - \cos \theta_L \cos \beta \cos (15\ t) \ . \tag{5}$$

Equations (3) and (4) can be combined to eliminate β:

$$\cos \alpha = \frac{\tan \gamma \sin \theta_L \sin \left[(N-80) \frac{360}{365} \right] - \cos \theta_L \cos (15\ t)}{\left\{ 1 + \tan^2 \gamma \sin^2 \left[(N-80) \frac{360}{365} \right] \right\}^{1/2}} . \qquad (6)$$

Equation (5) is useful for hand calculations if solar declination angles are obtained directly from a nautical almanac, as was the case for this study. Equation (6) is particularly useful for a computer program handling a large number of rocket flights.

In the derivations of the preceeding equations, spherical geometry has been assumed throughout. The largest net effect of this assumption is that the time t does not correspond to local standard time except on average. Thus to avoid errors in α of 5^o - 10^o one must use the correct values of t. The parameter t is seen to be a means for expressing the hour angle of the sun with respect to the lower meridian of the observing site, and corresponds to what, in astronomy, would be called the local apparent time of the rocket launch rather than to the standard mean time t_{std}.*

Local apparent time is related to standard mean time or zone time with two correction terms, one involving the location of the observing site relative to the longitude of the center of the standard time zone and another involving the equation of time which accounts for the variation in the rate of the apparent motion of the sun relative to the earth at different times of the year.

When the longitude correction above is applied to t_{std}, the resulting time is called local mean time $t_{\ell m}$. For sites at longitudes east of the center meridian or standard meridian of a time zone, the various solar phenomena occur earlier in standard time than on the center meridian. For sites west of the standard meridian the same phenomena occur later in standard time than on the center meridian. Every longitudinal position within a time zone has a different value of local mean time $t_{\ell m}$. At each longitude $t_{\ell m}$ leads or lags t_{std} by 4 minutes (or 1/15 hours) for each degree displacement from the standard meridian. For sites east of the standard meridian the longitude time correction is added to standard mean time to yield local mean time. For sites west of the standard meridian the correction is subtracted. On the standard meridian the two kinds of time are identical. Specifically the correction term consists of the product of the reciprocal of the earth's axial rotation rate times the difference between L_{std} the longitude of the standard meridian of the time zone and L_{os} the longitude of the observers site

$$t_{\ell m} = t_{std} + 1/15\ (L_{std} - L_{os}) , \qquad (7)$$

where $t_{\ell m}$ and t_{std} are in hours and L_{std} and L_{os} are in degrees of longitude.

*For a more comprehensive treatment of the concepts involved in the definitions of time the reader is referred to Reference 3.

In order that Equation (7) may apply for longitudes both east and west of Greenwich, it is necessary to define all longitudes east of Greenwich as negative numbers.

If the launch time is given as Greenwich Mean (Zulu) Time, conversion to standard mean (zone) time can be made in general by the following rule of thumb: divide the longitude of the launch site (in degrees) by 15 and take the nearest whole number; subtract this number of hours from the Greenwich Mean Time of launch if the site is west of Greenwich or add if it is east; also note whether the date changes. Alternately, zone time can be determined easily with a good atlas [4]. There are a number of exceptions to the rule, however. For convenience, the zone time of some areas is shifted by one half or a full hour from the expected zone time. Confusion resulting from such local variations can be avoided when applying Equation (7) if care is taken to make the standard longitude (L_{std}) agree with the local time for that zone (t_{std}).

Kwajalein (Marshall Islands) serves as an example. Although the longitude of Kwajalein is 167°E (the apparent zone time for 165° ± 7.5° is GMT + 11 hours), the zone time for that area corresponds to 180° ± 7.5°(GMT + 12 hours). Thus, while the local launch time is given in terms of GMT + 12, the launch actually occurs one hour earlier relative to the sun. L_{std} in this case is 180° and not 165° which is the standard meridian for the zone containing the Marshall Islands.

Another exception is Ascension Island (14°W). The actual standard meridian for this zone is 15°W (apparent zone time thus is GMT - 1 hour) while the zone time for that area corresponds to GMT. The correction term (1/15 (L_{std} - L_{os})) is -0.961 hours if t_{std} is taken as GMT.

For several reasons, the apparent period of the earth's rotation relative to the sun is not constant throughout the year. Two major factors contribute to this effect: (1) the eccentricity of the earth's orbit about the sun and (2) the angle between the plane of the earth's orbit and the plane of the earth's equator. The result of this variable period is to make the length of a day, the time between successive meridian transits, vary through the year. Since our civil time systems are based on the average or mean length of a solar day, as indicated by the names "Standard Mean Time" or "Local Mean Time," the small daily differences accumulate, and in general the sun lags or leads the local mean time by a quantity called the equation of time t_{eq} with values up to 16 minutes in February and November.

The sun's transit of the local meridian determines local apparent noon, and is the basis of local apparent time. During periods when the sun lags mean time, t_{eq} is subtracted from local mean time to yield local apparent time. The value of the equation of time is approximated by Figure 3 and may be obtained accurately for any particular day from a suitable almanac. Specifically then, in order to obtain local apparent time t in hours one uses

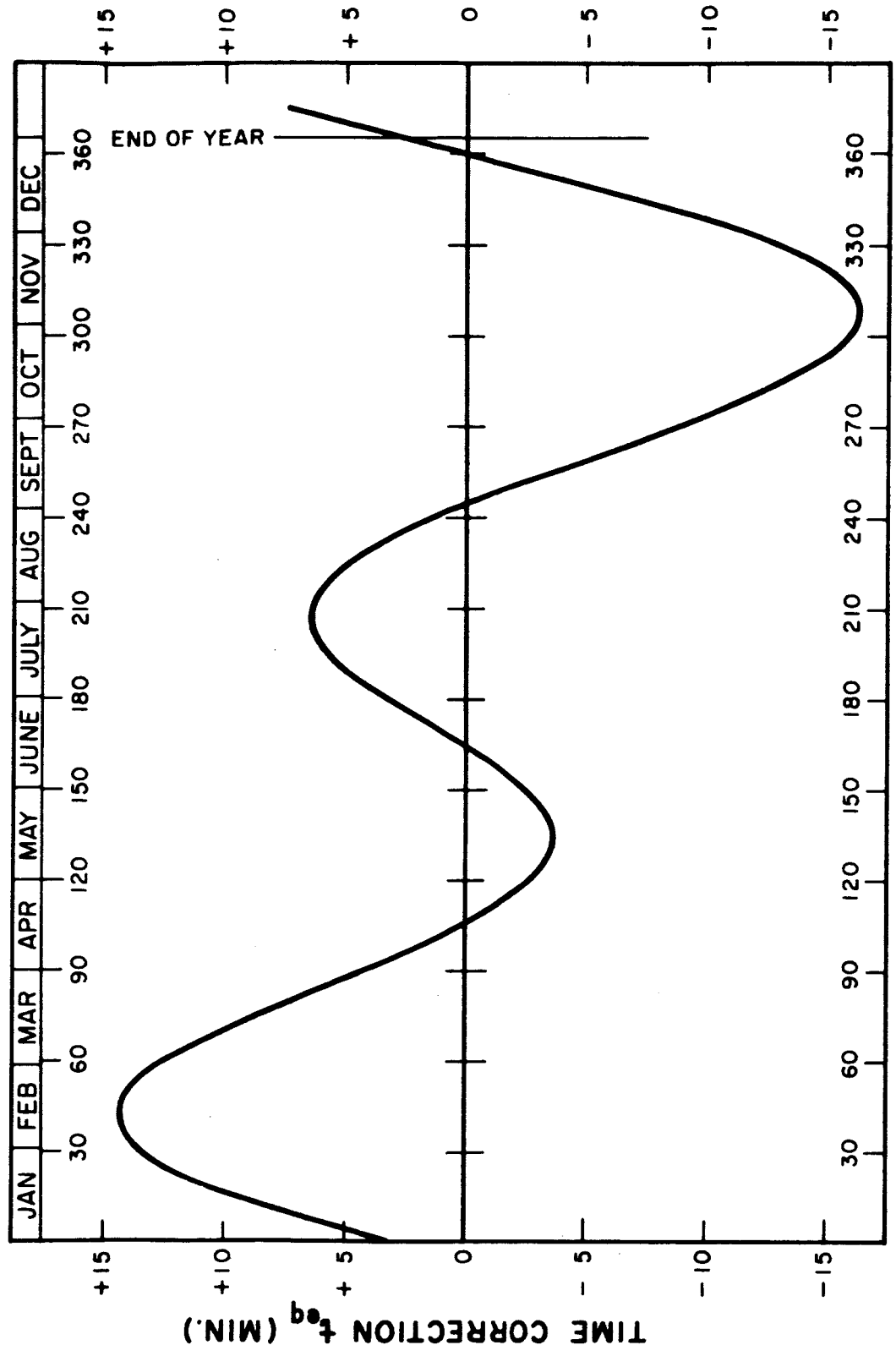

Figure 3. The equation of time correction.

$$t = t_{\ell m} - t_{eq}$$

$$= t_{std} + 1/15\ (L_{std} - L_{os}) - t_{eq} \qquad (8)$$

Thus the local apparent time does not agree with standard time except when the sum of the two correction terms is zero. The data of Figure 3 applied to Equation (8) shows the following: (1) for a narrow region within about 1-1/2° of the standard meridian, this situation ($t = t_{std}$) may exist on four different days throughout a year; (2) for regions where $|(L_{std} - L_{os})|$ is greater than about 4°, local apparent time is never equal to standard time; and (3) for intermediate regions the local apparent time may equal standard time on only two days of the year.

While in the present study, values for the equation of time (t_{eq}) were taken from a nautical almanac, approximate values can be obtained from the empirical formula

$$t_{eq}(\text{sec}) \simeq 97.8 \sin(\phi) + 431.3 \cos(\phi) - 596.6 \sin(2\phi)$$

$$+ 1.9 \cos(2\phi) - 41.0 \sin(3\phi) - 19.3 \cos(3\phi) \qquad (9)$$

where

$$\phi = \left(\frac{360}{365.272}\right)\left(\text{N}-80.608\right) .$$

N = the number of days past December 31. The number (80.608) refers to the time in days of the occurrence of the vernal equinox of a leap year. For each year after a leap year, 0.25 is subtracted from 80.608.

For an accurate determination of α it is always necessary to consider both the longitude correction and the equation-of-time correction. Despite these corrections the values of α are not accurate to better than about 2 degrees because the earth rotates a substantial amount during the rocket flight and because the latitude and longitude of even a so-called vertical sounding rocket change substantially during its flight.

Conversion of Units of Solar Flux

Solar flux values in the microwave regions (i.e., at 10.7 cm) are usually given in terms of energy per unit area per unit time per unit frequency. For example values of solar flux are given in Reference 1 in terms of some number times 10^{-22} joules m^{-2} sec^{-1} $(cps)^{-1}$. In the ultraviolet region values of solar flux are frequently given in terms of energy per unit area, per unit time, per unit wavelength; i.e., ergs cm^{-2} sec^{-1} $(\text{Å})^{-1}$. In order that the relative magnitudes for the solar fluxes in the several regions may be compared similar units must be employed. Conversion from one set of units to

the other is based on the following:

$$\lambda\nu = c \ , \tag{10}$$

where λ = wavelength, ν = frequency and c is the velocity of propagation. Differentiation of Equation (10) yields

$$d\lambda = c\ \nu^{-2}\, d\nu \ . \tag{11}$$

Eliminating ν between Equations (10) and (11) and expressing the differentials as finite increments, we have

$$\frac{d\lambda}{d\nu} = \frac{\lambda^2}{c} \ . \tag{12}$$

If the wavelength unit is 1Å, $\Delta\lambda/\Delta\nu$ = 0.382 (Å/cps). Thus at 10.7 cm, 1Å corresponds to 2.62 cps and

$$100 \times 10^{-22} \text{ joules m}^{-2} \text{ sec}^{-1} \text{ (cps)}^{-1} = \tag{13}$$

$$10^{-17} \text{ ergs cm}^{-2} \text{ sec}^{-1} \text{ (cps)}^{-1} = 2.62 \times 10^{-17} \text{ ergs cm}^{-2} \text{ sec}^{-1} (\text{Å})^{-1} \ .$$

The energy per photon at 10.7 cm is

$$\frac{hc}{\lambda} = \frac{1.9862 \times 10^{-16}}{10.7} = 1.86 \times 10^{-17} \text{ ergs (photon)}^{-1} \tag{14}$$

It follows that

$$10^{-17} \text{ ergs cm}^{-2} \text{ sec}^{-1} \text{ (cps)}^{-1} = 0.538 \text{ photons cm}^{-2} \text{ sec}^{-1} \text{ (cps)}^{-1} \tag{15}$$

and

$$2.62 \times 10^{-17} \text{ ergs cm}^{-2} \text{ sec}^{-1} (\text{Å})^{-1} = 1.41 \times 10^{-2} \text{ photons cm}^{-2} \text{ sec}^{-1} (\text{Å})^{-1} \tag{16}$$

In summary the 10.7 cm flux s whose numerical value is 100 is equivalently expressed in any of the following values

$$100 \times 10^{-22} \text{ joules m}^{-2} \text{ sec}^{-1} \text{ (cps)}^{-1}$$

$$1 \times 10^{-17} \text{ ergs cm}^{-2} \text{ sec}^{-1} \text{ (cps)}^{-1}$$

$$2.62 \times 10^{-17} \text{ ergs cm}^{-2} \text{ sec}^{-1} (\text{Å})^{-1}$$

$$0.538 \text{ photons cm}^{-2} \text{ sec}^{-1} \text{ (cps)}^{-1}$$

$$1.41 \times 10^{-2} \text{ photons cm}^{-2} \text{ sec}^{-1} (\text{Å})^{-1}$$

REFERENCES

1. National Bureau of Standards, Central Radio Propagation Laboratory, Boulder Colorado, Solar Geophysical Data -- 10.7 cm Solar Flux.

2. Peterson, L. R. and R. A. Minzner, "Considerations on Analysis of Atmospheric Structure Data with Emphasis on the Computation of the Angular Distance from the Sub Solar Point," GCA Technical Report No. 64-1-A, (1964).

3. Baker, R. H., Astronomy, Seventh Edition, Van Nostrand, New York (1959).

4. World Atlas, Encyclopedia Britanica, William Brenton Publishers, Chicago, (1963).

PLANETARY ATMOSPHERES GENERATED FROM SOLAR RADIATION AND ABSORPTION CONSIDERATIONS [1]

Introduction

The prediction of reentry trajectories of artificial earth satellites and interplanetary space vehicles, as well as the solution of various problems in atmospheric physics requires a knowledge of the variation of the distribution of the atmospheric density versus altitude, as a function of the many variable parameters influencing such a profile. The complete measurement of the earth's density field for any particular situation would be a suitable but prohibitively costly and unlikely solution. In lieu of such a capability, it would be desirable to be able to predict, with reasonable accuracy, the density-altitude profile as a function of the variable parameters influencing this profile.

A number of the variable parameters frequently recognized include the several earth-centered parameters, latitude, season, and time of day. These are basically related to a single general parameter, the magnitude and direction of solar radiation into the earth's atmosphere. Thus, a model developed in terms of such a general overall parameter might well provide the basis of a reliable predictive model. Nicolet [2] has shown how lumped values of solar uv radiation, lumped values of absorption cross section, and lumped values of conductivity coefficient may in principle be combined to compute an altitude profile of scale height according to the variations in uv solar radiation. Such profiles could then serve as the definition of an entire system of model atmospheres. Nicolet presented such a system of models in a Smithsonian publication [3] which contained only a vague discussion of the method for developing the temperature profiles. He also presented a much more extensive listing of the same system of models in an unpublished document [4] in which the absorption and conductivity concepts were discussed in some detail. References [3] and [4] imply that absorption, conductivity, and reradiation considerations determined the temperature-altitude profiles, although no specific equation is given. (A private communication [5] has since determined that the basic noonday temperature-altitude profile of the Nicolet models was not calculated from any specific equation, but rather was produced empirically.) The study of the Nicolet papers, however, has led the writer to a refinement of the Nicolet method, and to an equation which does serve as the basis for the generation of a complete static model atmosphere in terms of the following:

(1) solar radiation expressed as the mean value within successive bands as narrow as 1 Å or less over the significant wavelength region;

(2) radiation-absorption cross sections of each atmospheric species for each of the successive narrow bands of radiation into which the solar spectrum has been divided; and

(3) atmospheric conductivity which varies with altitude in accordance with the variation of the relative composition as deduced by the computed temperature-altitude profile.

In its present form, this model, unlike the Harris and Priester model [6], does not account for diurnal variations such as changing angle of incidence of the solar radiation and vertical mass transport due to diurnal heating and cooling. More correctly than in the Harris and Priester model, this model considers the proper space distribution of atmospheric heat sources on the basis of the solar radiation spectrum in narrow wavelength-band increments and by the use of related measured absorption cross section coefficients for each species for the corresponding narrow wavelength-band increments. Harris and Priester, on the other hand, take an estimated single effective flux and corresponding estimated single mean cross-section coefficients for each species.

General Concepts

The temperature-altitude profile of a static, horizontally symmetrical, planetary atmosphere is dependent upon: (1) size and vertical distribution of heat sources and sinks; (2) varieties and vertical distribution of the gas species comprising the atmosphere, and hence determining the altitude variation of the thermal conductivity coefficient; and (3) the value of the acceleration of gravity which, along with the temperature profile, controls the altitude distribution of the several species. The size of the positive, vertical, temperature gradient at any particular altitude in the thermosphere is proportional to the downward flux of thermal energy in that region, and inversely proportional to the square root of the temperature at that altitude.

The heat sources comprise two major types: corpuscular radiation and excited terrestrial gas molecules or atoms. Corpuscular radiation consists of various high-energy particles which come from the sun as well as from interstellar space and which are trapped in the earth's atmosphere. The kinetic energy of these particles may be considered to be a kind of thermal flux into the top of the atmosphere.

The second and perhaps more important heat source consists of terrestrial gas molecules or atoms which have absorbed solar radiation primarily in the uv region, in such a way that the radiation is converted to thermal or kinetic energy. The gas molecules near the top of the atmosphere, where the solar radiation flux is the greatest, have the greatest probability of absorbing a photon of radiant energy. Consequently, the mean kinetic energy per particle at any instant, i.e. the temperature at any instant in a unit volume, increases with increasing altitude, while the positive temperature gradient decreases toward zero because of a simultaneously, exponentially increasing mean free path and related considerations. Thus, at a sufficiently high altitude, above 500 km, one finds a high-temperature near-isothermal layer which Nicolet [4] calls the thermopause.

At lower altitudes, close to the base of the thermosphere, most of the uv radiation from the sun has already been absorbed, and very few of the particles in any unit volume absorb any photons of radiation. Consequently, in the lower region of the thermosphere, the temperature at any instant tends to remain low. In the steady-state equilibrium condition, any time-dependent buildup of the

temperature is prevented by the continuing thermal flux from high-temperature regions at high altitudes, to low-temperature regions at lower altitudes, and to the heat sinks which become increasingly numerous as altitude decreases.

The heat sinks consist of gas molecules or atoms which are capable of reradiating by some specific radiation process, some fraction of their energy at a longer wavelength (lower energy photon) than that of the originally absorbed energy. The wavelengths of the more important of these reradiation processes coincide with regions of atmospheric transmission, so that much of this reradiation energy is ultimately lost to outer space. Only specific particle species are capable of such a direct energy-loss process. At any given altitude, however, the total energy per unit volume tends to become distributed among all the particles of that volume, and hence each particle contributes energy indirectly to the specific radiation process. Thus, indirectly, all particles may be considered as heat sinks, and some energy loss occurs at all altitudes. Because of the very small number density at high altitudes, the energy loss is negligibly small at the thermopause but, as altitude decreases, and particle number density increases, the energy loss increases very rapidly to significant amounts near the base of the thermosphere.

The difference between the differential energy absorption and the differential energy reradiation in any differential altitude increment may be expressed mathematically and equated to the differential thermal-energy flux through that layer. This expression, after suitable integration, is in turn related to the scale height and scale-height gradient by means of an appropriate conductivity coefficient of the composite atmosphere. An additional integration finally yields an expression for the square root of scale height as a function of altitude in terms of: (1) the scale height at the base or reference level, which scale-height value is inferred from a set of assumed boundary conditions, i.e., the number density of each of the atmospheric constants and the temperature; (2) the total solar-radiation flux at the top of the atmosphere in each successive narrow wavelength band; (3) the absorption cross-section coefficients of the individual species of gases in each of the separate wavelength bands; (4) the reradiation coefficients for each of these species in each successive narrow wavelength band in the region of reradiation; and (5) the corpuscular (high energy particle) radiation flux into the top of the atmosphere. This equation then permits the calculation of scale height for small altitude increments by means of an iterative process which simultaneously yields number-density values of the several species for these same altitude increments. Other standard equations then permit the calculation of an entire model atmosphere.

Assumptions

For simplicity, the thermal-flux equation used in the development of the final scale-height equation is based on the assumption that the solar-radiation flux is directed only vertically downward and that the horizontal component of thermal conductivity is zero. These assumptions imply a static semi-infinite-plane atmosphere with an overhead sun located at infinite height. This

assumption is not mandatory, and the method may be extended to include diurnal variation.

A further assumption is that each gas species has a vertical distribution dependent only upon its own molecular mass, the temperature-altitude profile, and gravity; thereby, complete diffusive hydrostatic equilibrium is implicit. The application of the method is consequently restricted to altitudes where mechanical mixing has a negligible influence on the species distribution; i.e., above 130 or 140 km. The theory as presently developed does not account for changes in composition due to dissociation of diatomic molecules, although the energy absorbed by such dissociation processes is accounted for. No great change in composition above 150 km results from this assumption since most of the O_2 to O dissociation occurs at altitudes below this level.

All energy reradiated (primarily in the infrared region of the spectrum) is assumed to be completely lost to outer space since no intermediate reabsorption is accounted for in the present form of the theory. Nicolet [2] states, however, that for altitudes above about 150 km, the IR loss is small compared with the uv absorption, and consequently inaccuracies in that portion of the scale-height equation which considers IR reradiation do not seriously influence the model, when calculations are restricted to sufficiently high altitudes. In fact, under these conditions, the IR-loss term may in some instances be entirely omitted.

Summary of Equation Development

In particular, the method depends upon the expression of two quantities: (1) the incremental amount of energy extracted from $\sum_j I_j(h) \cdot \Delta\lambda_j$ the summation of the flux of all wavelength bands j of solar radiation passing through elemental volume ($cm^2 \cdot dh$) at level h of a vertical cm^2 - column of a planetary atmosphere containing various species of gas i, and (2) the incremental amount of energy reradiated from the same elemental volume of atmosphere by the total number of molecules of each species in that elemental volume.

The incremental amount of energy extracted dE_{ex} by $\sum_i n_i$ the total number of molecules of various species i within the volume ($cm^2 \cdot dh$) of the incremental cm^2 column is

$$dE_{ex} = \sum_j I_j(h) \cdot \Delta\lambda_j \cdot \sum_i \sigma_{ij} \cdot n_i(h) \cdot (-dh) , \qquad (1)$$

where σ_{ij} is the effective cross section of species i for wavelength band j.

The incremental rate of energy reradiation $d(E_{re})_j$ within wavelength band j by the molecules of various species i within incremental volume ($cm^2 \cdot dh$) is

$$d(E_{re})_j = \sum_i d(E_{re})_{ij} = \sum_i R_{ij}(h) \cdot \Delta\lambda_j \cdot n_i(h) \cdot (-dh) , \qquad (2)$$

where R_{ij} is the radiation rate per molecule of species i in wavelength band j.

Defining $\bar{R}_j(h)$ as the average value of the radiation rate per molecule within the wavelength band j averaged over all molecules at any height h, we have

$$\bar{R}_j(h) = \frac{\sum_i R_{ij}(h) \cdot n_i(h)}{\sum_i n_i(h)} \tag{3}$$

the quantity $\bar{R}_j$ is a function of h since n_i and all of the quantities R_{ij} are each individually functions of h in accordance with the radiation flux at level h.

Eliminating R_{ij} between Equations (2) and (3) we have

$$dE_{re} = \sum_j d(E_{re})_j = \sum_j \bar{R}_j(h) \cdot \Delta\lambda_j \cdot \sum_i n_i(h) \cdot (-dh) \; . \tag{4}$$

The difference between the differential rates of energy extraction from the solar beam and the energy reradiation (presumably to outer space or to the ground) is dE the differential energy available for heating the differential volume,

$$dE = \sum_j I_j(h) \cdot \Delta\lambda_j \cdot \sum_i \sigma_{ij} \cdot n_i(h) \cdot (-dh) - \sum_j \bar{R}_j(h) \cdot \Delta\lambda_j \cdot \sum_i n_i(h) \cdot (-dh) \; . \tag{5}$$

Applying the concepts of optical depth τ and Beers law, and integrating over the cm^2-column from h to ∞ yields E(h) the total rate of net energy absorption over the entire cm^2-column from h to infinity, [ergs$(cm^2\text{-column})^{-1}$ sec^{-1}]

$$E(h) = E(\infty) + \sum_j I_j(\infty) \cdot \Delta\lambda_j \cdot [1 - e^{-\tau_j(h)}] - \sum_j \bar{\bar{R}}_j(h) \cdot \Delta\lambda_j \cdot \tau_j(h) \; , \tag{6}$$

where

$$\bar{\bar{R}}_j(h) \equiv \frac{1}{\tau_j(h)} \int_{\tau(\infty)}^{\tau(h)} \frac{\bar{R}_j(h)}{\bar{\sigma}_j(h)} \cdot d\tau_j = \frac{1}{\tau_j(h)} \int_{\tau(\infty)}^{\tau(h)} \frac{\sum_i R_{ij}(h) \cdot n_i(h)}{n(h) \cdot \bar{\sigma}_j(h)} \cdot d\tau_j, \tag{7}$$

is a kind of average radiation-rate coefficient which varies more slowly with altitude, than $R_{ij}(h)$.

The term $E(\infty)$ appears as a result of integration limits and represents any thermal energy flux through the outer "surface" of the planetary atmosphere. If such flux exists at all, it most likely is directed toward the planet such that its sign will be positive and such that its direction implies

a positive temperature gradient at the extremities of the planetary atmosphere. Considering it to be corpuscular in nature it is hereafter designated by $C(\infty)$.

For an overhead sun, each cm^2-column of planetary atmosphere is heated in a manner identical to that of the adjacent columns, and no net heat conduction takes place from one column to the next. After a quasi-thermal equilibrium state has been established, increments of absorbed energy produce a thermal flux which cannot be directed upward since a negative temperature gradient has not been observed in the thermosphere. The thermal flux must be directed downward, and E the total number of ergs per sec flowing down through any cm^2-column at level h is equal to the total number of ergs per second absorbed as heat in the entire column above level h; i.e., from h to ∞.

The thermal flux E at level h is related to thermal conductivity A, temperature T, and temperature gradient dT/dh at level h according to

$$E = -A(h) \cdot T^{\frac{1}{2}} \cdot dT/dh \ . \tag{8}$$

In this expression the negative sign indicates that the direction of flux is downward, i.e., opposite to the direction for which increasing values of h are positive. For the case of a single-gas atmosphere, this thermal flux may also be related to geopotential scale height H' and its vertical gradient dH'/dh by direct transformation,

$$E = -B(h) \cdot (H')^{\frac{1}{2}} \cdot dH'/dh \ , \tag{9}$$

where, for an atmosphere of unvarying composition, B is a constant times A. (In a multigas atmosphere where composition varies with altitude, the value of B is dependent upon the varying mean molecular mass in accordance with Equations (23) and (24).)

The downward thermal flux, out of the bottom of the cm^2-column which is absorbing radiation as expressed by Equation (6), is identical to the thermal flux associated with the scale-height gradient of Equation (9). Equating the absolute magnitudes of the two expressions, therefore, performing some algebraic manipulations, and integrating between level h_b and level h_a (where $h_a > h_b$), we obtain an expression for scale height at level a in terms of scale height at level b, and in terms of the change in optical depth between levels a and b for each of the various wavelength bands involved in the absorption and reradiation phenomena:

$$[H'(a)]^{\frac{1}{2}} = [H'(b)]^{\frac{1}{2}} + \frac{\bar{\bar{\sigma}}_\alpha(\bar{h})}{2B(\bar{h}) \cdot \bar{\sigma}_\alpha(\bar{h})} \cdot C(\infty) \cdot \ell n \frac{\tau_\alpha(b)}{\tau_\alpha(a)} + \sum_j \frac{\bar{\bar{\sigma}}_j(h)}{2B(\bar{h}) \cdot \bar{\sigma}_j(\bar{h})}$$

$$\cdot I_j(\infty) \cdot \Delta\lambda_j \cdot \left\{(\ell n\, \tau_j(b) - Ei[-\tau_j(b)]) - (\ell n\, \tau_j(a) - Ei[-\tau_j(a)])\right\}$$

$$-\sum_j \frac{\bar{\bar{\sigma}}_j(\bar{h})}{2B(\bar{h}) \cdot \bar{\sigma}_j(\bar{h})} \cdot [\bar{\bar{R}}_j(\bar{h}) \cdot \Delta\lambda_j] \cdot [\tau_j(b) - \tau_j(a)] \ . \qquad (10)$$

In the last integration, the quantities $\bar{\bar{\sigma}}_\alpha(h)$, $\bar{\sigma}_\alpha(h)$, $\bar{\bar{\sigma}}_j(h)$, $\bar{\sigma}_j(h)$, $B(h)$, and $\bar{\bar{R}}_j(h)$ were all considered to be essentially constant within the small interval $h(a) - h(b)$, and in the resulting integrated expression as represented by Equation (10), these quantities are all designated with a bar over the h, i.e., $B(h)$ becomes $B(\bar{h})$ the mean value between $B(a)$ and $B(b)$, etc.

With a knowledge of the solar spectrum outside of the atmosphere, and a knowledge of the effective cross sections and reradiation coefficients for each of the atmospheric gases for the various wavelength regions, plus certain boundary conditions at a reference level near the base of the thermosphere of the planetary atmosphere, this equation permits the calculation of the atmospheric properties above the reference level.

Atmospheric Boundary Conditions

The required boundary-condition values are those of $H'(b)$ geopotential scale height at the reference level, and $n_1(b)$, $n_2(b)$, $n_3(b)$, $\cdots$ the number density of each of the atmospheric constituents at $h(b)$ the reference level. These quantities along with known cross-section values lead to the required values of $\tau_j(b)$ the optical depth of the composite atmosphere, from $h(\infty)$ to $h(b)$, for each of the various wavelength bands j, as well as $\tau_{ij}(b)$ the optical depths of the individual species for the same conditions. The evaluation of $\tau_j(b)$ is accomplished as follows: The number densities of the several species yield $\bar{m}(b)$ the mean molecular mass at level $h(b)$; i.e.,

$$\frac{\sum_i n_i(b) \cdot m_i}{\sum_i n_i(b)} = \frac{\sum_i n_i(b) \cdot m_i}{n(b)} = \bar{m}(b) \ . \qquad (11)$$

This quantity and $H'(b)$ yield $T(b)$ the kinetic temperature at level $h(b)$; i.e.,

$$H'(b) \cdot \bar{m}(b) \cdot \frac{G}{k} = T(b) \ , \qquad (12)$$

where k is Boltzmann's constant, and G is the geopotential constant, which by definition [7,8] for the planet earth under consideration, is 9.80665 $m^2\ sec^{-2}\ (m')^{-1}$ for latitudes near 45^o.

The values of $T(b)$ and values of m_i for the several species i, yield values of the individual scale heights $H_i'(b)$ for these species; i.e.,

$$\frac{T(b)k}{m_i G} = H_i'(b) \ . \tag{13}$$

The values of the individual scale heights and individual number densities at level h(b), together with individual cross-sections σ_{ij} for the various wavelength bands yield $\tau_{ij}(b)$ the individual optical depths of the several species for the various wavelengths bands, as indicated by the single terms of Equation (14) below. When these values of $\tau_{ij}(b)$ are summed over i, one obtains $\tau_j(b)$ the optical thickness of the composite atmosphere from $h(\infty)$ to h(b) for the particular wavelength band j;

$$\sum_i \sigma_{ij} \cdot n_i(b) \cdot H_i'(b) = \sum_i \tau_{ij}(b) = \tau_j(b) \ . \tag{14}$$

These values of $\tau_j(b)$ for the various wavelength bands together with the previously adopted value of H'(b) for the composite atmosphere are the only atmospheric properties required in the evaluation of Equation (10).

Required Parameters and Coefficients Related to Physical Constants

In addition to $\tau_j(b)$ and H'(b), the evaluation of Equation (10) requires values of a number of kinds of cross-section parameters $\bar{\sigma}_j(\bar{h})$, $\bar{\bar{\sigma}}_j(\bar{h})$, $\bar{\sigma}_\alpha(\bar{h})$, $\bar{\bar{\sigma}}_\alpha(\bar{h})$, and a conductivity parameter $B(\bar{h})$, all of which depend in some way upon the variation of composition with altitude. In each instance, the symbol $(\bar{h})$ designates the mean value of the quantity between the levels h(a) and h(b), i.e.,

$$\bar{\sigma}_j(\bar{h}) \equiv \frac{\bar{\sigma}_j(b) + \bar{\sigma}_j(a)}{2} \ , \tag{15}$$

$$\bar{\bar{\sigma}}_j(\bar{h}) \equiv \frac{\bar{\bar{\sigma}}_j(b) + \bar{\bar{\sigma}}_j(a)}{2} \ , \tag{16}$$

where h(a) - h(b) may be made as small as desired.

The quantity $\bar{\sigma}_j(b)$ represents the general member of the set of the average cross sections $\bar{\sigma}_\alpha(b)$, $\bar{\sigma}_\beta(b)$, $\bar{\sigma}_\gamma(b)$, $\cdots$ at altitude h(b) for each of the various wavelength bands j, such that $\bar{\sigma}_\alpha(b)$ represents $\bar{\sigma}$ at level h(b) for the particular wavelength band α. The quantity $\bar{\sigma}_\alpha(b)$ is then the weighted average cross section for wavelength band α, for the various species within an elemental layer dh at level h(b) of a cm^2-column of the atmosphere, and is defined by

$$\sigma_\alpha(b) \equiv \frac{\sum_i \sigma_{i\alpha} \cdot n_i(b)}{\sum_i n_i(b)} \ . \tag{17}$$

For each of the other wavelength bands, the α is replaced by the appropriate member of the set represented in general by j. The quantity $\bar{\sigma}_j(a)$ is, of course, $\bar{\sigma}_j$ evaluated at level h(a).

The quantity $\bar{\bar{\sigma}}_j(b)$ represents a set of a different kind of average cross sections for the various wavelength bands evaluated at level h(b) such that, for wavelength band α

$$\bar{\bar{\sigma}}_\alpha(b) \equiv \frac{\sum_i \sigma_{i\alpha} \cdot n_i(b) \cdot H_i(b)}{\sum_i n_i(b) \cdot H_i(b)} = \frac{\sum_i \sigma_{i\alpha} \cdot N_i(b)}{\sum_i N_i(b)} = \frac{\tau_\alpha(b)}{N(b)} . \qquad (18)$$

That is, $\bar{\bar{\sigma}}_\alpha(b)$ represents the weighted, average, cross section for wavelength band α for the entire cm^2-column from h(b) to h(∞). In Equation (13), $N_i(b)$ the column count at level h(b) for species i represents the total number of particles of species i in the cm^2-column from h(b) to h(∞), and N(b) is of course equal to $\sum_i N_i(b)$. The quantity $\bar{\bar{\sigma}}_\alpha(a)$ is defined in a similar manner relative to level h(a), while $\bar{\bar{\sigma}}_j(b)$ and $\bar{\bar{\sigma}}_j(a)$ represent the general members of their respective sets.

While equations for $\bar{\sigma}_j(b)$ and $\bar{\bar{\sigma}}_j(b)$ involve the boundary-layer values of $N_i(b)$ and the derived values of $H_i(b)$, the expressions for $\bar{\sigma}_j(a)$ and $\bar{\bar{\sigma}}_j(a)$ imply values of $N_i(a)$ and $H_i(a)$ which are not known directly from the boundary conditions. They are determined iteratively by means of one loop of the more general double loop computer program.

All of the above cross-section parameters depend upon σ_{ij} the sets of values of cross sections of each individual species for each wavelength band. These values have been determined for N_2, O_2, A, CO_2 and O_3 and are available on IBM cards for narrow bandwidths from 276Å to 3000Å. Values of σ_{ij} from O, N, He, H_2 and H are not now on IBM cards but the lack of these should not seriously affect a first approximation calculation.

The quantity $B(\bar{h})$ is the arithmetic mean of the quantities B(b) and B(a),

$$B(\bar{h}) = \frac{B(a) + B(b)}{2} \qquad (19)$$

where B is related to A through Equations (8) and (9) and where A is related to λ_c the thermal conductivity coefficient through the expression

$$\lambda_c = A\, T^{\frac{1}{2}} . \qquad (20)$$

Methods for computing values of λ_c for composite as well as simple gases are discussed in Chapman and Cowling [9]. It may be shown, that at level h(b) in a composite-gas atmosphere where composition changes with altitude, that

$$B(b) = A(b) \cdot \left(\frac{\bar{m}(b) \cdot G}{k}\right)^{3/2} \cdot \left[1 + \frac{d\ \ell n\ \bar{m}}{d\ \ell n\ H'}\right], \tag{21}$$

where $\bar{m}$ is the mean molecular weight. For a single gas species i, B_i is independent of altitude and may be expressed by

$$B_i = A \left(\frac{m\ G}{k}\right)^{3/2}, \tag{22}$$

or

$$B_i = f \cdot \frac{\eta}{2} \cdot \frac{5}{16} \cdot \left(\frac{G^3}{\pi}\right)^{\frac{1}{2}} \cdot \frac{m}{\sigma_c^2}, \tag{23}$$

where, for a monatonic gas, f and η have the values 5/2 and 3 respectively. For a diatomic gas f and η have the values 1.9 and 5 respectively. In this study, B(h) for a mixed atmosphere is taken as

$$B(h) = \frac{\sum_i B_i\ n_i(h)}{\sum_i n_i(h)}, \tag{24}$$

rather than a more complicated expression derived from Equation (21).

Computed values of B for the important individual atmospheric gases suggest that B does not vary by more than a factor of five between 200 and 500 km altitude, where the number densities of helium or hydrogen are small compared with that of dissociated oxygen.

The dimensions of B as defined in Equation (23) are ergs cm^{-2} sec^{-1} $(cm')^{-\frac{1}{2}}$.

Energy Input and Loss Factors

Equation (9) involves two energy input factors $E_j(\infty)$ and $c(\infty)$. The first of these $E_j(\infty)$, representing the solar flux through the top of the atmosphere, is now reasonably well known, and is available on the same IBM cards with the values of σ_{ij} for small bandwidths from 276Å to 3000Å. The quantity $C(\infty)$ which enters the equation as a constant of integration may be zero, or,

according to Nicolet, should be small compared with $E(\infty)$. Nicolet further states that if it were not small, we would not observe diurnal variations of temperature or density. For values of $C(\infty)$ equal to 1% of $\Sigma E_j(\infty)$, the influence on scale height would be negligible for altitudes below several thousand kilometers. The value of $C(\infty)$ might actually be considerably larger, as suggested by Harris and Priester [5] and models based on various values of $C(\infty)$ should be computed.

The last term of Equation (10) is the energy-loss term, and contains the loss factor $\bar{\bar{R}}_j$ which is the general symbol for a set of special loss factors, each member of which is associated with a particular, narrow, wavelength band. This loss factor is seen from Equation (7) to be a rather complicated function of R_{ij} the basic loss factor expressed in terms of ergs per molecule per second for each wavelength band and for each species. Replacing the factor $\bar{\bar{R}}_j(h)$ in the summation loss term of Equation (10) by its equivalent in Equation (7), the contribution of the energy-loss term to the scale height is seen to be

$$\sum_j \frac{\bar{\bar{\sigma}}_j(\bar{h})}{2B(\bar{h}) \cdot \bar{\sigma}_j(\bar{h})} \cdot \frac{1}{\tau_j(\bar{h})} \int_{\tau(\infty)}^{\tau(\bar{h})} \frac{\sum_i R_{ij}(\bar{h}) \cdot n_i(h)}{n(\bar{h}) \cdot \bar{\sigma}_j(\bar{h})} \cdot d\tau_j \cdot \Delta\lambda_j \left[\tau_j(b) - \tau_j(a)\right] . \tag{25}$$

Nicolet has estimated that the energy loss in the atmosphere above 150 km is primarily from atomic oxygen in the infrared region of the spectrum, particularly in the 63-micron band designated by I. In this instance, the only loss coefficient is R_{oI} and the summation term (Expression (25)) simplifies to the single term

$$\frac{\bar{\bar{\sigma}}_I(\bar{h})}{2B(\bar{h}) \cdot \sigma_I(\bar{h})} \cdot \frac{1}{\tau_I(\bar{h})} \int_{\tau(\infty)}^{\tau(\bar{h})} \frac{R_{oI}(\bar{h}) \cdot n_o(\bar{h})}{n(\bar{h}) \cdot \bar{\sigma}_I(\bar{h})} \, d\tau_I \cdot \Delta\lambda_I \left[\tau_I(b) - \tau_I(a)\right] . \tag{26}$$

If it is further assumed that atomic oxygen is the only species contributing to the optical depth at wavelength I, an assumption which is somewhat questionable, Expression (26) simplifies further to the form

$$\frac{1}{2B(\bar{h})} \frac{1}{n_o(\bar{h}) \cdot H_o(\bar{h})} \left[\int_{\infty}^{\bar{h}} \frac{R_{oI}(\bar{h}) \cdot [n_o(\bar{h})]^2}{n(\bar{h}) \cdot \bar{\sigma}_{oI}} \cdot dh \right] \cdot \left[n_o(b) \cdot H_o'(b) - n_o(a) \cdot H_o'(a)\right]. \tag{27}$$

In this form, the parallelism to the loss term in the relatively crude scale-height-generating Equation (5.45) of Nicolet is evident.

While the differences between Equation (10) and Nicolet's Equation (5.45) are significant in the energy absorption and corpuscular radiation terms, the differences in the loss term are only of academic interest, since, for the altitude region above 150 km, the influence of the loss term on the computed scale height is small. Nicolet has estimated a mean value of $R_{oI}(h)$ to be

5×10^{-19} ergs sec^{-1} $molecule^{-1}$. He has also estimated an oxygen cross section σ_{oI} for this radiation process to be $\geq 10^{-17}$ cm^2 $molecule^{-1}$, so that R_{oI}/σ_{oI} has a value of the order of 5×10^{-2} ergs per cm^2 column per second. Such a value is small compared to the estimated absorbed radiation of about 2 ergs cm^{-2} sec^{-1}.

Because the contribution of the summation loss term is small, and because the information for an accurate evaluation of this summation term is not presently at hand, the entire loss term is neglected in the planned calculations.

Description of Computer Program for Model Generation

A general, double-loop, iterative, computer program for generating a complete model atmosphere above 150 km in terms of absorbed solar radiation has been outlined. The calculation of the model by this program depends only upon the following input information: (1) the values of the boundary conditions at 150 km as indicated in a previous paragraph; (2) the values of the set of $I_j(\infty)$ the solar radiation incident upon the top of the atmosphere in each wavelength band j; and (3) the value of $C(\infty)$ the corpuscular radiation into the top of the atmosphere.

The loss term is neglected at present because not enough information concerning the actual loss coefficients at the various wavelengths is immediately available.

The computer program will generate a large number of atmospheric properties as a function of altitude for prescribed geometric altitude intervals, 5 km for example, from 150 km to 600 km or above, while the variation of gravity is taken care of through the geopotential concept. Temperature, pressure, density, number density, pressure scale height, and mean molecular weight for the composite atmosphere will be generated. The number densities and scale heights for each of the individual species would also be determined.

Significance of the Model

The model generated through Equation (10) and the other associated equations is a static noon-day model which in some respects may be inferior to the more dynamic-type model of Harris and Priester [5]. It will demonstrate, however, the variation of the several parameters with altitude on the basis of a more realistic energy-absorption pattern than the lumped value which Harris and Priester and Nicolet appear to have employed. The method may well be adapted for inclusion in a more sophisticated approach of the Harris and Priester type.

REFERENCES

1. Minzner, R. A. and G. O. Sauermann, "Planetary Atmospheres Generated from Solar Radiation and Absorption Considerations," GCA Technical Report (in preparation).

2. Nicolet, M., "Structure of the Thermosphere," Planet. Space Sci., 5, 1-32, (1961).

3. Nicolet, M., "Density of the Heterosphere Related to Temperature," Smithsonian Contributions to Astrophysics, Vol. 6, Research and Space Science, 175-187, Washington, D.C., (1963).

4. Nicolet, M., "Aeronomy," to be published Handbuck der Physik (Geophysik) Band XLIX.

5. Nicolet, M., Private communication by telephone between Dr. K. S. Champion and Dr. M. Nicolet, (July 1964).

6. Harris, I. and W. Priester, "Time-Dependent Structure of the Upper Atmosphere," NASA TND-1443, Washington, D.C. (July 1962).

7. Minzner, R. A. and W. S. Ripley, "The ARDC Model Atmosphere, 1956," Air Forces Surveys in Geophysics No. 86 Geophysics Research Directorate Air Force Cambridge Research Center, (Dec. 1956).

8. U. S. Standard Atmosphere, 1962, National Aeronautics and Space Administration, U. S. Air Force and U. S. Weather Bureau Government Printing Office, Washington, D. C. (1962).

9. Chapman, S. and T. G. Cowling, "The Mathematical Theory of Non Uniform Gases," Cambridge University Press, London and New York, (1960).

ANALYTICAL INVESTIGATION OF THE EXISTENCE OF SUCCESSIVE ISOPYCNIC LEVELS

Introduction

Cole [1] reported that a condition approximating a second isopycnic level exists over Fort Churchill, Canada at an altitude of 80 to 90 km. That is, the average density-altitude profiles for various seasons, as well as the instantaneous density-altitude profiles which, at any given altitude, may differ considerably from one to the other tend to converge to a common value of density in the region 80 to 90 km. This altitude, at which these density-altitude profiles converge, is called the isopycnic altitude.

The convergence of these density-altitude profiles is not exact, but rather is spread out over an altitude region such that the term isopycnic region is more descriptive in this situation.

The existence of this 90-km isopycnic region is not limited to the arctic region, but is probably formed rather generally at most latitudes in association with the isothermal layer at the mesopause, though not necessarily dependent upon it. Because of the general existence of this isopycnic region, it is interesting to examine its influence on the possible density-altitude profiles of model atmospheres above the mesopause, particularly as it may influence the existence of an additional isopycnic region at some greater altitude. Such a region would be of significance as the base level for models of the thermosphere, which models vary with changes in solar radiation and related properties. Currently, thermosphere models such as those presented by Jacchia [2] and Harris and Priester [3] tend to diverge upward from a common density point assigned arbitrarily to the altitude 120 km.

The present study demonstrates that the isopycnic level at or near 90 km implies near isopycnic conditions at about two scale heights above 90 km, i.e., at about 101 km. A mean density value at this altitude, therefore, would better serve as the boundary-condition values for thermospheric models than the mean-density value arbitrarily selected by several investigators for 120 km.

This study examines the behavior of possible density-altitude profiles between the isopycnic reference level h_b and a few scale heights above this altitude. For the sake of simplicity, the examination is limited to those profiles of relative density versus geopotential ($\rho(h)/\rho_b$ vs h), as defined by $(T_M)_b$ a common value of molecular scale temperature T_M at h_b, and by L_M' a single gradient of T_M with respect to h (i.e. $L_M' \equiv dT_M/dh$) which gradient may assume any single realistic positive or negative value including zero.

Density-Altitude Relationship for an Isothermal Layer

Since the reference isopycnic level lies within an isothermal layer, it is convenient to extend the density-altitude profile associated with this

isothermal region to altitudes a few scale heights above h_b, on the basis of the same isothermal conditions, and to use this density-altitude profile as a basis of comparison of various other density-altitude profiles.

The equation for the altitude profile of relative density for $L'_M = 0$ is the well-known expression [4,5]

$$\frac{\rho(h)}{\rho_b} = \exp\left[- \frac{G \cdot M_o}{R \cdot (T_M)_b} (h-h_b) \right] , \tag{1}$$

where G is the invariable acceleration-of-gravity parameter associated with the definition of standard geopotential meter,
M_o is the sea-level value of molecular weight, and
R is the universal gas constant.

In order to reduce the number of symbols, as well as to simplify the dimensional considerations, it is convenient to introduce two quantities. The first quantity is geopotential pressure scale height H′ which has the dimension of geopotential altitude, and is defined by

$$H' = \frac{R \cdot T_M}{G \cdot M_o} . \tag{2}$$

The second quantity is the dimensionless altitude parameter x defined by

$$x \equiv \frac{h - h_b}{H'_b} \tag{3}$$

In this expression H'_b is the reference-level value of H′, and x is seen to be positive for $h > h_b$. In terms of these two quantities, Equation (1) is simply expressed as

$$\frac{\rho(x)}{\rho_b} = \exp(-x) , \tag{4}$$

from which it follows that

$$\ell n \frac{\rho(x)}{\rho_b} = -x , \tag{5}$$

and

$$\frac{d \ \ell n \ [\rho(x)/\rho_b]}{dx} = -1 . \tag{6}$$

Thus, the graph of $\ell n\ \rho(x)/\rho b$ versus x in Figure 1 is represented by the straight line QAA′ with a slope of -1.

Density-Altitude Relationships for Constant Nonzero Gradients of T_M or H′

One of the density-altitude equations associated with a constant gradient of T_M is given by the following well-known expression [4,5]

$$\frac{\rho(h)}{\rho_b} = \left[\frac{(T_M)_b}{(T_M)_b + L'_M(h-h_b)}\right]^{\left(1 + \frac{G \cdot M_o}{R \cdot L'_M}\right)} . \tag{7}$$

The temperature gradient L'_M may be related to the geopotential scale height gradient $\beta' = dH'/dh$. Since H′ is directly proporational to T_M the differentiation of both sides of Equation (2) with respect to h yields

$$\beta' = \frac{R}{G \cdot M_o} \cdot L'_M . \tag{8}$$

In terms of geopotential scale height and its gradient, as given by Equations (2) and (8), and the transformation defined by Equation (3), one may rewrite Equation (7) as

$$\frac{\rho(x)}{\rho_b} = \left[\frac{1}{1 + \beta' \cdot x}\right]^{\frac{1 + \beta'}{\beta'}} . \tag{9}$$

This equation is defined for all values of β' except $\beta' = 0$, but for $\beta' < -1$, the density-altitude profiles become physically unrealistic.

Another form of density-altitude expression for constant scale-height gradient is defined for all values of β' including $\beta' = 0$. This expression, first presented by Nicolet [6], was defined by him in terms of geometric altitude z, geometric scale height H, and geometric scale-height gradient β, and, accordingly, it includes the nuisance gravity ratio $g(z)/g_b$. Minzner [7] has shown that when z, H, and β are properly transformed into their geopotential counterparts, the gravity ratio vanishes, and we have

$$\frac{\rho(h)}{\rho_b} = \exp\left\{-\frac{2(1 + \beta')\ (h-h_b)}{(H' + H'_b)}\left[1 + \frac{1}{3}\left(\frac{H' - H'_b}{H' + H'_b}\right) + \frac{1}{5}\left(\frac{H' - H'_b}{H' + H'_b}\right)^2 + \cdots\right]\right\} \tag{10}$$

Constant scale-height gradient β' implies the relationship

$$H' = H'_b + \beta'\ (h-h_b) \tag{11}$$

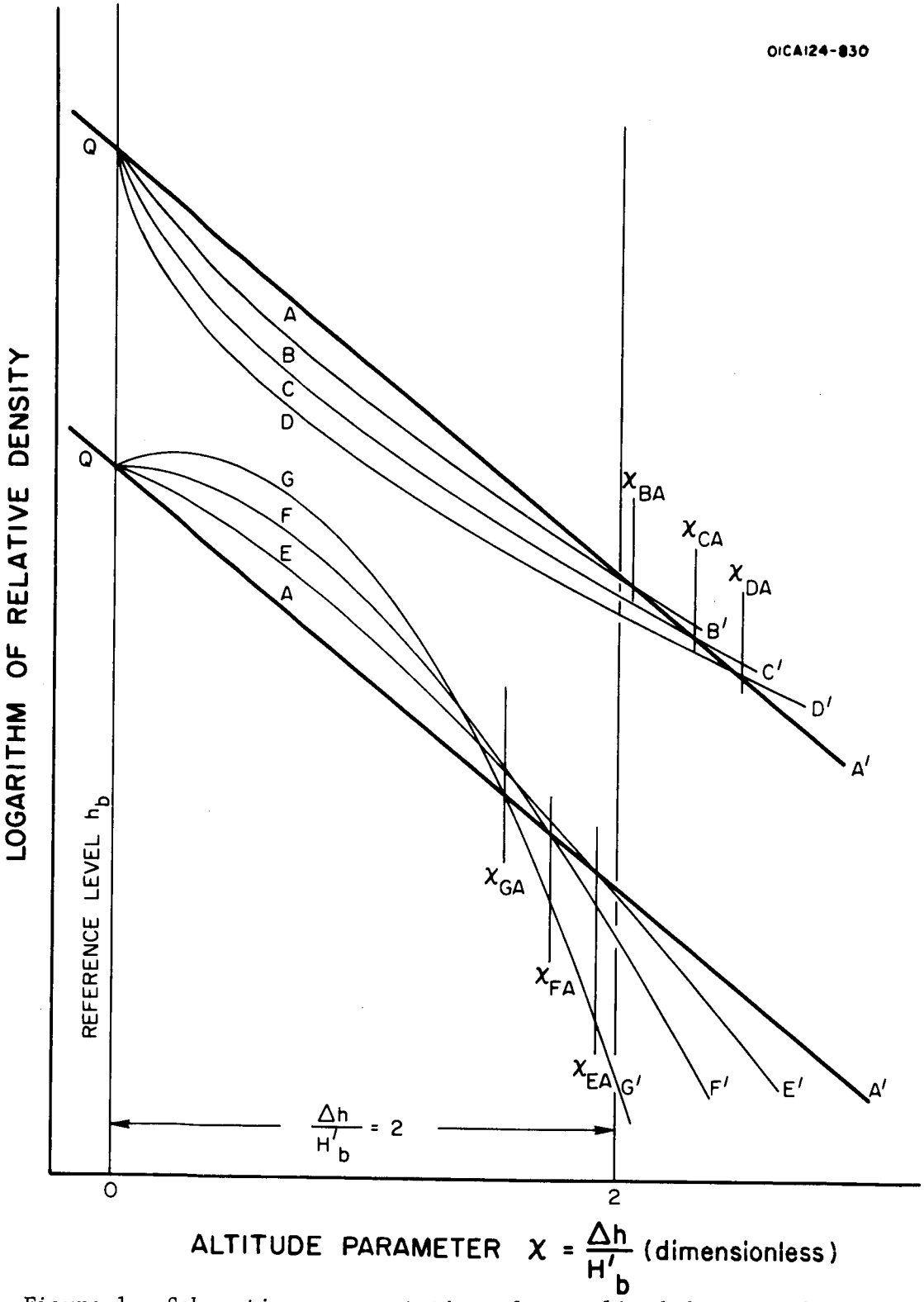

Figure 1. Schematic representation of normalized density-altitude profiles for various constant positive gradients of scale height versus altitude in the upper part of the figure, and for various constant negative gradients in the lower part of the figure.

It is apparent, therefore, from Equation (11) and (3), that

$$\frac{H' - H'_b}{H' + H'_b} = \frac{\beta'(h-h_b)}{2H'_b + \beta'(h-h_b)} = \frac{\beta' \cdot x}{2 + \beta' \cdot x} \tag{12}$$

and that

$$\frac{2(1 + \beta')\ (h-h_b)}{H' + H'_b} = \frac{2(1 + \beta')\ (h-h_b)}{2H'_b + \beta'\ (h-h_b)} = \frac{2(1 + \beta')x}{2 + \beta' \cdot x} \tag{13}$$

Introducing Equations (12) and (13) into Equation (10) yields,

$$\frac{\rho(x)}{\rho_b} = \exp\left\{-\frac{2(1 + \beta')x}{2 + \beta' \cdot x}\left[1 + \frac{1}{3}\left(\frac{\beta' \cdot x}{2 + \beta' \cdot x}\right)^2 + \frac{1}{5}\left(\frac{\beta' \cdot x}{2 + \beta' \cdot x}\right)^4 + \cdots\right]\right\} \tag{14}$$

It may be shown that the infinite series converges for all finite values of the product $\beta' \cdot x$ including $\beta' = 0$, for which value Equation (14) degenerates identically to Equation (4).

Form of Related Density-Altitude Curves

It can be shown that for positive values of β', Equations (9) and (14) will generate identical density-altitude profiles which when plotted in the form of $\ell n\ \rho(x)/\rho_b$ versus x appear concaved upward as in the cases schematically designated by curves $Q\beta\beta'$, QCC', and QDD' of Figure 1. Each curve represents successively increasing values of β'. The crossing points x_{BA}, x_{CA}, and x_{DA}, at which these three curves respectively cross the straight-line profile QAA', each have x-coordinate values greater than x = 2, and each successively greater than the preceding one, as will be demonstrated below. It is also noted that none of the curves for positive values of β' cross each other before first crossing the reference density-altitude profile for $\beta' = 0$.

For a set of realistic negative values of β', i.e. $-1 < \beta' < 0$, whose absolute magnitude increases successively from 0, the corresponding density-altitude profiles are represented successively by the lines QEE', QFF', and QGG' of Figure 1, all of which are concaved downward. These lines are each seen to cross the zero-gradient line QAA' at successively lower values of x, i.e., x_{EA}, x_{FA}, and x_{GA}, each of which is successively smaller than x = 2. It will also be noted that the curve for any negative value of β' crosses all density-altitude profiles for less-negative values of β' before crossing that one for $\beta' = 0$.

Analytical Determination of Crossing Points

The analytical determination of the coordinates for these various crossing points x_{BA} to x_{GA} is accomplished in principle by the solution of that equation which results from equating the right-hand member of Equation (4) to the right-hand member of either Equation (9) or Equation (14). The lack of a compatible format of Equation (9) eliminates that possibility, while the infinite series of Equation (14) effectively eliminates the second possibility. Minzner [7] has shown, however, that for small values of β' and x, the infinite series of Equation (14) converges very rapidly, and under these conditions the truncation of the series after the first term yields quite good results. More accurate results can be obtained if the first two terms of the series are retained, as in this study. Thus, the form of Equation (14) actually employed when the left-hand member is expressed as the natural logarithm is

$$\ell n \left[\frac{\rho_x}{\rho_b}\right] = - \frac{2(1 + \beta')x}{2 + \beta' \cdot x} \left[1 + \frac{1}{3}\left(\frac{\beta' \cdot x}{2 + \beta' \cdot x}\right)\right]^2 \qquad (15)$$

Now equating the right-hand members of the equivalent expressions, Equations (5) and (15), yields a cubic equation in x but a quadratic equation in β'. Thus,

$$x^2(3x - 8)(\beta')^2 + 2x(5x - 12)\,\beta' + 12(x - 2) = 0 \; . \qquad (16)$$

The relationship between β' and x expressed by Equation (16) is shown in Figure 2. For realistic values of β as represented by actual atmospheric conditions, i.e., for $-0.2 \leqslant \beta' \leqslant +0.6$, the corresponding values of x, i.e., $1.85 \leqslant x \leqslant 2.3$, are shown as a heavier line. This heavy line indicates the realistic range of crossing points of Figure 1. As β' approaches 0 from either direction, the crossing point approaches x = 2.

Discussion of the Results

Superimposing the two sections of Figure 1 yields the results shown in Figure 3. The lower extreme crossing point x_{GA} may not have an x value smaller than x = 1.85 for realistic negative-gradient considerations, while the upper-extreme crossing point x_{DA} may not have an x value greater than x = 2.3. The possible crossing points of these several density-altitude profiles is certainly confined with respect to altitude. The figure also indicates a confinement with respect to density. That part of the problem related to range of density values at any given altitude still requires analysis for accurate interpretation.

It is apparent, however, that an isopycnic region does exist in the vicinity of two scale heights above a common reference point, if temperature-altitude profiles or the related scale-height-altitude profiles are restricted to linear segments extending at least for two scale heights in altitude from this common density-temperature-altitude point.

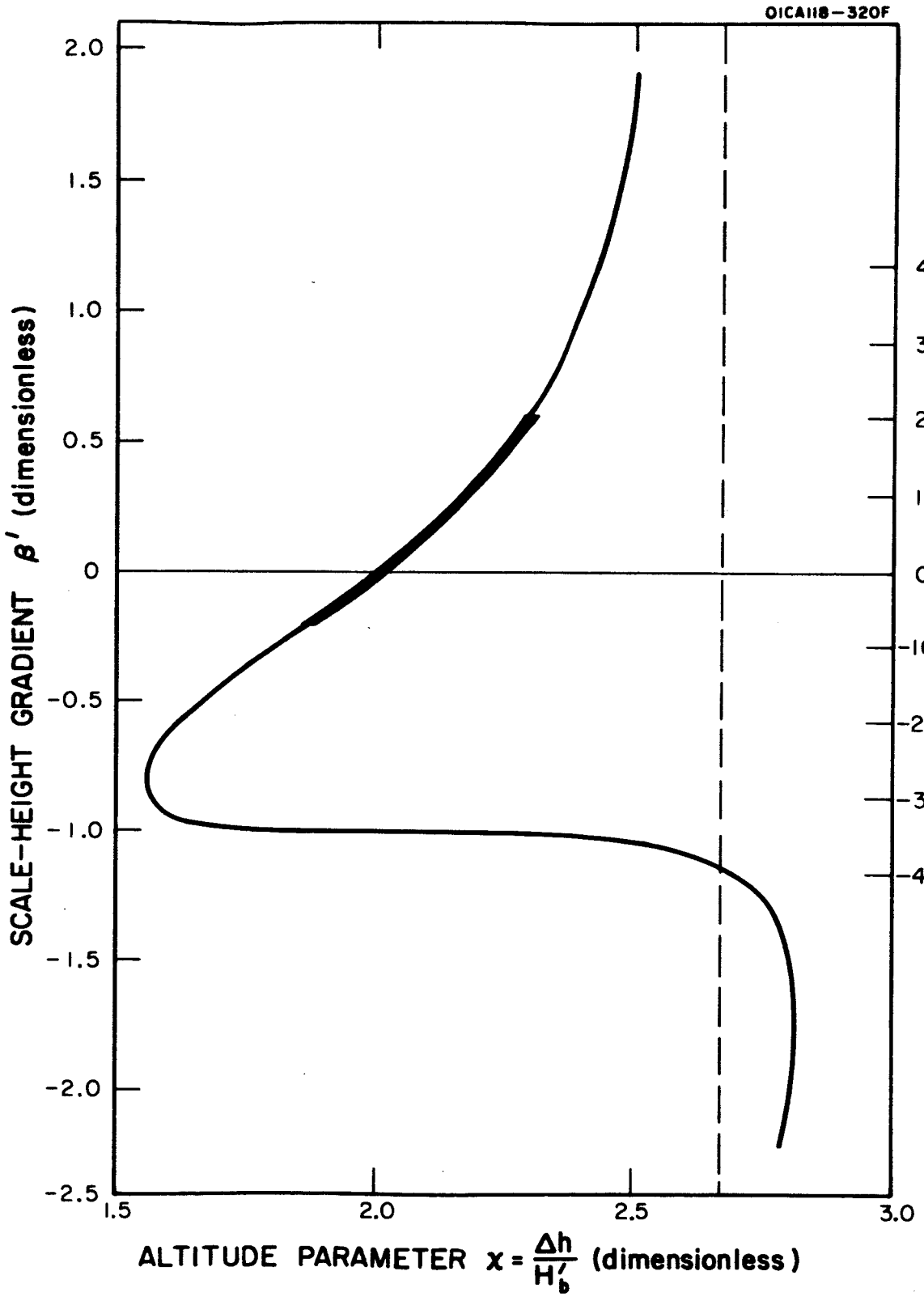

Figure 2. Crossing altitudes x_{BA}, x_{CA} ··· x_{GA}, etc. of Figure 1 in terms of parameter x for various values of scale-height gradients as determined by the solution of Equation 16.

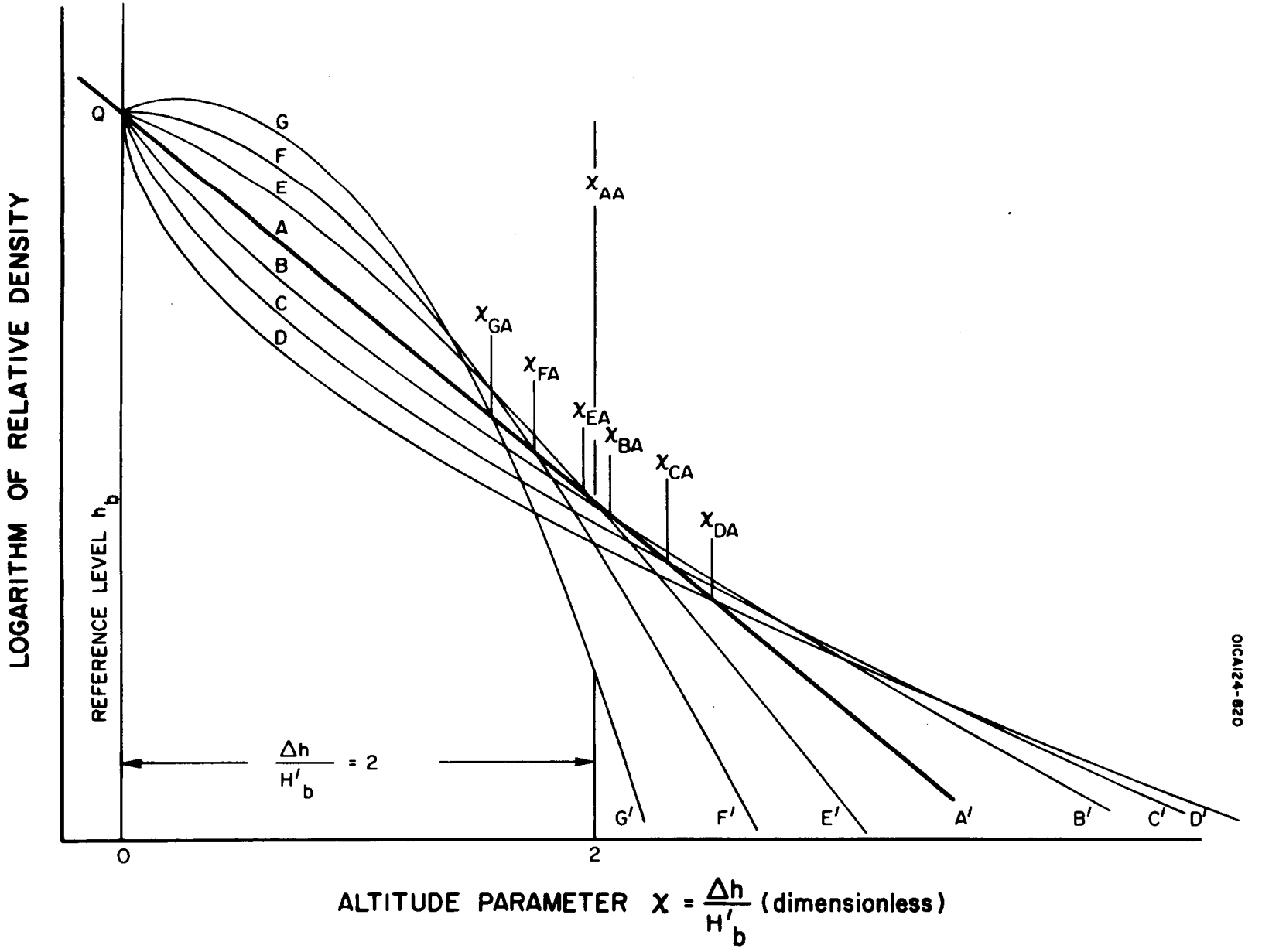

Figure 3. Schematic representation of normalized density-altitude profiles for various constant positive and negative scale-height gradients.

A density-altitude point within this region would appear to serve as a better reference point for atmospheric models of the thermosphere than the 120 km point now generally used.

Perhaps more significant is an implication of the above study regarding the required altitude interval between successive density observations if meaningful temperature-altitude profiles are to be inferred from these data. Obviously, two successive density-altitude observations made with normal measurement uncertainty, and separated by two scale heights are consistent with an almost infinite number of constant temperature-altitude gradients. These range from extreme positive to extreme negative values. It is apparent, therefore, that such density-altitude points treated in pairs will not yield significant temperature information. Density-altitude data should be collected with a sampling interval which is small compared with two scale heights.

REFERENCES

1. Cole, A. E., "Suggestion of a Second Isopycnic Level at 80 to 90 Km over Churchill, Canada," J. Geophys. Res., 66 (9), 2773-2778, (Sept. 1963).

2. Jacchia, L. J., "Static Diffusion Models of the Upper Atmosphere with Empirical Temperature Profiles," Special Report 170, Smithsonian Institution Astrophysical Observatories, (December 30, 1964).

3. Harris, I. and W. Priester, "Time-Dependent Structure of the Upper Atmosphere," NASA TND-1443, Washington, D. C., (July 1962).

4. Minzner, R. A., W. S. Ripley and T. P. Condron, U. S. Extension to the ICAO Standard Atmosphere, U. S. Government Printing Office, Washington, D. C., (1958).

5. Minzner, R. Q., K. S. W. Champion and H. L. Pond, "The ARDC Model Atmosphere 1959," AFCRC-TR-59-267, Air Force Surveys in Geophysics No. 115, (August 1959).

6. Nicolry, M., "Density of the Heterosphere Related to Temperature," Smithsonian Contributions to Astrophysics, Vol. 6, Research in Space Science, 175-186, Washington, D. C., (1963).

7. Minzner, R. A., "Pressure and Density Scale Heights Defining Atmospheric Models," GCA Technical Report No. 64-6-A, (April 1964).

TEMPERATURE DETERMINATION FROM DIFFUSION DATA

For several years, GCA has participated in a rocket program involving the formation of sodium vapor trails to altitudes above 200 km. In addition to the determination of wind profiles from these vapor trails, some molecular diffusion data has been obtained from 18 of these flights [1]. In two flights, only a single diffusion-altitude point exists, but in the remainder of the flights, values of diffusion exist for at least four different altitudes, and in two instances for eleven different altitudes.

These data have been indirectly related to temperature profiles by a comparison of diffusion data with diffusion-altitude profiles computed from two model atmospheres [2,3] and from the most recent U. S. Standard Atmosphere [4]. No temperature-altitude profiles had been computed, however, for any of these sets of data even though temperature-altitude data were inherently available from the data.

Recognizing the situation, the writer with the assistance of Dr. Herbert K. Brown developed an integral equation in which temperature-altitude data may be inferred from diffusion-altitude data without assuming any initial value of temperature or of any other atmospheric property.

The derived relationship is based upon an expression for diffusion D of molecules of mass m_1 into a medium of molecular mass m as used by Nicolet [5]:

$$D = \frac{3}{4} \frac{1}{(8\pi)^{\frac{1}{2}} \sigma^2} \left(1 + \frac{m}{m_1}\right)^{\frac{1}{2}} \frac{g^{\frac{1}{2}} H^{\frac{1}{2}}}{n} , \qquad (1)$$

where g is the local acceleration of gravity,
H is the local scale height,
n is the local number density of major species of molecular mass m, and
σ is the effective mean collision cross section of the two species.

This expression is in turn derived from an expression given by Chapman and Cowling [6]:

$$D_{1,2} = \frac{3}{8n\sigma_{1,2}^2} \left\{\frac{kTm_1 + m_2}{2\pi m_1 m_2}\right\}^{\frac{1}{2}} \qquad (2)$$

in which T is the temperature, k is Boltzmann's constant, and the subscripts 1 and 2 indicate the minor and major gases respectively. The Chapman and Cowling expression is listed as a first-approximation expression for the case where the gas molecules are considered to be rigid spheres.

Either of these expressions can be converted to the form

$$D = c' \cdot u' \cdot T_M^{2/3} \cdot p^{-1} \tag{3}$$

where T_M is molecular scale temperature,
p is atmospheric pressure,
c' is a composite constant given by Equation (4), and
u' is a molecular weight function given by Equation (5).

The value of the constant c' is given by

$$c' = \left(\frac{9}{128\pi}\right)^{\frac{1}{2}} \cdot \left(\frac{R}{M_o}\right)^{3/2} \cdot \frac{1}{N\sigma^2} , \tag{4}$$

where R is the universal gas constant,
M_o is the sea-level value of the mean molecular weight of the atmosphere,
N is Avogadro's number, and
σ is the effective collision cross section between air and the diffusing gas.

The molecular weight function u' is given by

$$u' = M \cdot \left(1 + \frac{M}{M_1}\right)^{\frac{1}{2}} , \tag{5}$$

where M is the mean molecular weight of the atmosphere at any geopotential altitude h, and
M_1 is the molecular weight of the substance diffusing into the atmosphere.

Defining a parameter $D' = D/u'$, we may write an expression for D', the right-hand side of which is free from any explicit expressions of molecular weight:

$$D' = c' \cdot T_M^{2/3} \cdot p^{-1} . \tag{6}$$

In the absence of simultaneous observations of atmospheric pressure or density along with diffusion observations, neither Equation (3) nor (6) may be evaluated for temperature. It is well known, however, that altitude profiles of pressure p yield altitude profiles of T_M as indicated by

$$\frac{d\ \ell n\ p}{dh} = \frac{G \cdot M_o}{R \cdot T_M} = \frac{Q}{T_M} , \tag{7}$$

where h is geopotential altitude,
G is numerically equal to the sea-level value of the acceleration of gravity, and
Q is a constant equal to $G \cdot M_o/R$.

It is similarly well known that T_M may also be derived from altitude profiles of density ρ as indicated by the following expression recently used by Minzner [7]:

$$(T_M)_r = \frac{\rho_a}{\rho_r} (T_M)_a + \frac{Q}{\rho_r} \int_{h_r}^{h_a} \rho dh \ . \tag{8}$$

In this expression subscript a is associated with the greatest altitude of a density observation and subscript r is associated with a running altitude varying between h_a and the lowest altitude of set of data.

From Equation (6) it is possible to write

$$\frac{d\ \ell n\ D'}{dh} = \frac{2}{3} \frac{d\ \ell n\ T_M}{dh} - \frac{d\ \ell n\ p}{dh} \ . \tag{9}$$

Combining Equations (7) and (9) leads to

$$a \cdot \frac{dT_M}{dh} - \frac{2a}{3} \cdot \frac{d\ \ell n\ D'}{dh} \cdot T_M = - \frac{2a}{3} \cdot Q \ , \tag{10}$$

where a is an arbitrary factor applied to both sides of the equation.

The left-hand side of Equation (10) has the form of the derivative of the product $a \cdot T_M$, i.e.,

$$\frac{d(a \cdot T_M)}{dh} = a \cdot \frac{dT_M}{dh} + T_M \cdot \frac{da}{dh} \ , \tag{11}$$

where "a" must have the form such that

$$\frac{da}{dh} = - \frac{2a}{3} \cdot \frac{d\ \ell n\ D'}{dh} \ . \tag{12}$$

The condition of Equation (12) is met for

$$a = e^v \tag{13}$$

or

$$\frac{da}{dh} = \frac{de^{v}}{dh} = e^{v} \cdot \frac{dv}{dh} , \tag{14}$$

where

$$\frac{dv}{dh} = - \frac{2}{3} \frac{d \ \ell n \ D'}{dh} , \tag{15}$$

and, hence, where

$$v = - \frac{2}{3} \int \frac{d \ \ell n \ D'}{dh} \cdot dh = - \frac{2}{3} \ \ell n \ D' , \tag{16}$$

such that

$$a = \left(\exp - \frac{2}{3} \ \ell n \ D' \right) . \tag{17}$$

Hence, Equation (10) may be rewritten as

$$\left(\exp - \frac{2}{3} \ \ell n \ D' \right) \cdot \frac{dT_M}{dh} - \frac{2}{3} \left(\exp - \frac{2}{3} \ \ell n \ D' \right) \cdot \frac{d \ \ell n \ D'}{dh} \cdot T_M = \frac{2Q}{3} \left(\exp - \frac{2}{3} \ \ell n \ D' \right) , \tag{18}$$

or

$$\frac{d}{dh} \left[T_M \left(\exp - \frac{2}{3} \ \ell n \ D' \right) \right] = - \frac{2Q}{3} \cdot \left(\exp - \frac{2}{3} \ \ell n \ D' \right) . \tag{19}$$

Recognizing that

$$\exp - \frac{2}{3} \ \ell n \ D' = \exp - \ell n (D')^{2/3} = \frac{1}{\exp \ \ell n (D')^{2/3}} = \frac{1}{(D')^{2/3}} ,$$

we rewrite Equation (19) as

$$\frac{d}{dh} \left[T_M \cdot (1/D')^{2/3} \right] = - \frac{2Q}{3} \cdot (1/D')^{2/3} . \tag{20}$$

Integrating between the limits of a and r we have

$$T_M \cdot (1/D')^{2/3} \Big|_a^r = - \frac{2Q}{3} \cdot \int_a^r (1/D')^{2/3} \cdot dh . \tag{21}$$

Introducing the limits on the left-hand side and reversing the limits on the right-hand side of Equation (21) yields

$$(T_M)_r \cdot (1/D'_r)^{2/3} = (T_M)_a \cdot (1/D'_a)^{2/3} + \frac{2Q}{3} \int_r^a (1/D')^{2/3} \cdot dh \ , \qquad (22)$$

from which we have

$$(T_M)_r = (T_M)_a \cdot (D'_r/D'_a)^{2/3} + \frac{2}{3} Q \cdot (D'_r)^{2/3} \cdot \int_r^a (1/D')^{2/3} \cdot dh \ . \qquad (23)$$

The similarity between this equation and Equation (8) is striking.

Multiplying the above equation by M/M_o transforms the expression to kinetic temperature, thus

$$T_r = T_a \cdot (D'_r/D'_a)^{2/3} + \frac{2}{3} \frac{G}{R} \cdot (D'_r)^{2/3} \int_r^a M \cdot (1/D')^{2/3} \cdot dh \ . \qquad (24)$$

In terms of the trapezoidal rule for numerical integration, this expression becomes

$$T_r = T_a \cdot (D'_r/D'_a)^{2/3} + \frac{2}{3} \frac{G}{R} \cdot (D'_r)^{2/3} \left[\frac{M_a}{(D'_a)^{2/3}} \cdot \frac{h_a - h_{a+1}}{2} + \right.$$

$$\left. + \frac{M_r}{(D'_r)^{2/3}} \cdot \frac{h_{r-1} - h_r}{2} + \sum_{j=a+1}^{r-1} \frac{M_j}{(D'_j)^{2/3}} \cdot \frac{h_{j-1} - h_{j+1}}{2} \right] \qquad (25)$$

Equation (25) programmed for an IBM 1620 digital computer was used to determine a family of profiles of T_M versus h for each of the sets of diffusion data previously referred to. It is apparent that T_r, the running value of T, is dependent upon the assumed value T_a. It is also apparent that, as altitude h_r drops increasingly below altitude h_a, the value of the ratio D'_r/D'_a becomes increasingly small, such that, for h_r sufficiently below h_a, the quantity $T_a(D'_r/D'_a)^{2/3}$ becomes small compared to T_r, and the choice of the value of T_a is then unimportant.

A family of T-h profiles from sodium diffusion data illustrates this convergence phenomena (see Figures 1 and 2). The wide range of temperature values, as shown in Figure 1, for successive values of diffusion also indicates, to some extent, the relative uncertainty in successive diffusion data points.

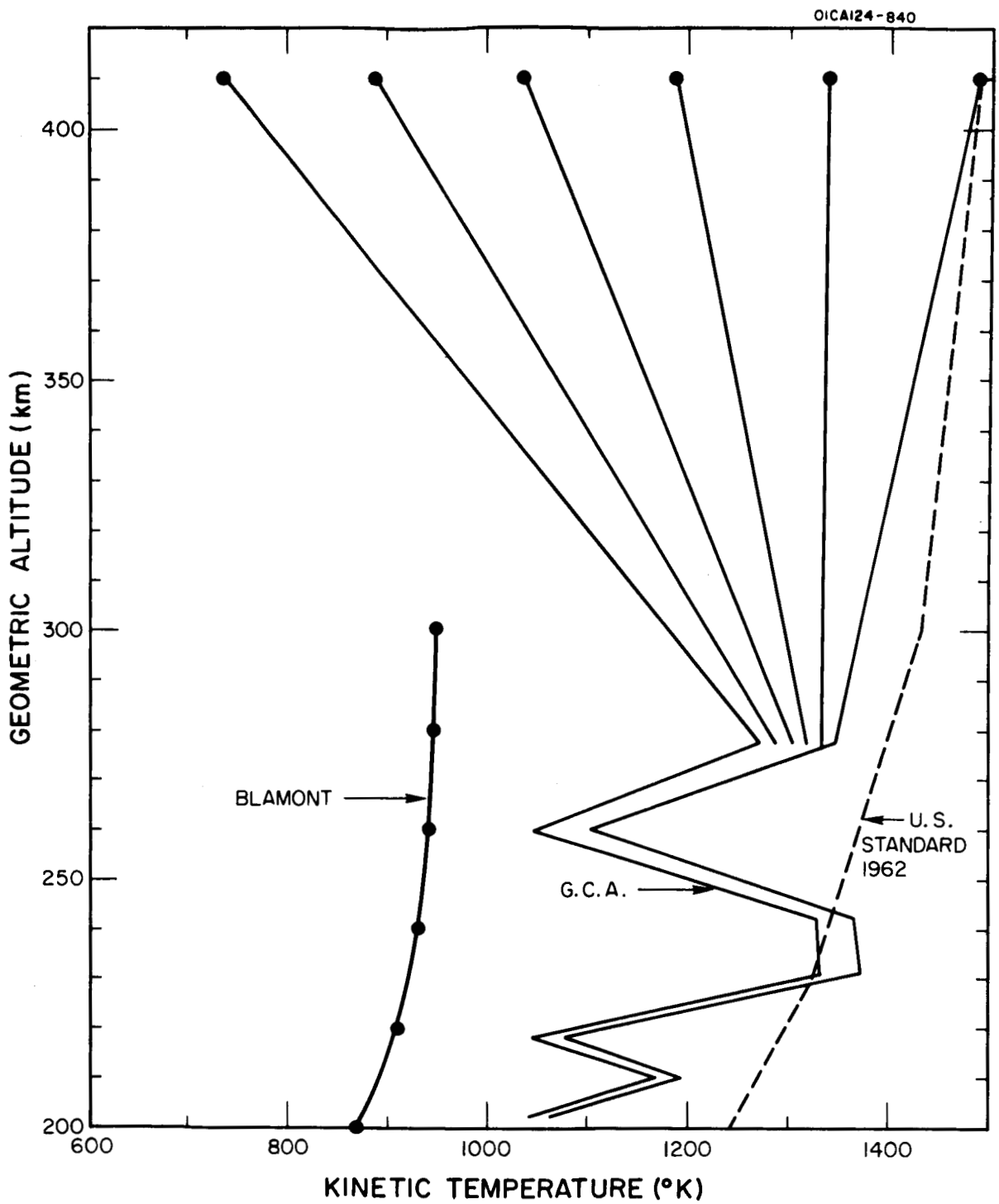

Figure 1. Temperature-altitude profile over Wallops Island at 0532 EST on September 13, 1961 as deduced from GCA sodium diffusion data, and six different reference temperatures at 410 km altitude, compared with Blamont's results for the same occasion and compared with the U. S. Standard Atmosphere.

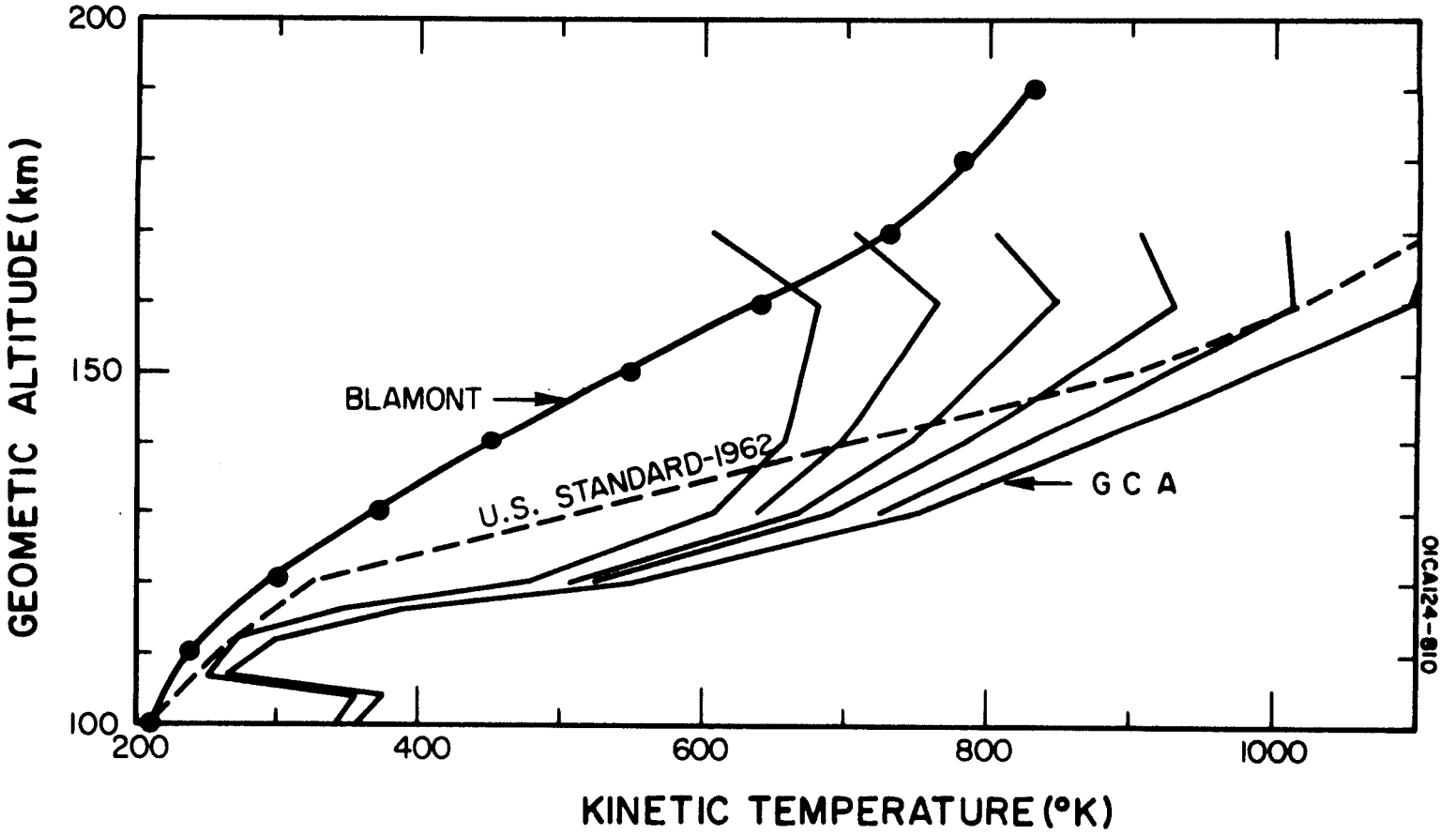

Figure 2. Temperature-altitude profile over Wallops Island at 0532 EST on 17 September 1961 as deduced from GCA sodium diffusion data and six different assumed reference temperatures at 170 km, compared with Blamont's results for the same occasion and compared with the U. S. Standard Atmosphere.

Tabular values of diffusion D, the quantity $D' = D/u'$ (designated in the IBM printout as DPPP), molecular weight, and a family of five sets of temperature versus altitude data are given for each of sixteen flights at specified times and locations.

The molecular weights used in the evaluation of Equation (25) are those of the U. S. Standard Atmosphere [4] and are shown in the computer printout.

TEMPERATURE VS. GEOMETRIC ALTITUDE
FROM D SODIUM DIFFUSION DATA WHERE COMPUTATIONS ACCOUNT
FOR GRAVITY THROUGH GEOPOTENTIAL AND FOR MOLECULAR WEIGHT
THROUGH TM MOLECULAR SCALE TEMPERATURE
CONVERSIONS TO T ARE THROUGH MOLECULAR WEIGHT OF THE 1962
US STANDARD ATMOSPHERE
THE UPPER PART OF THE T VS Z PROFILE IS BIASED
BY THE UPPER REFERENCE LEVEL VALUES OF TM IN THE RATIO
DPPA**(-2/3)/((DPP**(-Z/3))

19 APRIL 61 0436 EST WALLOPS ISLAND

Z	D	DPPP	TEMPERATURES						M.WT.
155000.	1.513E+05	2.693E-05	1144.	1036.	927.	819.	711.	603.	26.79
105000.	2.020E+06	7.695E-04	239.	236.	232.	228.	224.	221.	28.75
107000.	3.000E+06	5.899E-04	261.	256.	251.	247.	242.	237.	28.68
110000.	3.640E+06	5.167E-04	227.	222.	216.	211.	205.	200.	28.56
112000.	9.880E+06	2.648E-04	379.	368.	357.	346.	336.	325.	28.47
115000.	1.090E+07	2.469E-04	337.	326.	314.	303.	291.	280.	28.32
120000.	5.240E+07	8.605E-05	755.	722.	689.	656.	623.	591.	28.07
125000.	5.590E+07	8.177E-05	679.	645.	610.	576.	542.	508.	27.81
130000.	1.020E+08	5.437E-05	882.	831.	780.	729.	678.	627.	27.58
140000.	1.990E+08	3.442E-05	1110.	1031.	951.	872.	792.	713.	27.20
150000.	2.570E+08	2.877E-05	1093.	999.	904.	810.	716.	622.	26.92
155000.	2.820E+08	2.693E-05	1058.	958.	857.	757.	658.	558.	26.79

20 APRIL 61 19.12 EST WALLOPS ISLAND

Z	D	DPPP	TEMPERATURES						M.WT.
170000.	1.655E+05	1.523E-05	1211.	1102.	992.	882.	773.	663.	26.45
120000.	4.110E+07	1.011E-04	606.	590.	574.	558.	542.	526.	28.07
130000.	8.020E+07	6.383E-05	674.	650.	625.	600.	575.	550.	27.58
135000.	1.350E+08	4.481E-05	828.	793.	758.	723.	688.	652.	27.37
150000.	2.690E+08	2.790E-05	913.	857.	802.	746.	690.	635.	26.92
155000.	3.580E+08	2.297E-05	992.	925.	858.	791.	724.	656.	26.79
170000.	6.520E+08	1.523E-05	1105.	1006.	905.	805.	705.	606.	26.45

21 APRIL 61 0439EST WALLOPS ISLAND

Z	D	DPPP	TEMPERATURES						M.WT.
160000.	1.560E+05	2.128E-05	1111.	1002.	893.	784.	676.	567.	26.66
100000.	2.070E+06	7.600E-04	336.	333.	330.	327.	324.	321.	28.88
118000.	1.720E+07	1.813E-04	377.	364.	352.	339.	327.	314.	28.17
120000.	4.010E+07	1.028E-04	603.	581.	560.	538.	516.	494.	28.07
125000.	4.930E+07	8.891E-05	578.	553.	528.	503.	478.	453.	27.81
130000.	8.160E+07	6.310E-05	682.	647.	613.	578.	543.	508.	27.58
140000.	2.130E+08	3.289E-05	992.	926.	860.	794.	728.	662.	27.20
150000.	3.350E+08	2.411E-05	1101.	1011.	922.	833.	744.	655.	26.92
160000.	3.990E+08	2.128E-05	1022.	922.	822.	722.	622.	521.	26.66

13 SEPTEMBER 61 04.32 EST WALLOPS ISLAND ABOVE 200 KM.

Z	D	DPPP	TEMPERATURES						M.WT.
410000.	3.851E+05	2.687E-07	2186.	1966.	1745.	1525.	1304.	1084.	19.70
202000.	1.180E+09	1.297E-05	1062.	1058.	1054.	1050.	1046.	1042.	25.50
211000.	1.760E+09	9.842E-06	1192.	1186.	1181.	1176.	1171.	1165.	25.24
218000.	1.790E+09	9.661E-06	1074.	1069.	1063.	1058.	1053.	1047.	25 04
231000.	3.500E+09	6.091E-06	1373.	1365.	1357.	1348.	1340.	1332.	24.66
242000.	4.370E+09	5.190E-06	1378.	1368.	1359.	1349.	1340.	1330.	24.34
260000.	4.590E+09	4.923E-06	1101.	1091.	1081.	1071.	1061.	1051.	23.82
277000.	9.000E+09	3.083E-06	1348.	1333.	1318.	1302.	1287.	1271.	23.33
410000.	2.770E+11	2.687E-07	1486.	1337.	1186.	1037.	886.	737.	19 70

16 SEPT 61 1839 EST WALLOPS ISLAND

Z	D	DPPP	TEMPERATURES						M.WT.
200000.	1.938E+05	1.051E-05	1401.	1287.	1174.	1061.	947.	834.	25.56
107000.	3.550E+06	5.273E-04	362.	360.	357.	355.	353.	351.	28.68
110000.	5.850E+06	3.766E-04	427.	423.	420.	417.	414.	411.	28.56
114000.	8.090E+06	3.017E-04	432.	428.	424.	421.	417.	413.	28.37
115000.	1.070E+07	2.500E-04	497.	492.	488.	483.	478.	474.	28.32
145000.	2.240E+08	3.166E-05	1026.	991.	956.	921.	886.	850.	27.05
160000.	5.530E+08	1.712E-05	1444.	1379.	1315.	1251.	1187.	1123.	26.66
170000.	5.540E+08	1.698E-05	1245.	1181.	1117.	1053.	989.	925.	26.45
180000.	8.040E+08	1.312E-05	1370.	1288.	1206.	1124.	1042.	960.	26.15
190000.	8.640E+08	1.238E-05	1237.	1151.	1065.	980.	894.	808.	25.85
200000.	1.090E+09	1.051E-05	1236.	1135.	1036.	936.	835.	735.	25.56

17 SEPT 61 05032 EST WALLOPS ISLAND

Z	D	DPPP	TEMPERATURES						M.WT.
170000.	1.655E+05	1.612E-05	1211.	1102.	992.	882.	773.	663.	26.45
100000.	2.510E+06	6.684E-04	355.	352.	350.	347.	344.	342.	28.88
104000.	3.920E+06	4.950E-04	375.	371.	368.	364.	361.	357.	28.78
107000.	3.220E+06	5.628E-04	267.	264.	261.	258.	255.	251.	28.68
112000.	6.860E+06	3.378E-04	298.	293.	287.	282.	277.	272.	28.47
116000.	1.510E+07	1.984E-04	388.	379.	370.	362.	353.	344.	28.27
120000.	3.420E+07	1.143E-04	552.	537.	522.	507.	492.	477.	28.07
130000.	9.100E+07	5.867E-05	749.	721.	692.	664.	635.	606.	27.58
140000.	1.690E+08	3.838E-05	871.	828.	785.	741.	698.	655.	27.20
150000.	2.800E+08	2.717E-05	974.	914.	853.	793.	732.	672.	26.92
160000.	4.490E+08	1.967E-05	1094.	1012.	929.	847.	764.	681.	26.66
170000.	5.990E+08	1.612E-05	1105.	1006.	905.	805.	705.	606.	26.45

1 MARCH 62 1823 EST WALLOPS ISLAND

Z	D	DPPP	TEMPERATURES						M.WT.
130000.	1.273E+05	7.029E-05	707.	634.	560.	487.	413.	340.	27.58
106000.	3.420E+06	5.412E-04	298.	288.	279.	269.	260.	250.	28.72
110000.	6.860E+06	3.387E-04	361.	346.	331.	316.	301.	286.	28.56
115000.	1.260E+07	2.242E-04	406.	383.	361.	338.	315.	293.	28.32
120000.	2.290E+07	1.494E-04	471.	437.	403.	370.	336.	303.	28.07
125000.	4.190E+07	9.910E-05	571.	521.	471.	421.	371.	321.	27.81
130000.	6.940E+07	7.029E-05	673.	603.	533.	463.	393.	323.	27.58

2 MARCH 62 05.54 EST WALLOPS ISLAND

Z	D	DPPP	TEMPERATURES						M.WT.
125000.	1.225E+05	1.191E-04	565.	512.	460.	408.	356.	304.	27.81
104000.	1.040E+06	1.199E-03	193.	188.	183.	178.	173.	167.	28.78
106000.	2.360E+06	6.931E-04	274.	265.	256.	248.	239.	230.	28.72
108000.	3.960E+06	4.897E-04	335.	322.	310.	297.	285.	272.	28.64
110000.	6.510E+06	3.507E-04	414.	397.	379.	362.	344.	327.	28.56
112000.	6.170E+06	3.625E-04	357.	340.	323.	306.	290.	273.	28.47
115000.	9.180E+06	2.769E-04	390.	368.	347.	325.	303.	281.	28.32
125000.	3.180E+07	1.191E-04	542.	492.	442.	392.	342.	292.	27.81

23 MARCH 62 18.44 EST WALLOPS ISLAND

Z	D	DPPP	TEMPERATURES						M.WT.
132000.	1.293E+05	9.860E-05	674.	600.	526.	452.	379.	305.	27.49
106000.	5.860E+06	3.780E-04	472.	453.	434.	415.	396.	377.	28.72
114000.	1.050E+07	2.535E-04	480.	452.	424.	396.	368.	340.	28.37
120000.	2.080E+07	1.593E-04	591.	547.	503.	459.	414.	370.	28.07
122000.	2.950E+07	1.258E-04	698.	642.	587.	531.	475.	419.	27.97
132000.	4.160E+07	9.860E-05	639.	569.	499.	429.	359.	289.	27.49

27 MARCH 62 18.48 EST WALLOPS ISLAND

Z	D	DPPP	TEMPERATURES						M.WT.
119000.	1.168E+05	2.160E-04	453.	402.	350.	299.	247.	196.	28.12
105000.	2.980E+06	5.938E-04	368.	350.	331.	313.	294.	275.	28.75
107000.	3.830E+06	5.013E-04	388.	366.	344.	322.	300.	278.	28.68
110000.	3.980E+06	4.869E-04	331.	309.	286.	264.	241.	219.	28.56
113000.	6.220E+06	3.600E-04	370.	340.	309.	279.	249.	219.	28.42
119000.	1.320E+07	2.160E-04	440.	390.	340.	290.	240.	190.	28.12

30 NOV 62 06.15 EST WALLOPS ISLAND

Z	D	DPPP	TEMPERATURES						M.WT.
160000.	1.560E+05	1.643E-05	1111.	1002.	893.	784.	676.	567.	26.66
106000.	2.700E+06	6.336E-04	247.	245.	242.	239.	236.	233.	28.72
110000.	5.220E+06	4.063E-04	273.	268.	264.	260.	255.	251.	28.56
114000.	7.810E+06	3.088E-04	257.	251.	245.	240.	234.	228.	28.37
120000.	4.710E+07	9.239E-05	573.	554.	535.	517.	498.	479.	28.07
130000.	1.090E+08	5.202E-05	711.	678.	645.	612.	580.	547.	27.58
140000.	2.080E+08	3.342E-05	829.	779.	728.	678.	628.	578.	27.20
150000.	2.850E+08	2.685E-05	794.	732.	670.	608.	547.	485.	26.92
160000.	5.880E+08	1.643E-05	1022.	922.	822.	722.	622.	521.	26.66

21 FEB 63 18.16 EST WALLOPS ISLAND

Z	D	DPPP	TEMPERATURES						M.WT.
140000.	1.369E+05	3.407E-05	867.	760.	654.	547.	441.	334.	27.20
110000.	8.640E+06	2.904E-04	377.	365.	353.	340.	328.	316.	28.56
115000.	1.320E+07	2.173E-04	374.	358.	342.	325.	309.	293.	28.32
130000.	1.080E+08	5.234E-05	709.	643.	577.	511.	445.	378.	27.58
140000.	2.020E+08	3.407E-05	814.	714.	614.	514.	414.	314.	27.20

23 MAY 63 19.45 EST WALLOPS ISLAND

Z	D	DPPP	TEMPERATURES						M.WT.
175000.	1.703E+05	1.397E-05	1246.	1135.	1025.	915.	805.	694.	26.30
111000.	5.550E+06	3.895E-04	311.	307.	304.	300.	296.	292.	28.51
115000.	1.130E+07	2.411E-04	387.	381.	375.	369.	362.	356.	28.32
120000.	2.360E+07	1.464E-04	492.	482.	471.	461.	451.	441.	28.07
125000.	4.240E+07	9.831E-05	595.	580.	565.	550.	535.	520.	27.81
150000.	3.400E+08	2.387E-05	1076.	1016.	956.	896.	836.	776.	26.92
175000.	7.370E+08	1.397E-05	1131.	1030.	930.	831.	730.	630.	26.30

22 MAY 63 04.10 GMT CHURCHILL

Z	D	DPPP	TEMPERATURES						M.WT
124000.	1.216E+05	1.490E-04	544.	492.	440.	388.	336.	284.	27.86
106000.	3.690E+06	6.777E-04	280.	269.	258.	246.	235.	224.	28.72
110000.	9.900E+06	3.491E-04	413.	392.	370.	348.	326.	304.	28.56
117000.	2.720E+07	1.760E-04	587.	544.	501.	458.	416.	373.	28.22
124000.	3.430E+07	1.490E-04	523.	473.	423.	373.	323.	273.	27.86

22 MAY 63 07.51 GMT CHURCHILL

Z	D	DPPP	TEMPERATURES						M.WT
124000.	1.216E+05	1.381E-04	544.	492.	440.	388.	336.	284.	27.86
108000.	5.860E+06	4.965E-04	352.	338.	323.	309.	295.	280.	28.64
112000.	8.710E+06	3.791E-04	358.	340.	321.	302.	284.	265.	28.47
116000.	1.330E+07	2.840E-04	375.	350.	325.	301.	276.	251.	28.27
118000.	2.060E+07	2.114E-04	452.	419.	386.	352.	319.	286.	28.17
124000.	3.840E+07	1.381E-04	523.	473.	423.	373.	323.	273.	27.86

23 MAY 63 04.13 GMT CHURCHILL

Z	D	DPPP	TEMPERATURES						M.WT.
136000.	1.331E+05	6.689E-05	733.	680.	627.	574.	521.	468.	27.33
112000.	1.270E+07	2.948E-04	414.	402.	391.	379.	367.	355.	28.47
114000.	1.570E+07	2.551E-04	431.	417.	403.	390.	376.	363.	28.37
120000.	2.810E+07	1.713E-04	476.	456.	436.	415.	395.	375.	28.07
127000.	7.550E+07	8.764E-05	702.	663.	624.	586.	547.	508.	27.72
136000.	1.110E+08	6.689E-05	692.	642.	592.	542.	492.	441.	27.33

REFERENCES

1. Bedinger, J. F., H. Knaflich and G. Best, "Experimental Study on the Dynamics and Structure of the Upper Atmosphere," GCA Technical Report 64-10-N, (June 1964).

2. Minzner, R. A. and W. S. Ripley, "The ARDC Model Atmosphere 1956," AFCRC TN-56-204, Air Force Surveys in Geophysics, No. 86, (Dec. 1956).

3. Minzner, R. A., K. S. W. Champion and H. L. Pond, "The ARDC Model Atmosphere 1959," U. S. Air Force Surveys in Geophysics, No. 115, AFCRC-TR-59-267, (August 1959).

4. United States Standard Atmosphere, National Aeronautics and Space Administration, U. S. Air Force and U. S. Weather Bureau, Government Printing Office, Washington, D. C. (1962).

5. Nicolet, M., "Dynamic Effects in the High Atmosphere," Equation 29, page 656 of The Earth as a Planet, Edited by G. P. Kuiper, University of Chicago Press, Chicago, Illinois, (1954).

6. Chapman, S. and T. G. Cowling, "The Mathematical Theory of Non-Uniform Gases," p. 250, Second Edition, Cambridge University Press, (1960).

7. Minzner, R. A., G. O. Sauermann and G. A. Faucher, "Low Mesopause Temperatures over Eglin Test Range Deduced from Density Data," J. Geophys. Res., 70, 743-745, (1965).

PROPOSED TRANSITION MODEL ATMOSPHERES AND PROBLEMS ASSOCIATED WITH THEIR GENERATION

Introduction

At a recent meeting of the Committee for the Extension of the Standard Atmosphere (COESA) (January 20-23, 1965), the Jacchia-type models [1] were adopted as a basis for that portion of the proposed publication U. S. Standard Atmosphere Supplements 1965 describing the atmosphere above 120 kilometers altitude. At a previous meeting of COESA, the Cole-Kantor models [2] had been adopted for the region below 90 kilometers altitude. A working group of which the writer is a member was directed to select a set of transition atmospheres to rigorously connect the Cole-Kantor models to the Jacchia models. The accompanying graphs and tables represent one possible set of such transition models.

This set is a kind of minimum-confusion set in that each transition model is characterized by a mesopause isothermal region, connecting directly or indirectly to the related Cole-Kantor Model, and by a single positive value of temperature gradient between this isothermal region and the base of the Jacchia models. In some instances minor adjustments were made to the Cole-Kantor models in the region of negative temperature gradient directly below the mesopause isothermal layer.

Presentation of the Models

The solid-line profiles of Figure 1 represent the defining temperature-altitude relationships of the proposed transition models A through G (including the adjustments to the Cole-Kantor models) for mean January and July conditions, for each of the latitudes 30°N, 45°N, and 60°N, as well as for the annual average conditions at 15°N. The dashed-line extensions represent the corresponding Cole-Kantor models to which the transition atmospheres must connect at about 89 km′ or at some lower altitude in the case of models F and G.

The solid-line profiles of Figure 2, models H and I, represent the transition models related to the Cole-Kantor models for 60°N cold and 60°N warm, which are similarly shown as dashed lines both above and below the lowest altitude of the solid-line profiles.

Complete tables of kinetic temperature T, molecular scale temperature T_M, molecular weight M, density ρ, geometric pressure scale height H, and geopotential pressure scale height H′, as a function of both geometric altitude Z and geopotential altitude h, are given for each transition model in the section Tables of the Transition Models. Percent departure of the density of these models from that of the U. S. Standard Atmosphere as a function of geopotential altitude is given in Figure 3.

The altitude values of the base of the mesopause isothermal layers of each model are integral multiples of one geopotential kilometer (km′). The

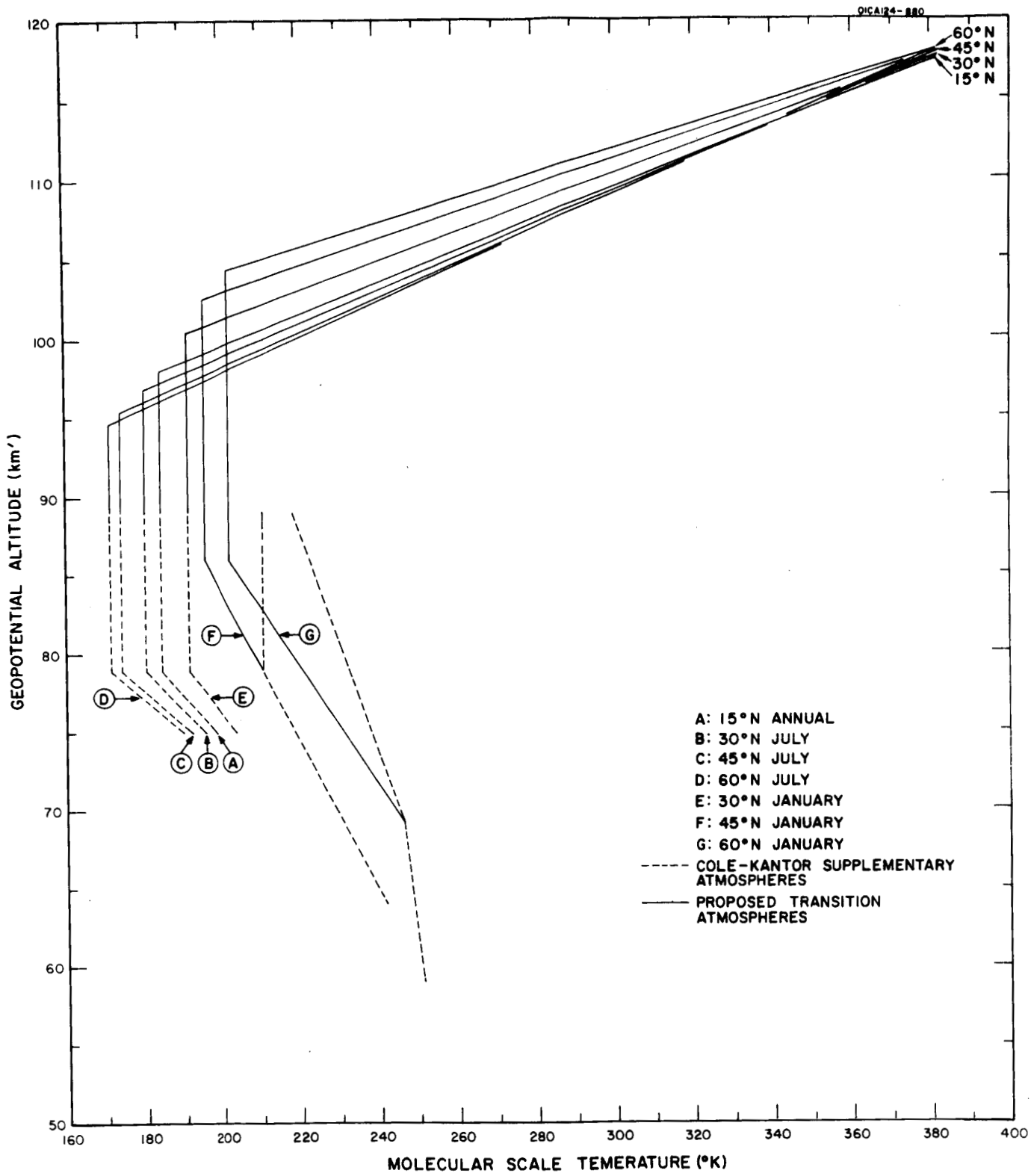

Figure 1. Defining temperature-altitude profiles for seven proposed transition models connecting supplementary atmospheres to thermosphere models.

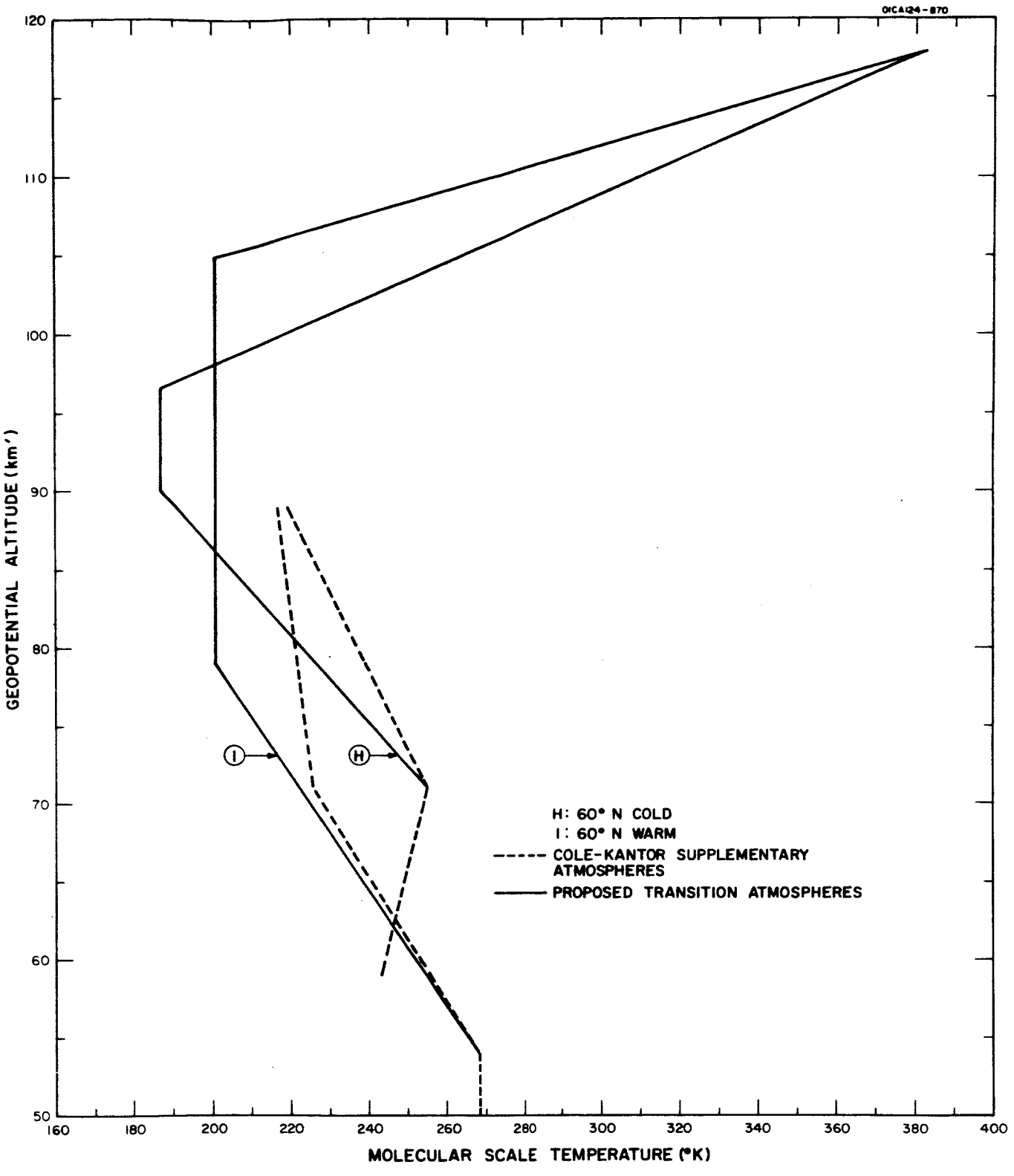

Figure 2. Defining temperature-altitude profiles for two proposed transition models connecting supplementary atmospheres to thermosphere models.

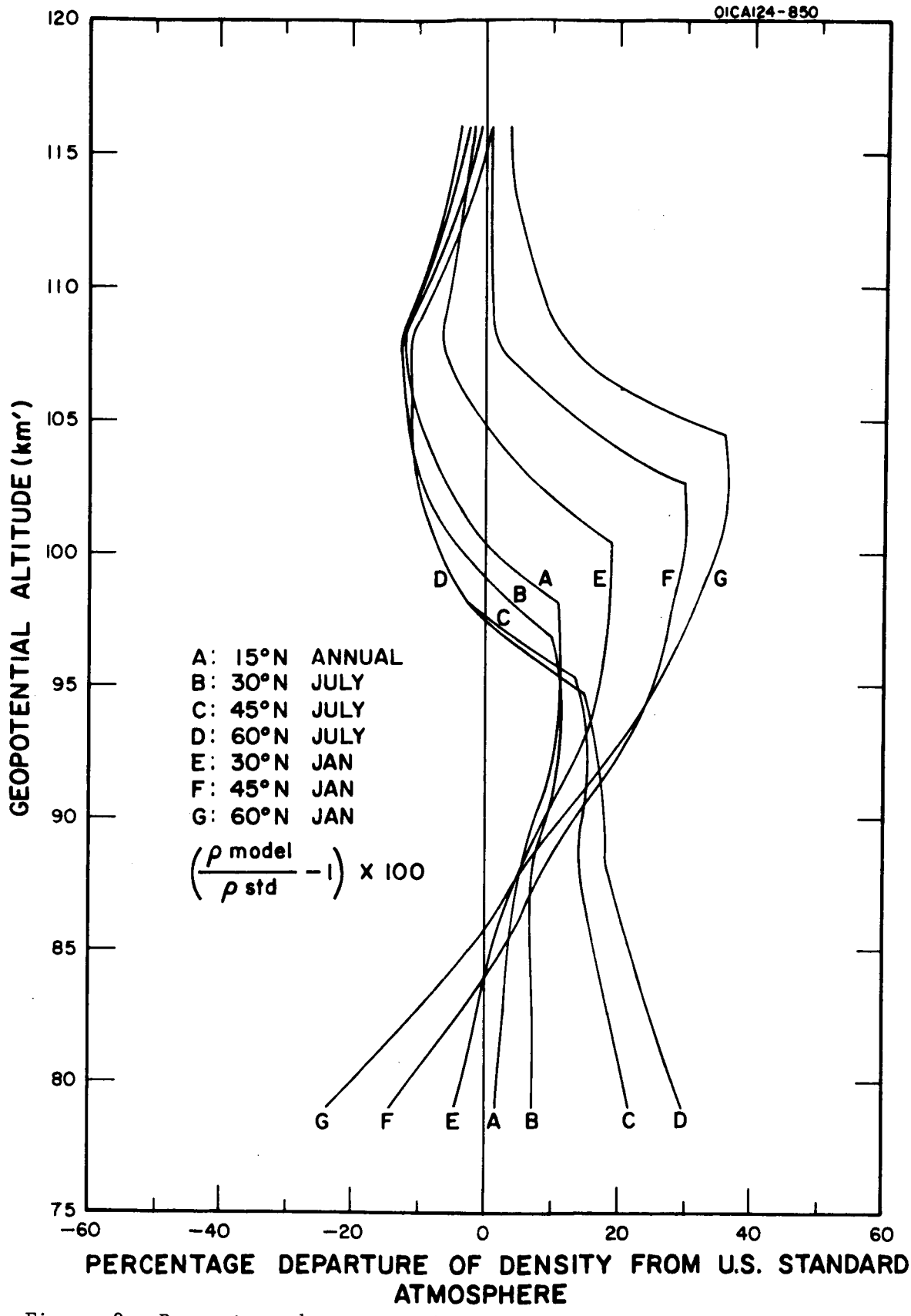

Figure 3. Percentage departure of the density of various models from that of the U. S. Standard Atmosphere versus geopotential altitude.

altitude of the breakpoint at the top of this isothermal layer for each model is a seven-significant-figure number resulting from the solution of Equation (11), and is the only altitude at which the breakpoint may occur for the particular set of adopted boundary conditions. This altitude designated by x is given in the heading of the tabulation of each model along with the value of the positive gradient of temperature above x. The value and altitude range of any negative gradient given in the heading represent an adjustment in the altitude range of the existing gradient or in the size of the gradient from that of the Cole-Kantor models. In addition, the positive temperature gradient from x to the base of the Jacchia models expressed in terms of the corresponding gradient of geopotential pressure scale height with respect to h is also listed in the heading.

Compatible System for Defining Gradients of Temperature with Respect to Altitude

The Cole-Kantor models are defined as linear functions of temperature with respect to geopotential altitude h, after the manner of the U. S. Standard Atmosphere, 1962 [3]. Since these supplementary atmospheres are limited to altitudes below 90 km, where molecular weight is constant, and consequently where the temperatures T_M and T are identical, the Cole-Kantor temperatures may be taken to be either T_M or T. For this study T_M was used so that existing gradients of T_M with respect to h in the Cole-Kantor models could be extended as required above 90 km without first defining molecular weight as a unique function of altitude.

The Jacchia models are tabulated in terms of kinetic temperature and geometric altitude, but since molecular weight is simultaneously tabulated, with a value of 26.90 at 120 km, the molecular scale temperature is implied. When the base level of these models (Z_a = 120 km) is suitably transformed to geopotential h_a, it becomes possible to specify gradients of T_M with respect to h which terminate identically at the base of the Jacchia models. The further assumption of some reasonable altitude-dependent function of M such as a linear decrease of molecular weight between 90 geometric kilometers and Z_a the base of the Jacchia models, after the manner of

$$M(Z) = M_o + \left(\frac{29.60 - M_o}{Z_a - 90}\right)(Z - 90) , \qquad (1)$$

permits one to transform the transition-model values of T_M to values of T as a function of geometric altitude after all other calculations have been made. Thus, values of kinetic temperature may be made continuously available from the top of Jacchia's models down to sea level.

The Cole-Kantor models, defined in terms of geopotential, are specified for four latitudes 15°N, 30°N, 45°N, and 60°N. For each latitude a different relationship exists between geopotential and geometric altitude, in accordance with the latitude variation of the effective earth's radius $r\Phi$ and the sea-level

value of the acceleration of gravity $g\phi$. Consequently, for any particular value of Z, there is a different value of h for each latitude in accordance with the relationship

$$h = \left(\frac{r\phi Z}{r\phi + Z}\right) \frac{(g\phi)_o}{9.80665} \cdot \qquad (2)$$

Here values of $r\phi$ and $g\phi$ are the effective earth radius and the sea-level values of the acceleration of gravity for various latitudes as given by Smithsonian Meteorological Tables [4]. These are reproduced in Table 1 for the four specified latitudes along with the corresponding values of h for Z = 120 km.

Table 1

Values of Effective Earth's Radius, Sea-Level Value of Acceleration of Gravity, and Geopotential for Z = 120 km as a Function of Latitude

Latitude	$r\phi$ (km)	$(g\phi)_o$	h for Z = 120 km
15°N	6,337.838	9.78381	117.49586
30°N	6,345.653	9.79324	117.61179
45°N	6,356.360	9.80665	117.77652
60°N	6,367.103	9.81911	117.92986

The Jacchia models, defined in terms of a single value of T, M, and ρ at Z = 120 km, indicate no specified latitude dependence for the 120 km level and consequently imply no specific relationship* between Z and h at that level.

Since these Jacchia models must be merged rigorously into each of the Cole-Kantor models, a different Z-to-h transformation must be applied for each latitude in question. Thus, the single geometric-altitude, no-latitude point representing the base of the Jacchia models assumes four different values of geopotential in accordance with the four different latitudes as indicated by the values in Table 1 and by the four termination points at the upper end of the temperature-altitude profiles shown in Figure 1.

When either T or T_M of the transition models are plotted as a function of Z, the line segments are not straight except in the isothermal regions

*See Section entitled "Implication of Gravity Variation with Latitude" for discussion of inconsistencies in applying the Jacchia models to latitudes other than 45°.

below 90 km, but they all merge into a common point at Z = 120 km as in Figure 4, where the temperature-altitude profiles of Models A, D, and G previously shown in Figure 1 are replotted in terms of T and Z.

Compatible Boundary-Condition Values

Each of the transition models comprises an internally consistent set of values of h, ρ, and T_M (or pressure scale height H' which is directly proportional to T_M) which values satisfy the equation of state, the hydrostatic equation, and a set of boundary conditions. The boundary conditions consist of a set of values of h, ρ, and T_M for the upper end of the transition models, and a similar set for the lower end of the transition models. The upper-end values designated by h_a, ρ_a, and $(T_M)_a$ are the corresponding values of the Jacchia models. The lower-end values designated by h_b, ρ_b, and $(T_M)_b$ are the corresponding values of the Cole-Kantor models or are derived directly from the Cole-Kantor models.

The Jacchia-model values of T and M at Z = 120 km are $T_{120} = 355^{o}K$ and $M_{120} = 26.90$. These imply a value $(T_M)_{120} = (T_M)_a = 382.24393^{o}K$, as the related boundary-layer value of T_M by means of the relationship

$$T_M = \frac{T}{M} \cdot M_o \ , \tag{3}$$

where $M_o = 28.9644$ when carried to six significant figures from the data in Table I.2.7 of the U. S. Standard Atmosphere, 1962.

The corresponding value of geopotential pressure scale height, and consequently an alternative boundary-condition value, is seen to be $H'_a = 11.18876$ km′, according to the relationship

$$H' \equiv \frac{R \cdot T}{G \cdot M} = \frac{R \cdot T_M}{G \cdot M_o} \ , \tag{4}$$

where $G \cdot M_o/R$ is taken to be exactly $34.1632\ ^{o}K/km'$.

The quantity geopotential pressure scale height is introduced as a boundary-condition value for reasons of simplicity of notation in a subsequent equation, so that the explicit presence of three constants in the form of $R/G \cdot M_o$ can be eliminated. It is emphasized that the geopotential pressure scale height must be employed in contrast to geometric pressure scale height H since the latter, defined as

$$H \equiv \frac{R \cdot T}{g\phi \cdot M} = \frac{R \cdot T_M}{g\phi \cdot M_o} \ , \tag{5}$$

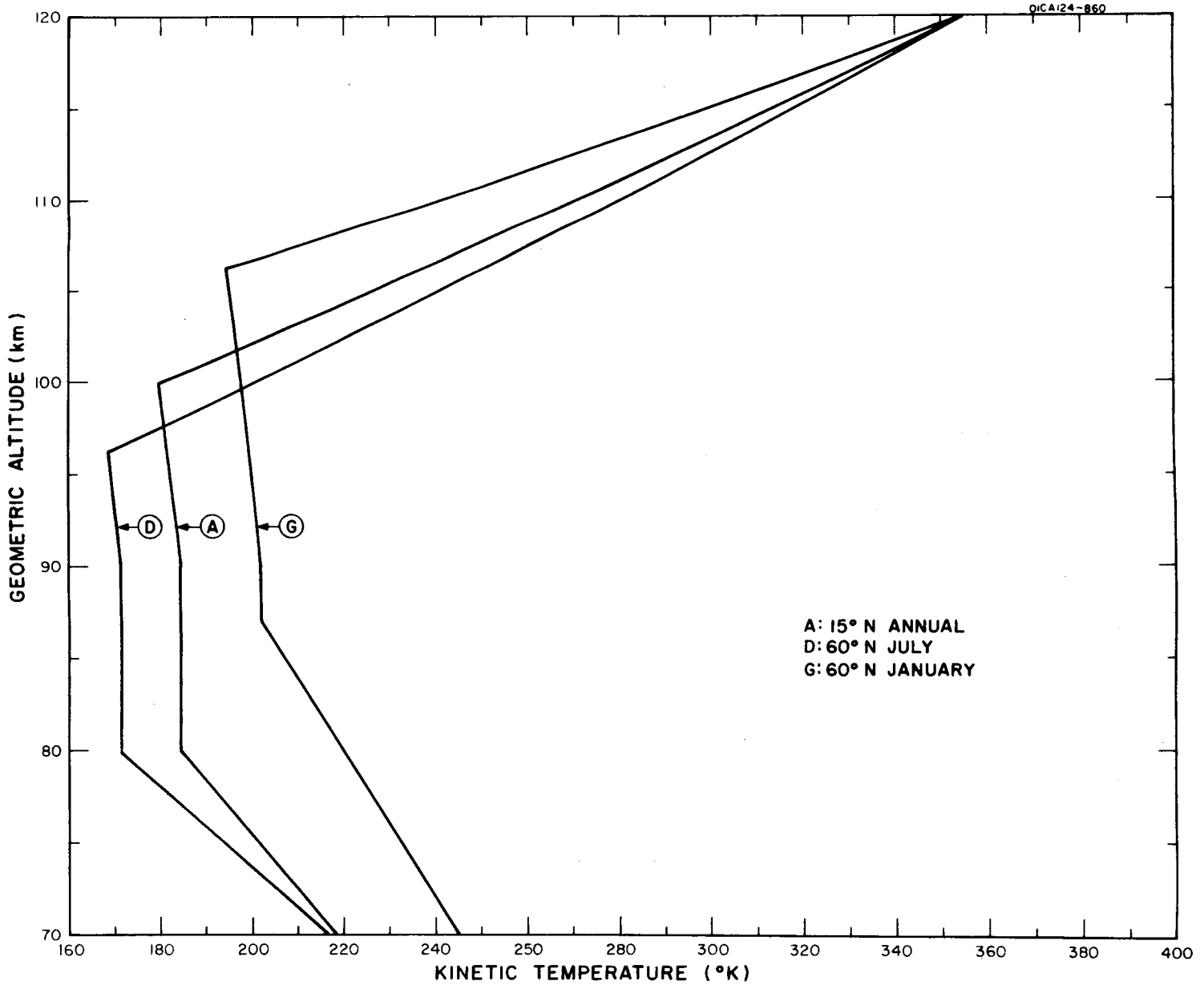

Figure 4. Defining temperature-altitude profiles for proposed transition models expressed in an alternate system of units.

involves the variable $g\phi$, and hence, T_M and H are not directly proportional. The value of $g\phi$ is given by

$$g\phi = (g\phi)_o \left(\frac{r\phi}{r\phi + Z}\right) \tag{6}$$

where values of $r\phi$ and $(g\phi)_o$ are given in Table 1 according to the latitude.

Thus, the upper-level boundary conditions for the transition model consist of the following: the above listed value of H'_a or of $(T_M)_a$, the Jacchia value of density at 120 km (geometric), i.e., $\rho_a = .24610 \times 10^{-4}$ grams per cubic meter (in accordance with the units of the Cole-Kantor atmospheres), and the four values of h of Table 1, each being the equivalent of Z = 120 km at a specified latitude. These values are summarized in relation to the applicable latitudes in Table 2.

The lower-level boundary conditions designated by subscript b stem directly from self-consistent sets of values of T_M (and hence H'), ρ and h at some altitude in each of the Cole-Kantor models. For five of the transition models which connect identically to the upper end of the corresponding five Cole-Kantor models, the lower-level boundary conditions assumed are those existing at the 79 km' level (i.e., at the base of the mesopause isothermal layer) of the appropriate Cole-Kantor models. (At the time of the initial calculations, it was not known whether the top of the isothermal layer in the transition atmospheres would be above or below the top of the Cole-Kantor models. Hence, calculations in all cases were made from the base of the isothermal layer rather than from the top.) The five models for which this situation prevails are

Model A	15°N Annual
Model B	30°N July
Model C	45°N July
Model D	60°N July
Model E	30°N January

The boundary-condition values H'_b or $(T_M)_b$, ρ_b, and h_b for the base of the mesopause isothermal layer for each of these transition models as well as those of the remaining transition models F through I are given in Table 2.

Transition Model Theory

In general it is not possible to take an arbitrary density-temperature-altitude point and rigorously connect it to an existing model at some other altitude without including an isothermal layer of unspecified thickness somewhere within the transition region. The possibility of joining the Jacchia models to the Cole-Kantor models exists by virtue of the presence of the mesopause isothermal layer in the transition region.

TABLE 2

Boundary-Condition Values which were used in Deducing the Value of x and the Positive Temperature-Altitude Gradient for Each of the Transition Models A through I

		h_{bb} km′	ρ_{bb} g/m^3	$(T_M)_{bb}$ ^oK	L_{bb} ^oK/km′	h_b km′	ρ_b	$(T_M)_b$ ^oK	H'_b km′	h_a km′	ρ_a g/m^3	$(T_M)_a$ ^oK	H'_a km′
A	15°N Annual					79	$.20265 \times 10^{-1}$	184.15	5.3903031	117.4958	$.24610 \times 10^{-4}$	382.244	11.18876
B	30°N July					79	$.21523 \times 10^{-1}$	180.15	5.2732180	117.6118	$.24610 \times 10^{-4}$	382.244	11.18876
C	45°N July					79	$.24315 \times 10^{-1}$	174.15	5.0975904	117.7765	$.24610 \times 10^{-4}$	382.244	11.18876
D	60°N July					79	$.25997 \times 10^{-1}$	171.15	5.0097767	117.9299	$.24610 \times 10^{-4}$	382.244	11.18876
E	30°N Jan.					79	$.19096 \times 10^{-1}$	191.15	5.5952019	117.6118	$.24610 \times 10^{-4}$	382.244	11.18876
F	45°N Jan.	64	.14361	241.65	-2.1	86	$.562606 \times 10^{-2}$	195.45	5.7210682	117.7765	$.24610 \times 10^{-4}$	382.244	11.18876
F′	45°N Jan. alt.	52	.65845	265.65	-2.1	85	$.651826 \times 10^{-2}$	196.35	5.7474122	117.7765	$.24610 \times 10^{-4}$	382.244	11.18876
G	60°N Jan.	69	$.59480 \times 10^{-1}$	246.15	-2.6	86	$.53815 \times 10^{-2}$	201.95	5.9113313	117.9299	$.24610 \times 10^{-4}$	382.244	11.18876
H	60°N Cold	71	$.34111 \times 10^{-1}$	255.15	-3.6	90	$.24111 \times 10^{-2}$	186.75	5.4664082	117.9299	$.24610 \times 10^{-4}$	382.244	11.18876
I	60°N Warm	54	.54953	268.15	-2.7	79	$.18725 \times 10^{-1}$	200.65	5.8732787	117.9299	$.24610 \times 10^{-4}$	382.244	11.18876

The problem therefore is to extend the mesopause isothermal layer upward to some geopotential altitude x where the density will be ρ_x such that a single linear segment of T_M versus h with gradient $L_M = (T_M)_a - (T_M)_b / h_a - x$ will cause the density to decrease exactly from ρ_x to ρ_a, within the altitude interval $h_a - x$. The decrease of density from ρ_b to ρ_x as altitude increases from h_b to x within an isothermal layer is given by

$$\rho_x = \rho_b \exp\left\{-\frac{G \cdot M_o \cdot (x - h_b)}{R \cdot (T_M)_b}\right\} = \rho_b \exp\left\{-\frac{(x - h_b)}{H'_b}\right\} \qquad (7)$$

For an altitude region within which dT_M/dh or dH/dh is constant, the increase in density from ρ_a to ρ_x as altitude decreases from h_a to x is given by

$$\rho_x = \rho_a\left[\frac{(T_M)_a}{(T_M)_b}\right]^{1 + \frac{G \cdot M_o}{R}\left[\frac{h_a - x}{(T_M)_a - (T_M)_b}\right]} = \rho_a\left[\frac{H'_a}{H'_b}\right]^{1 + \left(\frac{h_a - x}{H'_a - H'_b}\right)} . \qquad (8)$$

Equation (8) implies the following linear relationship of T_M versus h for altitudes between x and h_a:

$$T_M = (T_M)_b + L_b(h - x) , \qquad (9)$$

where

$$L_b = \frac{dT_M}{dh} = \frac{(T_M)_a - (T_M)_b}{h_a - x} . \qquad (10)$$

Since ρ_x must be the same from both Equations (7) and (8) in order that the density and temperature profiles both may be continuous, we equate the corresponding sections of each of these expressions (the scale height version is used here) to obtain an equation in which x is the only unknown:

$$\rho_b \exp\left\{-\frac{x - h_b}{H'_b}\right\} = \rho_a\left[\frac{H'_a}{H'_b}\right]^{1 + \left(\frac{h_a - x}{H'_a - H'_b}\right)} \qquad (11)$$

The solution of Equation (11) for x yields the value of the only possible interface level between an isothermal layer with base-level values h_b, $(T_M)_b$ and ρ_b and a single positive-gradient layer with upper-level values h_a, $(T_M)_a$, and ρ_a. Equation (11) is solved by numerical methods with an IBM 1620 Digital Computer and a program which, involving Equations (1) through (10) simultaneously determines the various atmospheric properties of the model. These considerations completely determine the transition models A through E.

Modifications to Some of the Cole-Kantor Models

Transition Models A through E extend continuously from the top of the Cole-Kantor models without modifying these in the slightest. Each of the remaining transition models involves some modification of the upper end of the corresponding Cole-Kantor model. In the development of Model F for 45°N January, the isothermal layer of the Cole-Kantor model from 79 km′ to 89 km′ at 210.15°K was eliminated, and the negative gradient of -2.1°/km′ of the next-lower layer was extended from 79 to 86 where a new isothermal layer at 195.45°K is begun. If the transition model were to be built upon the original isothermal layer, it would have to extend upward about 30 km′ to 109.49597 km′ where a gradient of about 20.78°/km′ would begin.

The proposed modification of the Cole-Kantor model reduces the required thickness of the isothermal layer to about 16 km′ and reduces the succeeding positive gradient to about 12°/km′. With this modification, the values of ρ_b and $(T_M)_b$ for h_b = 86 km′ are not available from an existing table and it is necessary to generate these values from the data applicable to some lower altitude of the Cole-Kantor models. In the case at hand, the base of the altitude region for which the gradient is -2.1°/km, i.e., 64 km′ becomes h_{bb} the reference level. The quantities ρ_{bb} and $(T_M)_{bb}$, as well as the value of ρ and of T_M at level h_{bb}, become secondary boundary conditions for an initial calculation from which the primary boundary conditions are obtained. Thus ρ_b and $(T_M)_b$ for h_b = 86 km′ are determined by the expressions

$$\rho_b = \rho_{bb}\left[\frac{(T_M)_b}{(T_M)_{bb}}\right]^{1 + \frac{G \cdot M}{R \cdot L_{bb}}} , \tag{12}$$

and

$$(T_M)_b = (T_M)_{bb} + L_{bb}(h_b - h_{bb}) , \tag{13}$$

where L_{bb} is the existing (or the adjusted) gradient in the layer immediately below the mesopause isothermal layer, which gradient for the case in question has a value of -2.1°/km′.

The related values of ρ_{bb}, $(T_M)_{bb}$, h_{bb}, and L_{bb} for Model F are presented in the left-hand section of Table 2 while the derived related values of ρ_b, $(T_M)_b$, H_b', and h_b are given in the mid-portion of that table along with values ρ_a, $(T_M)_a$, H_a', and h_a, in the right-hand section. The application of Equation (11) determines the value of x which leads to profile F shown in Figure 1. The departure of Model F from the original Cole-Kantor model is shown by a comparison of solid and dashed lines.

The Cole-Kantor model for 60°N January has no mesopause isothermal layer but rather terminates at 88.858 km′ with a T_M value of 218.3488°K above a region defined by a gradient of -1.4°/km′ which extends upward from 69 km′. If this gradient is extended to exactly 89 km′ where the temperature would be

218.15°K, and an isothermal layer at this temperature is established for the transition atmosphere, the boundary conditions require that the isothermal layer be extended for about 26 km′ to 114.73827 km′ where an unrealistically large gradient of 51.4138°K/km′ up to 117.929 km′ would follow. Numerous trials finally resulted in the choice of a new gradient of -2.6°K/km′ from 69 km′ to 86 km′ where an isothermal at 201.95° is begun. Equations (12), (13) and (4) applied to tabulated values at 69 km′ in the Cole-Kantor model produced the necessary values of ρ_b, $(T_M)_b$, and H'_b for h_b = 86 km′ and L_{bb} = -2.6°/km′. These values then introduced into Equation (11) with the appropriate values of h_a, ρ_a, and H'_a, all listed in Table 2, determine an isothermal layer of about 18 km′ thickness from 86 km′ to 104.43142 km′, followed by a positive gradient of 13.35533°/km′. The resulting Model G and its departure from the Cole-Kantor model are shown in Figure 1.

Similar treatments have been applied to the 60°N cold and 60°N warm models resulting in transition models H and I respectively, as depicted in Figure 2. Model H for 60°N cold was adjusted so that its positive gradient is nearly identical to that of Model D for 60°N July, i.e., 9.09937°/km′ and 9.11176°/km′ respectively. Similarly, Model I was adjusted so that its positive gradient of 13.94325°/km′ is in close agreement with 13.35533°/km′ of Model G for 60°N January. The temperatures of the isothermals for Models I and G are also quite close 200.65 and 201.95° respectively. This agreement could possibly be improved by a slightly more negative gradient in Model I below 79 km, but the extra effort did not seem worthwhile.

Choice of Properties Tabulated in the Transition Models

The tabulated transition models are intended to match not only the boundary conditions of the Jacchia and the Cole-Kantor models but also ought to match the content of the two sets of adjoining models. Table 3 shows a comparative listing of the contents of each of the three models.

It is apparent that the existing format of the transition models does not quite meet the condition of including all the tabulations of both the Jacchia models and the Cole-Kantor models.

The transition models include T_M and H'. Either item can serve as the defining property of the transition models, although neither is explicitly included in the adjacent models. T_M is omitted from the Cole-Kantor models since these models are limited to altitudes below 90 km where $M = M_o$ and consequently where $T_M = T$; hence the specific inclusion of T_M in the Cole-Kantor models is unnecessary.

Values of H' are included in the transition model since these actually served to define the model through Equation (6), although Equation (6) could have been written in terms of T_M instead. In addition, values of H' are independent of latitude whereas values of H are latitude dependent in the fourth significant figure and, as noted in the next section which discusses gravity variation, Jacchia's values of H do imply a 45° latitude. It appears therefore that

TABLE 3

Comparison of the Tabulations of the Jacchia models, the Cole-Kantor models, and the Attached Proposed Transition Models as Regards the Parameters Calculated

	Jacchia	Transition	Cole-Kantor
Geometric Altitude	Z	Z	Z
Geopotential Altitude	-	h	h
Kinetic Temperature	T	T	T
Molecular Scale Temp.	-	T_M	(T_M)
Molecular Weight	M	M	-
Pressure	-	-	p
Density	ρ	ρ	ρ
Geometric Pressure Scale Height	H	H	-
Geopotential Pressure Scale Height	-	H'	-
Number Density O_2	$N(O_2)$	-	-
Number Density O	N(O)	-	-
Number Density N_2	$N(N_2)$	-	-
Number Density He	N(He)	-	-
Number Density H	N(H)	-	-

values of H′ for this and other reasons would be preferable to values of H in the supplementary-atmosphere tabulation of a Jacchia-type model, unless separate listings of values of H are to be given for each latitude.

Values of pressure are not included in the transition models, but a column could be added if the space between other columns were to be reduced, particularly if values of H were to be omitted.

Number densities of the various species are not included in the transition models primarily because their ratios at any given altitude do not change significantly below 120 km. In addition, they could not be added to the other properties in IBM 1620 program without a separate printout.

Implication of Gravity Variation with Latitude

Jacchia's values of geometric pressure scale height are calculated using a value of g determined on the basis of an inverse-square-law relationship in which the sea-level value is 9.80665 and the effective earth's radius is 6.35677×10^8 cm. Hence that parameter is in fact tied to a latitude of about 45° 32' as indicated by Minzner, et al. [5]. The decrease of ρ or number density of the various constituents with increasing altitude is also related to the value of gravity employed in the calculations and these properties too are tied to a model for only 45° 32' latitude. Thus, the assumption that the Jacchia model can in principle be tied to the Cole-Kantor models and can thus be applied to any latitude merely be properly transforming Z to the appropriate value of h is not rigorously correct except at the boundary layer, i.e., at Z = 120 km, when the value of H is ignored.

For any latitude other than 45°, the variation of g with Z is different from that assumed by Jacchia and values of density and number density, as determined by the specified temperature profiles should therefore differ increasingly from the tabulated Jacchia values as altitude increases from 120 km.

The use of the Jacchia models to deduce temperature from density observation, or vice-versa, at latitudes other than 45° latitude is consequently subject to some error. Similarly, supplementary atmospheres based on the Jacchia calculation above 120 km would involve similar small errors.

In the light of this discrepancy there appears to be three alternatives:

(1) Use the Jacchia approach unmodified and accept the errors in density at latitudes other than 45°.

(2) Recalculate the Jacchia tables three additional times each time with that g of Z function applicable to 15°, 30°, and 60° latitude. This would increase the bulk of that part of the tables four-fold.

(3) Redefine the Jacchia temperature functions in terms of geopotential, such as

$$T = T_\infty - (T_\infty - T_{h_a}) \exp[- S(h - h_a)]$$

and calculate a single set of densities, number densities and scale heights as a function of geopotential for each of the comparable 30 temperature profiles. The value of h_a could be fixed at h_a = 120 km' and again 30 pages of tables would result. There would then be four additional columns each listing the geometric altitude at one of the four latitudes desired, as a function of geopotential, the primary argument. In order to get tabulations in which the geometric altitudes for each latitude were to be listed for exactly those values now used by Jacchia, the total number of entries would have to be increased by four.

Of the three alternatives (2) and (3) would be equivalent in bulk through not exactly equivalent in concept or in values of density. The proposed transition models would apply in alternatives (1) and (2) but would have to be recalculated in the case of alternative (3).

TABULATIONS OF THE TRANSITION MODELS

MODEL A

PROPERTIES OF TRANSITION ATMOSPHERE
TROPICAL (15N) ANN TOO JACCHIA MODELS

15N ANN X = 98.04819 KM DEN X = .59161824E-03 G/M3
GEOPOT SCALE HT AT 117.4958 KM = 11.18876, AT X KM = 5.3903031
GRADIENT OF GEOP SCALE HT ABOVE X = .29815782E 00
GRADIENT OF MOL. TEMP. ZERO FOR H BTWN 79 AND X
GRADIENT OF MOL. TEMP. 10.18602 DEG/KM FOR H BTWN X AND 117.4958

ALTITUDE KM GEOMET	GEOPOT	TEMP DEG KELVIN MOL.	KINETIC	MOL WT	DENSITY G/M3	SCALE HT KM GEOMET	GEOPOT
80.186	79.000	184.15	184.15	28.96	.20265E-01	5.540	5.390
81.214	80.000	184.15	184.15	28.96	.16833E-01	5.542	5.390
82.000	80.764	184.15	184.15	28.96	.14608E-01	5.543	5.390
83.271	82.000	184.15	184.15	28.96	.11615E-01	5.545	5.390
84.000	82.708	184.15	184.15	28.96	.10185E-01	5.547	5.390
85.329	84.000	184.15	184.15	28.96	.80149E-02	5.549	5.390
86.000	84.651	184.15	184.15	28.96	.71030E-02	5.550	5.390
87.389	86.000	184.15	184.15	28.96	.55304E-02	5.552	5.390
88.000	86.592	184.15	184.15	28.96	.49545E-02	5.553	5.390
89.450	88.000	184.15	184.15	28.96	.38161E-02	5.556	5.390
90.000	88.533	184.15	184.15	28.96	.34567E-02	5.557	5.390
91.512	90.000	184.15	183.48	28.86	.26331E-02	5.560	5.390
92.000	90.472	184.15	183.27	28.82	.24122E-02	5.560	5.390
93.576	92.000	184.15	182.58	28.71	.18169E-02	5.563	5.390
94.000	92.410	184.15	182.39	28.68	.16837E-02	5.564	5.390
95.641	94.000	184.15	181.68	28.57	.12537E-02	5.567	5.390
96.000	94.347	184.15	181.52	28.55	.11754E-02	5.567	5.390
97.707	96.000	184.15	180.77	28.43	.86509E-03	5.570	5.390
98.000	96.282	184.15	180.64	28.41	.82085E-03	5.571	5.390
99.775	98.000	184.15	179.87	28.29	.59693E-03	5.574	5.390
99.825	98.048	184.15	179.85	28.28	.59161E-03	5.574	5.390
100.000	98.217	185.87	181.45	28.27	.56810E-03	5.626	5.440
101.844	100.000	204.03	198.28	28.14	.37860E-03	6.180	5.972
102.000	100.150	205.56	199.70	28.13	.36645E-03	6.226	6.017
103.914	102.000	224.40	216.98	28.00	.25016E-03	6.801	6.568
104.000	102.082	225.24	217.75	28.00	.24611E-03	6.827	6.593
105.986	104.000	244.77	235.47	27.86	.17136E-03	7.423	7.164
106.000	104.013	244.91	235.60	27.86	.17094E-03	7.428	7.168
108.000	105.943	264.56	253.25	27.72	.12214E-03	8.029	7.744
108.058	106.000	265.14	253.77	27.72	.12098E-03	8.046	7.761
110.000	107.871	284.21	270.70	27.58	.89424E-04	8.630	8.319
110.133	108.000	285.51	271.86	27.57	.87654E-04	8.670	8.357
112.000	109.798	303.84	287.96	27.45	.66859E-04	9.232	8.893
112.208	110.000	305.89	289.75	27.43	.64931E-04	9.295	8.953
114.000	111.724	323.46	305.01	27.31	.50915E-04	9.834	9.468
114.285	112.000	326.26	307.43	27.29	.49038E-04	9.920	9.550
116.000	113.649	343.06	321.87	27.17	.39407E-04	10.437	10.042
116.364	114.000	346.63	324.92	27.15	.37671E-04	10.547	10.146
118.000	115.573	362.66	338.53	27.03	.30941E-04	11.040	10.615
118.443	116.000	367.00	342.20	27.00	.29378E-04	11.174	10.742
120.000	117.495	382.24	355.00	26.90	.24610E-04	11.643	11.189

MODEL B

PROPERTIES OF TRANSITION ATMOSPHERE
SUBTROP (30N) JULY TOO JACCHIA MODELS

30N JULY X = 96.78893 KM DEN X = .73761983E-03 G/M3
GEOPOT SCALE HT AT 117.6118 KM = 11.18876, AT X KM = 5.2732180
GRADIENT OF GEOP SCALE HT ABOVE X = .28408870E 00
GRADIENT OF MOL. TEMP. ZERO FOR H BTWN 79 AND X
GRADIENT OF MOL. TEMP. 9.70537 DEG/KM FOR H BTWN X AND 117.6118

ALTITUDE KM GEOMET	GEOPOT	TEMP DEG KELVIN MOL.	KINETIC	MOL WT	DENSITY G/M3	SCALE HT KM GEOMET	GEOPOT
80.106	79.000	180.15	180.15	28.96	.21523E-01	5.415	5.273
81.133	80.000	180.15	180.15	28.96	.17805E-01	5.416	5.273
82.000	80.843	180.15	180.15	28.96	.15173E-01	5.418	5.273
83.188	82.000	180.15	180.15	28.96	.12185E-01	5.420	5.273
84.000	82.789	180.15	180.15	28.96	.10491E-01	5.421	5.273
85.244	84.000	180.15	180.15	28.96	.83389E-02	5.423	5.273
86.000	84.734	180.15	180.15	28.96	.72553E-02	5.425	5.273
87.302	86.000	180.15	180.15	28.96	.57068E-02	5.427	5.273
88.000	86.677	180.15	180.15	28.96	.50186E-02	5.428	5.273
89.361	88.000	180.15	180.15	28.96	.39054E-02	5.430	5.273
90.000	88.620	180.15	180.15	28.96	.34722E-02	5.431	5.273
91.421	90.000	180.15	179.54	28.87	.26727E-02	5.434	5.273
92.000	90.561	180.15	179.29	28.83	.24029E-02	5.435	5.273
93.483	92.000	180.15	178.66	28.72	.18291E-02	5.437	5.273
94.000	92.501	180.15	178.44	28.69	.16632E-02	5.438	5.273
95.546	94.000	180.15	177.78	28.58	.12517E-02	5.441	5.273
96.000	94.439	180.15	177.58	28.55	.11515E-02	5.441	5.273
97.610	96.000	180.15	176.89	28.44	.85665E-03	5.444	5.273
98.000	96.377	180.15	176.73	28.41	.79746E-03	5.445	5.273
98.424	96.788	180.15	176.54	28.38	.73762E-03	5.446	5.273
99.675	98.000	191.90	187.49	28.30	.55431E-03	5.803	5.617
100.000	98.313	194.95	190.32	28.28	.51622E-03	5.896	5.706
101.742	100.000	211.31	205.42	28.16	.35860E-03	6.394	6.185
102.000	100.249	213.73	207.64	28.14	.34063E-03	6.468	6.256
103.810	102.000	230.73	223.15	28.01	.24104E-03	6.986	6.754
104.000	102.183	232.50	224.77	28.00	.23283E-03	7.040	6.806
105.880	104.000	250.14	240.70	27.87	.16731E-03	7.579	7.322
106.000	104.115	251.26	241.71	27.86	.16395E-03	7.613	7.355
107.950	106.000	269.55	258.05	27.73	.11935E-03	8.172	7.890
108.000	106.047	270.01	258.46	27.73	.11843E-03	8.186	7.903
110.000	107.977	288.74	275.02	27.59	.87455E-04	8.759	8.452
110.022	108.000	288.96	275.21	27.59	.87161E-04	8.766	8.458
112.000	109.906	307.47	291.40	27.45	.65834E-04	9.333	9.000
112.096	110.000	308.37	292.18	27.44	.64967E-04	9.361	9.026
114.000	111.834	326.18	307.58	27.31	.50405E-04	9.907	9.548
114.171	112.000	327.78	308.96	27.30	.49302E-04	9.956	9.595
116.000	113.761	344.88	323.57	27.18	.39178E-04	10.482	10.095
116.247	114.000	347.19	325.54	27.16	.38012E-04	10.553	10.163
118.000	115.687	363.57	339.38	27.04	.30863E-04	11.057	10.642
118.324	116.000	366.60	341.93	27.02	.29726E-04	11.150	10.731
120.000	117.611	382.24	355.00	26.90	.24610E-04	11.632	11.189

MODEL C

PROPERTIES OF TRANSITION ATMOSPHERE
MIDLAT (45N) JULY TOO JACCHIA MODELS

45N JULY X = 95.46527 KM DEN X = .96182984E-03 G/M3
GEOPOT SCALE HT AT 117.7765 KM = 11.18876, AT X KM = 5.0975904
GRADIENT OF GEOP SCALE HT ABOVE X = .27300915E 00
GRADIENT OF MOL. TEMP. ZERO FOR H BTWN 79 AND X
GRADIENT OF MOL. TEMP. 9.32686 DEG/KM FOR H BTWN X AND 117.7765

ALTITUDE KM		TEMP DEG KELVIN		MOL WT	DENSITY G/M3	SCALE HT KM	
GEOMET	GEOPOT	MOL.	KINETIC			GEOMET	GEOPOT
79.994	79.000	174.15	174.15	28.96	.24315E-01	5.226	5.097
80.000	79.005	174.15	174.15	28.96	.24288E-01	5.226	5.097
81.019	80.000	174.15	174.15	28.96	.19983E-01	5.228	5.097
82.000	80.955	174.15	174.15	28.96	.16567E-01	5.229	5.097
83.071	82.000	174.15	174.15	28.96	.13498E-01	5.231	5.097
84.000	82.904	174.15	174.15	28.96	.11304E-01	5.233	5.097
85.124	84.000	174.15	174.15	28.96	.91178E-02	5.235	5.097
86.000	84.851	174.15	174.15	28.96	.77145E-02	5.236	5.097
87.179	86.000	174.15	174.15	28.96	.61588E-02	5.238	5.097
88.000	86.798	174.15	174.15	28.96	.52660E-02	5.239	5.097
89.235	88.000	174.15	174.15	28.96	.41601E-02	5.241	5.097
90.000	88.743	174.15	174.15	28.96	.35955E-02	5.242	5.097
91.292	90.000	174.15	173.61	28.87	.28100E-02	5.245	5.097
92.000	90.687	174.15	173.32	28.82	.24555E-02	5.246	5.097
93.351	92.000	174.15	172.76	28.73	.18981E-02	5.248	5.097
94.000	92.630	174.15	172.49	28.68	.16774E-02	5.249	5.097
95.410	94.000	174.15	171.91	28.59	.12821E-02	5.251	5.097
96.000	94.571	174.15	171.66	28.55	.11461E-02	5.252	5.097
96.920	95.465	174.15	171.28	28.48	.96183E-03	5.254	5.097
97.472	96.000	179.13	175.95	28.45	.84317E-03	5.405	5.243
98.000	96.512	183.91	180.41	28.41	.74583E-03	5.550	5.383
99.534	98.000	197.79	193.31	28.30	.53127E-03	5.972	5.789
100.000	98.451	201.99	197.19	28.27	.48160E-03	6.100	5.912
101.598	100.000	216.44	210.48	28.16	.34898E-03	6.539	6.335
102.000	100.389	220.07	213.79	28.13	.32295E-03	6.650	6.441
103.663	102.000	235.09	227.46	28.02	.23735E-03	7.107	6.881
104.000	102.325	238.13	230.21	28.00	.22356E-03	7.200	6.970
105.729	104.000	253.75	244.26	27.88	.16625E-03	7.676	7.427
106.000	104.261	256.18	246.45	27.86	.15900E-03	7.751	7.498
107.797	106.000	272.40	260.88	27.73	.11943E-03	8.246	7.973
108.000	106.195	274.23	262.50	27.72	.11577E-03	8.302	8.027
109.866	108.000	291.05	277.32	27.59	.87700E-04	8.816	8.519
110.000	108.128	292.26	278.37	27.58	.86032E-04	8.853	8.554
111.937	110.000	309.71	293.57	27.45	.65645E-04	9.387	9.065
112.000	110.060	310.27	294.06	27.45	.65089E-04	9.405	9.082
114.000	111.991	328.28	309.56	27.31	.50033E-04	9.957	9.609
114.008	112.000	328.36	309.63	27.31	.49977E-04	9.959	9.611
116.000	113.921	346.28	324.89	27.17	.39010E-04	10.509	10.136
116.081	114.000	347.02	325.51	27.16	.38626E-04	10.532	10.157
118.000	115.849	364.26	340.03	27.03	.30806E-04	11.062	10.662
118.156	116.000	365.67	341.21	27.02	.30258E-04	11.105	10.703
120.000	117.776	382.24	355.00	26.90	.24610E-04	11.615	11.189

MODEL D

PROPERTIES OF TRANSITION ATMOSPHERE
SUBARCTIC (60N) JULY TOO JACCHIA MODELS

60N JULY X = 94.76273 KM DEN X = .11180513E-02 G/M3
GEOPOT SCALE HT AT 117.9299 KM = 11.18876, AT X KM = 5.0097767
GRADIENT OF GEOP SCALE HT ABOVE X = .26671289E 00
GRADIENT OF MOL. TEMP. ZERO FOR H BTWN 79 AND X
GRADIENT OF MOL. TEMP. 9.11176 DEG/KM FOR H BTWN X AND 117.9299

ALTITUDE KM GEOMET	GEOPOT	TEMP DEG KELVIN MOL.	KINETIC	MOL WT	DENSITY G/M3	SCALE HT KM GEOMET	GEOPOT
79.889	79.000	171.15	171.15	28.96	.25997E-01	5.130	5.010
80.000	79.107	171.15	171.15	28.96	.25444E-01	5.130	5.010
80.913	80.000	171.15	171.15	28.96	.21292E-01	5.131	5.010
82.000	81.060	171.15	171.15	28.96	.17231E-01	5.133	5.010
82.963	82.000	171.15	171.15	28.96	.14284E-01	5.135	5.010
84.000	83.011	171.15	171.15	28.96	.11672E-01	5.136	5.010
85.013	84.000	171.15	171.15	28.96	.95824E-02	5.138	5.010
86.000	84.961	171.15	171.15	28.96	.79087E-02	5.139	5.010
87.065	86.000	171.15	171.15	28.96	.64283E-02	5.141	5.010
88.000	86.910	171.15	171.15	28.96	.53599E-02	5.143	5.010
89.118	88.000	171.15	171.15	28.96	.43123E-02	5.144	5.010
90.000	88.858	171.15	171.15	28.96	.36333E-02	5.146	5.010
91.172	90.000	171.15	170.67	28.88	.28929E-02	5.148	5.010
92.000	90.804	171.15	170.34	28.83	.24635E-02	5.149	5.010
93.228	92.000	171.15	169.84	28.74	.19407E-02	5.151	5.010
94.000	92.750	171.15	169.52	28.69	.16708E-02	5.152	5.010
95.285	94.000	171.15	169.00	28.60	.13019E-02	5.154	5.010
96.000	94.694	171.15	168.71	28.55	.11334E-02	5.155	5.010
96.070	94.762	171.15	168.68	28.55	.11180E-02	5.156	5.010
97.344	96.000	182.42	179.24	28.46	.82581E-03	5.497	5.340
98.000	96.637	188.23	184.65	28.41	.71165E-03	5.673	5.510
99.403	98.000	200.65	196.16	28.32	.52539E-03	6.050	5.873
100.000	98.578	205.92	201.03	28.28	.46448E-03	6.211	6.028
101.464	100.000	218.87	212.91	28.18	.34767E-03	6.604	6.407
102.000	100.519	223.60	217.23	28.14	.31409E-03	6.748	6.545
103.526	102.000	237.09	229.47	28.03	.23780E-03	7.158	6.940
104.000	102.458	241.27	233.25	28.00	.21886E-03	7.286	7.062
105.590	104.000	255.32	245.86	27.89	.16729E-03	7.714	7.473
106.000	104.396	258.93	249.09	27.86	.15648E-03	7.824	7.579
107.655	106.000	273.54	262.07	27.75	.12057E-03	8.269	8.007
108.000	106.333	276.58	264.75	27.73	.11441E-03	8.362	8.096
109.721	108.000	291.76	278.09	27.61	.88765E-04	8.826	8.540
110.000	108.269	294.22	280.24	27.59	.85304E-04	8.901	8.612
111.789	110.000	309.99	293.94	27.47	.66569E-04	9.383	9.074
112.000	110.203	311.85	295.55	27.45	.64708E-04	9.440	9.128
113.858	112.000	328.21	309.61	27.32	.50751E-04	9.941	9.607
114.000	112.137	329.46	310.68	27.31	.49844E-04	9.979	9.644
115.928	114.000	346.44	325.09	27.18	.39264E-04	10.500	10.141
116.000	114.069	347.07	325.63	27.18	.38926E-04	10.519	10.159
117.999	116.000	364.66	340.40	27.04	.30778E-04	11.059	10.674
118.000	116.000	364.66	340.40	27.04	.30778E-04	11.059	10.674
120.000	117.929	382.24	355.00	26.90	.24610E-04	11.600	11.189

MODEL E

PROPERTIES OF TRANSITION ATMOSPHERE
SUBTROP (30N) JAN TOO JACCHIA MODELS

30N JAN X = 100.47223 KM DEN X = .41142163E-03 G/M3
GEOPOT SCALE HT AT 117.6118 KM = 11.18876, AT X KM = 5.5952019
GRADIENT OF GEOP SCALE HT ABOVE X = .32635346E 00
GRADIENT OF MOL. TEMP. ZERO FOR H BTWN 79 AND X
GRADIENT OF MOL. TEMP. 11.14927 DEG/KM FOR H BTWN X AND 117.6118

ALTITUDE KM GEOMET	GEOPOT	TEMP DEG KELVIN MOL.	KINETIC	MOL WT	DENSITY G/M3	SCALE HT KM GEOMET	GEOPOT
80.106	79.000	191.15	191.15	28.96	.19096E-01	5.745	5.595
81.133	80.000	191.15	191.15	28.96	.15970E-01	5.747	5.595
82.000	80.843	191.15	191.15	28.96	.13736E-01	5.749	5.595
83.188	82.000	191.15	191.15	28.96	.11170E-01	5.751	5.595
84.000	82.789	191.15	191.15	28.96	.97012E-02	5.752	5.595
85.244	84.000	191.15	191.15	28.96	.78135E-02	5.754	5.595
86.000	84.734	191.15	191.15	28.96	.68528E-02	5.756	5.595
87.302	86.000	191.15	191.15	28.96	.54652E-02	5.758	5.595
88.000	86.677	191.15	191.15	28.96	.48418E-02	5.759	5.595
89.361	88.000	191.15	191.15	28.96	.38227E-02	5.762	5.595
90.000	88.620	191.15	191.15	28.96	.34217E-02	5.763	5.595
91.421	90.000	191.15	190.50	28.87	.26738E-02	5.765	5.595
92.000	90.561	191.15	190.24	28.83	.24186E-02	5.767	5.595
93.483	92.000	191.15	189.57	28.72	.18702E-02	5.769	5.595
94.000	92.501	191.15	189.33	28.69	.17099E-02	5.770	5.595
95.546	94.000	191.15	188.63	28.58	.13081E-02	5.773	5.595
96.000	94.439	191.15	188.43	28.55	.12092E-02	5.774	5.595
97.610	96.000	191.15	187.69	28.44	.91499E-03	5.777	5.595
98.000	96.377	191.15	187.52	28.41	.85528E-03	5.777	5.595
99.675	98.000	191.15	186.76	28.30	.63999E-03	5.780	5.595
100.000	98.313	191.15	186.61	28.28	.60507E-03	5.781	5.595
101.742	100.000	191.15	185.82	28.16	.44765E-03	5.784	5.595
102.000	100.249	191.15	185.70	28.14	.42815E-03	5.784	5.595
102.230	100.472	191.15	185.60	28.12	.41142E-03	5.785	5.595
103.810	102.000	208.18	201.35	28.01	.29081E-03	6.303	6.094
104.000	102.183	210.22	203.23	28.00	.27951E-03	6.366	6.154
105.880	104.000	230.48	221.79	27.87	.19231E-03	6.983	6.747
106.000	104.115	231.77	222.96	27.86	.18799E-03	7.022	6.784
107.950	106.000	252.78	242.00	27.73	.13213E-03	7.664	7.399
108.000	106.047	253.31	242.48	27.73	.13101E-03	7.680	7.415
110.000	107.977	274.83	261.77	27.59	.94058E-04	8.337	8.045
110.022	108.000	275.08	261.99	27.59	.93715E-04	8.345	8.052
112.000	109.906	296.34	280.85	27.45	.69247E-04	8.995	8.674
112.096	110.000	297.38	281.77	27.44	.68270E-04	9.027	8.705
114.000	111.834	317.84	299.71	27.31	.52095E-04	9.654	9.303
114.171	112.000	319.68	301.32	27.30	.50887E-04	9.710	9.357
116.000	113.761	339.32	318.36	27.18	.39935E-04	10.313	9.932
116.247	114.000	341.97	320.65	27.16	.38689E-04	10.394	10.010
118.000	115.687	360.79	336.79	27.04	.31122E-04	10.972	10.561
118.324	116.000	364.27	339.76	27.02	.29929E-04	11.079	10.663
120.000	117.611	382.24	355.00	26.90	.24610E-04	11.632	11.189

MODEL F

PROPERTIES OF TRANSITION ATMOSPHERE
MIDLAT (45N) JAN TOO JACCHIA MODELS

45N JAN X = 102.55970 KM DEN X = .31126404E-03 G/M3
GEOPOT SCALE HT AT 117.7765 KM = 11.18876, AT X KM = 5.7210682
GRADIENT OF GEOP SCALE HT ABOVE X = .35931943E 00
GRADIENT OF MOL. TEMP. -2.1 FOR H BTWN 64 AND 86
GRADIENT OF MOL. TEMP. ZERO FOR H BTWN 86 AND X
GRADIENT OF MOL. TEMP. 12.27550 DEG/KM FOR H BTWN X AND 117.7765

ALTITUDE KM		TEMP DEG KELVIN		MOL WT	DENSITY G/M3	SCALE HT KM	
GEOMET	GEOPOT	MOL.	KINETIC			GEOMET	GEOPOT
79.994	79.000	210.15	210.15	28.96	.17023E-01	6.307	6.151
80.000	79.005	210.14	210.14	28.96	.17009E-01	6.307	6.151
81.019	80.000	208.05	208.05	28.96	.14603E-01	6.246	6.090
82.000	80.955	206.04	206.04	28.96	.12594E-01	6.188	6.031
83.071	82.000	203.85	203.85	28.96	.10696E-01	6.124	5.967
84.000	82.904	201.95	201.95	28.96	.92717E-02	6.069	5.911
85.124	84.000	199.65	199.65	28.96	.77836E-02	6.002	5.844
86.000	84.851	197.86	197.86	28.96	.67841E-02	5.949	5.792
87.179	86.000	195.45	195.45	28.96	.56260E-02	5.879	5.721
88.000	86.798	195.45	195.45	28.96	.48932E-02	5.881	5.721
89.235	88.000	195.45	195.45	28.96	.39662E-02	5.883	5.721
90.000	88.743	195.45	195.45	28.96	.34828E-02	5.884	5.721
91.292	90.000	195.45	194.85	28.88	.27961E-02	5.887	5.721
92.000	90.687	195.45	194.52	28.83	.24795E-02	5.888	5.721
93.351	92.000	195.45	193.89	28.73	.19712E-02	5.890	5.721
94.000	92.630	195.45	193.59	28.69	.17656E-02	5.892	5.721
95.410	94.000	195.45	192.94	28.59	.13896E-02	5.894	5.721
96.000	94.571	195.45	192.66	28.55	.12575E-02	5.895	5.721
97.472	96.000	195.45	191.98	28.45	.97968E-03	5.898	5.721
98.000	96.512	195.45	191.74	28.41	.89581E-03	5.899	5.721
99.534	98.000	195.45	191.02	28.31	.69065E-03	5.902	5.721
100.000	98.451	195.45	190.81	28.28	.63828E-03	5.902	5.721
101.598	100.000	195.45	190.06	28.17	.48689E-03	5.905	5.721
102.000	100.389	195.45	189.88	28.14	.45488E-03	5.906	5.721
103.663	102.000	195.45	189.11	28.02	.34325E-03	5.909	5.721
104.000	102.325	195.45	188.95	28.00	.32425E-03	5.910	5.721
104.241	102.559	195.45	188.84	27.98	.31126E-03	5.910	5.721
105.729	104.000	213.13	205.17	27.88	.22431E-03	6.448	6.239
106.000	104.261	216.34	208.11	27.86	.21198E-03	6.545	6.332
107.797	106.000	237.68	227.63	27.74	.14849E-03	7.195	6.957
108.000	106.195	240.08	229.82	27.73	.14295E-03	7.268	7.028
109.866	108.000	262.23	249.86	27.60	.10238E-03	7.944	7.676
110.000	108.128	263.81	251.28	27.59	.10008E-03	7.992	7.722
111.937	110.000	286.78	271.84	27.45	.72976E-04	8.693	8.395
112.000	110.060	287.53	272.50	27.45	.72263E-04	8.716	8.416
114.000	111.991	311.23	293.48	27.31	.53553E-04	9.440	9.110
114.008	112.000	311.33	293.58	27.31	.53484E-04	9.443	9.113
116.000	113.921	334.92	314.23	27.18	.40576E-04	10.164	9.803
116.081	114.000	335.89	315.07	27.17	.40135E-04	10.194	9.832
118.000	115.849	358.59	334.73	27.04	.31338E-04	10.890	10.496
118.156	116.000	360.44	336.33	27.03	.30734E-04	10.946	10.550
120.000	117.776	382.24	355.00	26.90	.24610E-04	11.615	11.189

MODEL G

PROPERTIES OF TRANSITION ATMOSPHERE
SUBARCTIC (60N) JAN TOO JACCHIA MODELS

60N JAN X = 104.43142 KM DEN X = .23817473E-03 G/M3
GEOPOT SCALE HT AT 117.9299 KM = 11.18876. AT X KM = 5.9113313
GRADIENT OF GEOP SCALE HT ABOVE X = .39096597E 00
GRADIENT OF MOL. TEMP. -2.6 FOR H BTWN 69 TO 86
GRADIENT OF MOL. TEMP. ZERO FOR H BTWN 86 AND X
GRADIENT OF MOL. TEMP. 13.35533 DEG/KM FOR H BTWN X AND 117.9299

ALTITUDE KM GEOMET	GEOPOT	TEMP DEG KELVIN MOL.	KINETIC	MOL WT	DENSITY G/M3	SCALE HT KM GEOMET	GEOPOT
69.666	69.000	246.15	246.15	28.96	.59480E-01		7.205
70.000	69.326	245.30	245.30	28.96	.57037E-01	7.330	7.180
70.687	70.000	243.55	243.55	28.96	.52287E-01	7.279	7.129
72.000	71.285	240.21	240.21	28.96	.44213E-01	7.182	7.031
72.730	72.000	238.35	238.35	28.96	.40236E-01	7.128	6.977
74.000	73.242	235.12	235.12	28.96	.34092E-01	7.034	6.882
74.774	74.000	233.15	233.15	28.96	.30783E-01	6.977	6.825
76.000	75.198	230.03	230.03	28.96	.26142E-01	6.886	6.733
76.819	76.000	227.95	227.95	28.96	.23410E-01	6.826	6.672
78.000	77.153	224.95	224.95	28.96	.19931E-01	6.738	6.585
78.865	78.000	222.75	222.75	28.96	.17690E-01	6.674	6.520
80.000	79.107	219.87	219.87	28.96	.15105E-01	6.590	6.436
80.913	80.000	217.55	217.55	28.96	.13280E-01	6.523	6.368
82.000	81.060	214.79	214.79	28.96	.11375E-01	6.442	6.287
82.963	82.000	212.35	212.35	28.96	.99004E-02	6.371	6.216
84.000	83.011	209.72	209.72	28.96	.85103E-02	6.294	6.139
85.013	84.000	207.15	207.15	28.96	.73272E-02	6.219	6.064
86.000	84.961	204.65	204.65	28.96	.63228E-02	6.145	5.990
87.065	86.000	201.95	201.95	28.96	.53815E-02	6.066	5.911
88.000	86.910	201.95	201.95	28.96	.46131E-02	6.068	5.911
89.118	88.000	201.95	201.95	28.96	.38367E-02	6.070	5.911
90.000	88.858	201.95	201.95	28.96	.33182E-02	6.072	5.911
91.172	90.000	201.95	201.39	28.88	.27354E-02	6.074	5.911
92.000	90.804	201.95	200.99	28.83	.23872E-02	6.076	5.911
93.228	92.000	201.95	200.40	28.74	.19502E-02	6.078	5.911
94.000	92.750	201.95	200.03	28.69	.17178E-02	6.079	5.911
95.285	94.000	201.95	199.41	28.60	.13904E-02	6.082	5.911
96.000	94.694	201.95	199.07	28.55	.12363E-02	6.083	5.911
97.344	96.000	201.95	198.43	28.46	.99133E-03	6.086	5.911
98.000	96.637	201.95	198.11	28.41	.89005E-03	6.087	5.911
99.403	98.000	201.95	197.44	28.32	.70678E-03	6.090	5.911
100.000	98.578	201.95	197.15	28.28	.64085E-03	6.091	5.911

101.464	100.000	201.95	196.45	28.18	.50390E-03	6.093	5.911
102.000	100.519	201.95	196.19	28.14	.46152E-03	6.095	5.911
103.526	102.000	201.95	195.46	28.03	.35926E-03	6.097	5.911
104.000	102.458	201.95	195.23	28.00	.33244E-03	6.098	5.911
105.590	104.000	201.95	194.47	27.89	.25613E-03	6.101	5.911
106.000	104.396	201.95	194.27	27.86	.23951E-03	6.102	5.911
106.027	104.422	201.95	194.26	27.86	.23845E-03	6.102	5.911
107.655	106.000	223.00	213.65	27.75	.16754E-03	6.742	6.528
108.000	106.333	227.45	217.73	27.73	.15615E-03	6.877	6.658
109.721	108.000	249.70	238.00	27.61	.11203E-03	7.553	7.309
110.000	108.269	253.29	241.26	27.59	.10647E-03	7.663	7.414
111.789	110.000	276.39	262.09	27.47	.78039E-04	8.366	8.090
112.000	110.203	279.11	264.53	27.45	.75366E-04	8.449	8.170
113.858	112.000	303.09	285.91	27.32	.56206E-04	9.180	8.872
114.000	112.137	304.92	287.53	27.31	.55014E-04	9.236	8.925
115.928	114.000	329.79	309.47	27.18	.41619E-04	9.995	9.653
116.000	114.069	330.71	310.28	27.18	.41206E-04	10.024	9.680
117.999	116.000	356.48	332.77	27.04	.31547E-04	10.811	10.435
118.000	116.000	356.48	332.77	27.04	.31547E-04	10.811	10.435
120.000	117.929	382.24	355.00	26.90	.24610E-04	11.600	11.189

MODEL H

PROPERTIES OF TRANSITION ATMOSPHERE
SUBARCTIC (60N) COLD TOO JACCHIA MODELS

60N COLD X = 96.44558 KM DEN X = .74152773E-03 G/M3
GEOPOT SCALE HT AT 117.9299 KM = 11.18876, AT X KM = 5.4664082
GRADIENT OF GEOP SCALE HT ABOVE X = .26635016E 00
GRADIENT OF MOL. TEMP. -3.6 FOR H BTWN 71 TO 90
GRADIENT OF MOL. TEMP. ZERO FOR H BTWN 90 AND X
GRADIENT OF MOL. TEMP. 9.09937 DEG/KM FOR H BTWN X AND 117.9299

ALTITUDE KM		TEMP DEG KELVIN		MOL WT	DENSITY G/M3	SCALE HT KM	
GEOMET	GEOPOT	MOL.	KINETIC			GEOMET	GEOPOT
71.709	71.000	255.15	255.15	28.96	.34111E-01		7.468
72.000	71.285	254.12	254.12	28.96	.32962E-01	7.598	7.438
72.730	72.000	251.55	251.55	28.96	.30234E-01	7.523	7.363
74.000	73.242	247.08	247.08	28.96	.25961E-01	7.392	7.232
74.774	74.000	244.35	244.35	28.96	.23628E-01	7.312	7.152
76.000	75.198	240.03	240.03	28.96	.20310E-01	7.186	7.026
76.819	76.000	237.15	237.15	28.96	.18329E-01	7.101	6.942
78.000	77.153	233.00	233.00	28.96	.15775E-01	6.979	6.820
78.865	78.000	229.95	229.95	28.96	.14108E-01	6.890	6.731
80.000	79.107	225.96	225.96	28.96	.12161E-01	6.773	6.614
80.913	80.000	222.75	222.75	28.96	.10769E-01	6.678	6.520
82.000	81.060	218.93	218.93	28.96	.92995E-02	6.566	6.408
82.963	82.000	215.55	215.55	28.96	.81477E-02	6.467	6.309
84.000	83.011	211.91	211.91	28.96	.70504E-02	6.359	6.203
85.013	84.000	208.35	208.35	28.96	.61062E-02	6.255	6.099
86.000	84.961	204.89	204.89	28.96	.52965E-02	6.153	5.997
87.065	86.000	201.15	201.15	28.96	.45301E-02	6.042	5.888
88.000	86.910	197.87	197.87	28.96	.39402E-02	5.946	5.792
89.118	88.000	193.95	193.95	28.96	.33243E-02	5.830	5.677
90.000	88.858	190.86	190.86	28.96	.29006E-02	5.738	5.587
91.172	90.000	186.75	186.23	28.88	.24111E-02	5.617	5.466
92.000	90.804	186.75	185.86	28.83	.20810E-02	5.618	5.466
93.228	92.000	186.75	185.32	28.74	.16723E-02	5.621	5.466
94.000	92.750	186.75	184.98	28.69	.14578E-02	5.622	5.466
95.285	94.000	186.75	184.40	28.60	.11599E-02	5.624	5.466
96.000	94.694	186.75	184.09	28.55	.10215E-02	5.625	5.466
97.344	96.000	186.75	183.49	28.46	.80450E-03	5.628	5.466
97.802	96.445	186.75	183.29	28.43	.74152E-03	5.628	5.466
98.000	96.637	188.49	184.91	28.41	.70949E-03	5.681	5.517
99.403	98.000	200.89	196.41	28.32	.52405E-03	6.058	5.880
100.000	98.578	206.16	201.26	28.28	.46338E-03	6.218	6.035

101.464	100.000	219.09	213.13	28.18	.34699E-03	6.611	6.413
102.000	100.519	223.82	217.44	28.14	.31351E-03	6.754	6.551
103.526	102.000	237.29	229.67	28.03	.23744E-03	7.164	6.946
104.000	102.458	241.46	233.43	28.00	.21855E-03	7.291	7.068
105.590	104.000	255.49	246.03	27.89	.16710E-03	7.719	7.479
106.000	104.396	259.10	249.25	27.86	.15631E-03	7.829	7.584
107.655	106.000	273.69	262.21	27.75	.12047E-03	8.274	8.011
108.000	106.333	276.72	264.89	27.73	.11432E-03	8.367	8.100
109.721	108.000	291.89	278.21	27.61	.88710E-04	8.830	8.544
110.000	108.269	294.34	280.35	27.59	.85253E-04	8.905	8.616
111.789	110.000	310.09	294.03	27.47	.66540E-04	9.386	9.077
112.000	110.203	311.94	295.64	27.45	.64681E-04	9.443	9.131
113.858	112.000	328.29	309.68	27.32	.50737E-04	9.943	9.609
114.000	112.137	329.53	310.74	27.31	.49830E-04	9.982	9.646
115.928	114.000	346.48	325.14	27.18	.39257E-04	10.501	10.142
116.000	114.069	347.11	325.67	27.18	.38920E-04	10.521	10.160
117.999	116.000	364.68	340.42	27.04	.30776E-04	11.060	10.675
118.000	116.000	364.68	340.42	27.04	.30776E-04	11.060	10.675
120.000	117.929	382.24	355.00	26.90	.24610E-04	11.600	11.189

MODEL 1

PROPERTIES OF TRANSITION ATMOSPHERE
SUBARCTIC (60N) WARM TOO JACCHIA MODELS

60N WARM X = 104.90612 KM DEN X = .22741341E-03 G/M3
GEOPOT SCALE HT AT 117.9299 KM = 11.18876, AT X KM = 5.8732787
GRADIENT OF GEOP SCALE HT ABOVE X = .40813658E 00
GRADIENT OF MOL. TEMP. -2.7 FOR H BTWN 54 TO 79
GRADIENT OF MOL. TEMP. ZERO FOR H BTWN 79 AND X
GRADIENT OF MOL. TEMP. 13.94325 DEG/KM FOR H BTWN X AND 117.9299

ALTITUDE KM		TEMP DEG KELVIN		MOL WT	DENSITY G/M3	SCALE HT KM	
GEOMET	GEOPOT	MOL.	KINETIC			GEOMET	GEOPOT
54.392	54.000	268.15	268.15	28.96	.54953E 00	7.974	7.849
56.000	55.582	263.88	263.88	28.96	.45573E 00	7.851	7.724
56.424	56.000	262.75	262.75	28.96	.43354E 00	7.818	7.691
58.000	57.549	258.57	258.57	28.96	.35959E 00	7.697	7.569
58.458	58.000	257.35	257.35	28.96	.34036E 00	7.662	7.533
60.000	59.515	253.26	253.26	28.96	.28238E 00	7.544	7.413
60.493	60.000	251.95	251.95	28.96	.26584E 00	7.506	7.375
62.000	61.480	247.95	247.95	28.96	.22065E 00	7.391	7.258
62.529	62.000	246.55	246.55	28.96	.20652E 00	7.350	7.217
64.000	63.443	242.65	242.65	28.96	.17152E 00	7.237	7.103
64.566	64.000	241.15	241.15	28.96	.15954E 00	7.194	7.059
66.000	65.405	237.35	237.35	28.96	.13261E 00	7.083	6.948
66.605	66.000	235.75	235.75	28.96	.12254E 00	7.037	6.901
68.000	67.366	232.06	232.06	28.96	.10195E 00	6.930	6.793
68.645	68.000	230.35	230.35	28.96	.93543E-01	6.880	6.743
70.000	69.326	226.77	226.77	28.96	.77927E-01	6.776	6.638
70.687	70.000	224.95	224.95	28.96	.70951E-01	6.723	6.585
72.000	71.285	221.48	221.48	28.96	.59193E-01	6.622	6.483
72.730	72.000	219.55	219.55	28.96	.53455E-01	6.566	6.427
74.000	73.242	216.19	216.19	28.96	.44673E-01	6.468	6.328
74.774	74.000	214.15	214.15	28.96	.39990E-01	6.408	6.268
76.000	75.198	210.91	210.91	28.96	.33486E-01	6.314	6.174
76.819	76.000	208.75	208.75	28.96	.29696E-01	6.251	6.110
78.000	77.153	205.63	205.63	28.96	.24923E-01	6.160	6.019
78.865	78.000	203.35	203.35	28.96	.21881E-01	6.093	5.952
79.889	79.000	200.65	200.65	28.96	.18725E-01	6.014	5.873
80.000	79.107	200.65	200.65	28.96	.18384E-01	6.014	5.873
80.913	80.000	200.65	200.65	28.96	.15793E-01	6.016	5.873
82.000	81.060	200.65	200.65	28.96	.13184E-01	6.018	5.873
82.963	82.000	200.65	200.65	28.96	.11235E-01	6.020	5.873
84.000	83.011	200.65	200.65	28.96	.94577E-02	6.022	5.873
85.013	84.000	200.65	200.65	28.96	.79928E-02	6.024	5.873
86.000	84.961	200.65	200.65	28.96	.67856E-02	6.025	5.873
87.065	86.000	200.65	200.65	28.96	.56860E-02	6.027	5.873
88.000	86.910	200.65	200.65	28.96	.48694E-02	6.029	5.873
89.118	88.000	200.65	200.65	28.96	.40450E-02	6.031	5.873
90.000	88.858	200.65	200.65	28.96	.34950E-02	6.033	5.873

91.172	90.000	200.65	200.09	28.88	.28776E-02	6.035	5.873
92.000	90.804	200.65	199.70	28.83	.25091E-02	6.037	5.873
93.228	92.000	200.65	199.11	28.74	.20471E-02	6.039	5.873
94.000	92.750	200.65	198.74	28.69	.18016E-02	6.040	5.873
95.285	94.000	200.65	198.13	28.60	.14563E-02	6.043	5.873
96.000	94.694	200.65	197.79	28.55	.12939E-02	6.044	5.873
97.344	96.000	200.65	197.15	28.46	.10360E-02	6.047	5.873
98.000	96.637	200.65	196.84	28.41	.92952E-03	6.048	5.873
99.403	98.000	200.65	196.17	28.32	.73702E-03	6.050	5.873
100.000	98.578	200.65	195.88	28.28	.66785E-03	6.052	5.873
101.464	100.000	200.65	195.18	28.18	.52431E-03	6.054	5.873
102.000	100.519	200.65	194.93	28.14	.47995E-03	6.055	5.873
103.526	102.000	200.65	194.20	28.03	.37299E-03	6.058	5.873
104.000	102.458	200.65	193.98	28.00	.34498E-03	6.059	5.873
105.590	104.000	200.65	193.22	27.89	.26534E-03	6.062	5.873
106.000	104.396	200.65	193.02	27.86	.24802E-03	6.063	5.873
106.525	104.906	200.65	192.77	27.83	.22741E-03	6.064	5.873
107.655	106.000	215.90	206.85	27.75	.17661E-03	6.527	6.320
108.000	106.333	220.55	211.12	27.73	.16409E-03	6.668	6.456
109.721	108.000	243.79	232.37	27.61	.11615E-03	7.375	7.136
110.000	108.269	247.54	235.78	27.59	.11018E-03	7.489	7.246
111.789	110.000	271.68	257.61	27.47	.79935E-04	8.224	7.952
112.000	110.203	274.52	260.17	27.45	.77116E-04	8.310	8.035
113.858	112.000	299.56	282.58	27.32	.57059E-04	9.073	8.769
114.000	112.137	301.47	284.28	27.31	.55820E-04	9.132	8.824
115.928	114.000	327.45	307.28	27.18	.41971E-04	9.924	9.585
116.000	114.069	328.41	308.13	27.18	.41547E-04	9.954	9.613
117.999	116.000	355.33	331.70	27.04	.31658E-04	10.776	10.401
118.000	116.000	355.34	331.70	27.04	.31658E-04	10.777	10.401
120.000	117.929	382.24	355.00	26.90	.24610E-04	11.600	11.189

REFERENCES

1. Jacchia, L. G., "Static Diffusion Models of the Upper Atmosphere with Empirical Temperature Profiles," Special Report 170, Smithsonian Institution, Astrophysical Observatory, Cambridge, Mass. (Dec. 30, 1964).

2. Cole, A. E., A. J. Kantor, "Air Force Interim Supplemental Atmospheres to 90 kilometers," Air Force Surveys in Geophysics No. 153, AFCRL-63-936 (December 1963).

3. United States Standard Atmosphere, National Aeronautics and Space Administration, U. S. Air Force and U. S. Weather Bureau, Government Printing Office, Washington, D. C. (1962).

4. List (Editor), Smithsonian Meteorological tables, Sixth Edition, Washington, D. C. (1951).

5. Minzner, R. A., et al., "U. S. Extension to the ICAO Standard Atmosphere," Dept. of Commerce and U. S. Air Force Government Printing Office, Washington, D. C., page 4 (1958).

APPENDIX

Summary of that work accomplished under Contract No. NASw-976 which has been previously published in GCA Corporation Technical Reports.

This section consists of brief summaries of previously published GCA Corportaion reports. These summaries indicate the detail and scope of the work of the original report and consist of:

(1) Original title page,

(2) The original table of contents (if any),

(3) Abstract,

(4) List of references.

In the case of GCA TR 65-1-N, a reprint of the entire journal artical is given.

GCA Technical Report 64-9-N

TEMPERATURE DETERMINATION OF PLANETARY ATMOSPHERES

Raymond A. Minzner Gerhard O. Sauermann Lennart R. Peterson

June 1964

Contract No. NASw-976

GEOPHYSICS CORPORATION OF AMERICA
Bedford, Massachusetts

Prepared for

NATIONAL AERONAUTICS AND SPACE ADMINISTRATION
Washington 25, D.C.

ABSTRACT

A method is presented whereby accurate temperature-altitude profiles of planetary atmospheres may be determined from the number-density profiles of two inert gases having markedly different molecular weights M. In the earth's atmosphere, such gases would preferably be helium and argon. In contrast to previous methods in which mass-density profiles permitted the calculation of only the ratio T/M at altitudes sufficiently below the highest altitude of density data, the two-gas method yields values of kinetic temperature T, not only at low altitudes where number-density data for both gases exist, but also up to the greatest altitude for which the light-gas number-density data have been measured. The method depends upon recently developed mass spectrometers with detection sensitivities of the order of 10^5 particles per cubic centimeter.

A rigorous error analysis predicts the accuracy of the resulting temperatures on the basis of sensor and telemeter characteristics, and allows for optimizing any actual experiment as far as range and number of measurements are concerned.

TABLE OF CONTENTS

REFERENCES

1. Bjerknes, V., et al., "Dynamic Meteorology and Hydrography," Carnegie Institute of Washington, Publication 88, Washington, D. C. (1910).

2. Champion, K. S. W., AFCRL; W. J. O. Sullivan, Jr., NASA; and S. Teweles, U. S. Weather Bureau (co-editors), "U. S. Standard Atmosphere 1962," U. S. Government Printing Office, Washington, D. C. (1962).

3. Champion, K. S. W., Minzner, R. A., "Revision of United States Standard Atmosphere 90 to 700 Km," Rev. of Geophys. 1, 57-84 (1963).

4. Elterman, L., "A Series of Stratospheric Temperature Profiles Obtained with the Searchlight Technique," J. Geophys. Res. 58, 519 (1953).

5. Harrison, L. P., "Relation Between Geopotential and Geometric Height," Smithsonian Meteorological Tables, R. S. List, Editor, 6th ed., p. 217-219, Washington, D.C. (1951).

6. Minzner, R. A., and W. S. Ripley, "The ARDC Model Atmosphere 1956," Air Force Surveys in Geophysics #86, AFCRC TN-56-204, Astia Document 110233 (December 1956).

7. Minzner, R. A., W. S. Ripley and T. P. Condron, "U. S. Extension of the ICAO Standard Atmosphere," Washington, D.C. (1958).

8. Minzner, R. A., K. S. W. Champion, H. L. Pond, "The ARDC Model Atmosphere 1959," Air Force Surveys in Geophysics #115, AFCRC-TR-59-267 (August 1959).

9. Minzner, R. A., G. O. Sauermann, L. R. Peterson, "Temperature Determination Method for Planetary Atmospheres," GCA Tech. Report 63-10-N (May 1963).

10. Sauermann, G., and R. Herzog, "A Rocket-Borne Helium Mass Spectrometer," GCA Tech. Report 61-8-N (November 1961).

GCA Technical Report 65-1-N

LOW MESOPAUSE TEMPERATURES OVER EGLIN TEST RANGE DEDUCED FROM DENSITY DATA

R. A. Minzner G. O. Sauermann

G. A. Faucher*

January 1965

Contract No. NASw-976

GCA CORPORATION
Bedford, Massachusetts

*Air Force Cambridge Research Laboratories

Prepared for
NATIONAL AERONAUTICS AND SPACE ADMINISTRATION
Washington, D. C.

ABSTRACT

Unusually low values of temperature (about 156 $\pm$ 16°K) have been found to exist in the region of 100 km altitude over Eglin Gulf Test Range in Florida (30° 24'N, 86° 43' W) at 2315 hours GMT on December 7, 1961. These low temperatures have been determined from 50 density-altitude data points over the altitude range of 97.8 km to 132.2 km, without the use of any independent temperature information. The basic density data and their associated uncertainties were deducted from measurements of drag accelerations on a falling sphere of 2.74 meters diameter [1].* The data are shown graphically in Figure 10 of that paper and numerical values of density ρ and its uncertainties $\delta\rho$ are summarized in Table 2 of that same paper. The uncertainties in temperature which are dependent upon $\delta\rho$ have been calculated. From the extent of the temperature uncertainty, it is apparent that the temperature-altitude profile is well bounded for altitudes below 110 km, especially for the lower two kilometers of the profile, and these low mesopause temperatures are therefore indeed significant.

*Numbers in [ ] throughout text indicate reference numbers.

REFERENCES

1. Faucher, G. A., Procunier, R. W., and Sherman, F. S., "Upper-Atmosphere Density Obtained from Measurements of Drag on a Falling Sphere," J. Geophys. Res. 68, 3437-3450 (1963).

2. Elterman, L., "A Series of Stratospheric Temperature Profiles Obtained with the Searchlight Technique," J. Geophys. Res. 58, 519-530 (1953).

3. Newell, H. E., Jr., "High Altitude Rocket Research," Academic Press, Inc., New York, 1953 (p. 112).

4. Champion, K. S. W. and Minzner, R.A., "Revision of United States Standard Atmosphere 90 to 700 km," Rev. of Geophys. 1, 57-84 (1963).

5. Minzner, R. A. and Ripley, W. S., "The ARDC Model Atmosphere 1956," Air Force Surveys in Geophysics No. 86, ARCRC TN-56-204 (1956).

6. Minzner, R. A., Ripley, W. S., and Condron, T. F., "U. S. Extension of the ICAO Standard Atmosphere," Washington, D. C. (1958).

7. Minzner, R. A., Champion, K. S. W., and Pond, H. L., "The ARDC Model Atmosphere 1959," Air Force Surveys in Geophysics No. 115, AFCRC TR-59-267 (1959).

8. "U. S. Standard Atmosphere," National Aeronautics and Space Administration, U. S. Air Force, and U. S. Weather Bureau, Government Printing Office, Washington, D. C. (1962).

9. Harrison, L. P., "Relation between Geopotential and Geometric Height," Smithsonian Meteorological Tables, R. S. List, Ed., 6th Edition, 217-218, Washington, D. C. (1951).

10. Miller, L. E., "Molecular Weight of Air at High Altitudes," J. Geophys. Res. 62, 351-356 (1957).

11. Sauermann, G. O. and Herzog, R. F. K., "Helium on the Earth's Atmosphere," GCA Tech. Rpt. No. 61-6-N (1961).

12. Spencer, N. W., Newton, G. P., Reber, C. A., Brace, L. H., and Horowitz, R., "New Knowledge of the Earth's Atmosphere from the Aeronomy Satellite (Explorer XVII)," X-651-64-114, Goddard Space Flight Center, Greenbelt, Maryland (1964).

13. Court, A., Kantor, A. J., and Cole, A. E., "Supplementary Atmospheres," AFCRL-62-889 (September 1962).

REFERENCES (Continued)

14. Peterson, J. W., private communication (1964).

15. Stroud, W. G., Nordberg, W., Bandeen, W. R., Bartman, F. L., and Titus, P.,"Rocket-Grenade Measurements of Temperatures and Winds in the Mesosphere over Churchill, Canada," J. Geophys. Res. 65, 2307-2323 (1960).

16. Mikhnevich, V. V. and Khvostikov, I. A., "Study of the Upper Layers of the Atmosphere," Akademiia Nau SSSR, Leningrad, Izvestiia, Seriia Geofizicheskiia No. 11, 1393-1409 (1957).

JOURNAL OF GEOPHYSICAL RESEARCH VOL. 70, NO. 3 FEBRUARY 1, 1965

Low Mesopause Temperatures over Eglin Test Range Deduced from Density Data

R. A. MINZNER AND G. O. SAUERMANN

Geophysics Corporation of America, Bedford, Massachusetts

G. A. FAUCHER

Air Force Cambridge Research Laboratories, Bedford, Massachusetts

Unusually low temperatures (about 156° ± 16°K) were found in the region of 100-km altitude over Eglin Gulf Test Range, Florida (30°24'N, 86°43'W), at 2315 GMT, December 7, 1961. These low temperatures were determined from 50 density-altitude data points over the altitude range 97.8 to 132.2 km without the use of any independent temperature information. The basic density data and their associated uncertainties were deduced from measurements of drag accelerations on a falling sphere of 2.74 meters diameter. The data are shown graphically in Figure 10 of a recent paper by *Faucher et al.* [1963], and numerical values of density ρ and its uncertainties $\delta\rho$ are summarized in Table 2 of the same paper. The uncertainties in temperature, which are dependent on $\delta\rho$, have been calculated. From the extent of the temperature uncertainty, it is apparent that the temperature-altitude profile is well bounded for altitudes below 110 km, especially for the lower 2 km of the profile, and these low mesopause temperatures are therefore indeed significant.

The method for obtaining the temperature T_r at any altitude Z_r involves the downward integration of atmospheric mass density ρ with respect to Z from Z_a to Z_r, where Z_a is the greatest altitude of usable data. The basic form of the equation for extracting the temperature information from the density-altitude data is a well-known relationship [*Elterman*, 1953; *Newell*, 1953; *Champion and Minzner*, 1963] based on the hydrostatic equation and the equation of state:

$$T_r = \frac{\rho_a}{\rho_r} T_a + \frac{\bar{M}}{R\rho_r} \int_{Z_r}^{Z_a} (g\rho)\, dZ \qquad (1)$$

where

ρ_a and ρ_r are densities at altitudes Z_a and Z_r, respectively.

T_a is the temperature at Z_a.

$\bar{M}$ is the mean molecular weight of the gas (considered to be constant).

R is the universal gas constant.

g is the acceleration of gravity.

At first glance it would appear that the presence of T_a in (1) would prevent the evaluation of T_r, since no information about T_a is available. It is seen, however, that when the density-altitude gradient is negative, as it is in the atmosphere, the term $(\rho_a/\rho_r)T_a$ becomes negligibly small as altitude Z_r is taken sufficiently below Z_a, while the integral term approaches the full value of T_r. The highest 15 to 20 km of mass-density data are consumed in essentially eliminating the T_a term, and the more reliable values of T_r are determined only for lower altitudes; i.e., below 110 km for the data at hand.

In dealing with real mass-density data of a multigas atmosphere where the acceleration of gravity and the mean molecular weight are variables with respect to altitude, it is convenient to introduce two transformations. First, the two variables T and $\bar{M}$ are combined into a single new variable T_M (molecular scale temperature) through the relationship $T_M \equiv (T/\bar{M})M_0$, where M_0 is the sea-level value of $\bar{M}$ [*Minzner and Ripley*, 1956; *Minzner et al.*, 1958, 1959; *Champion and Minzner*, 1963; *United States Standard Atmosphere*, 1962]. Second, the two variables g and Z are combined into a single new variable h (geopotential) through the relationship $G \cdot dh = g \cdot dZ$, where G is a constant numerically equal to the sea-level value of g [*Harrison*, 1951; *Minzner and Ripley*, 1956; *Minzner et al.*, 1958, 1959]. In addition, the existence of the data in the form of discrete density-altitude points makes it desirable to introduce the trapezoidal rule for numerical integration. Together, these trans-

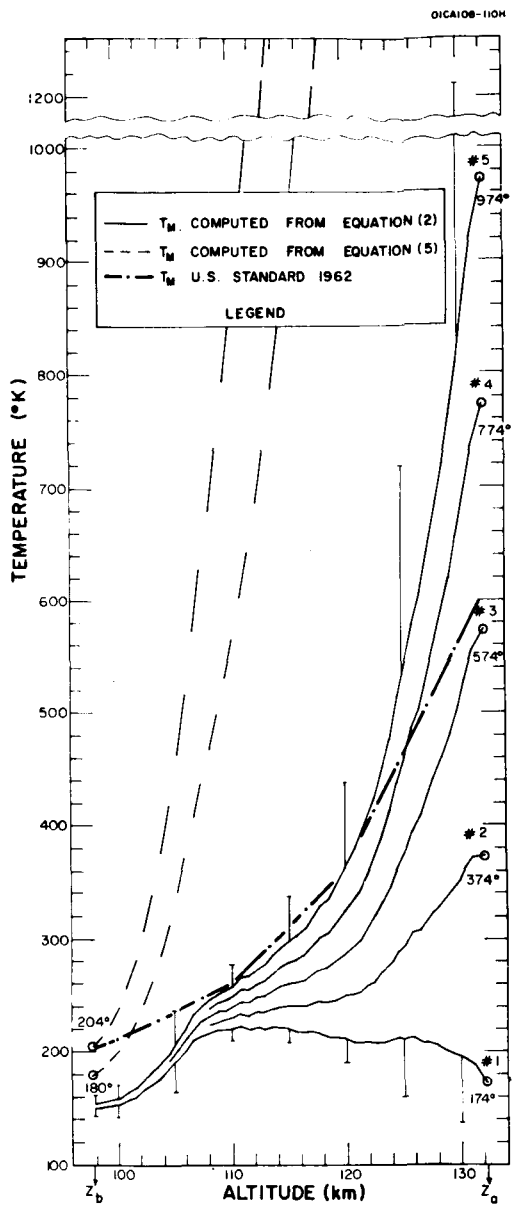

Fig. 1

formations lead to

$$(T_M)_r = \frac{\rho_a}{\rho_r}(T_M)_a + \frac{GM_0}{R\rho_r}\left[\rho_a\left(\frac{h_a - h_{a+1}}{2}\right) + \rho_r\left(\frac{h_{r-1} - h_r}{2}\right) + \sum_{i=a+1}^{r-1}\rho_i\left(\frac{h_{j-1} - h_{j+1}}{2}\right)\right] \quad (2)$$

In this expression the density-data points are considered to be numbered consecutively so that the numbers increase downward from the point at Z_a which is identically point a or point 1.

From this equation, T_M is determined as a function of h in geopotential meters (m'), but, by a reverse transformation, the values of h are independently related to appropriate values of Z, so that T_M is finally available as a function of geometric altitude Z.

In Figure 1, a series of five solid-line profiles of T_M versus Z computed from the data by means of (2) are compared with T_M of the *United States Standard Atmosphere* [1962]. These five curves are representative of an infinite number of profiles which might be computed from the data, each differing solely by virtue of the assumed value of $(T_M)_a$ at 132.2 km, the upper end of the useful available density data. Each of the series of five values of $(T_M)_a$ employed differs by 200°K from the preceding value, with the range extending from 173.7°K to 973.7°K. The T_M profiles are seen to converge with decreasing altitude.

Since any expected true value of T_M at 132.2 km should be well within the extremes of the five values of $(T_M)_a$ presented, the true T_M versus Z profile should also always lie between the extreme curves even at low altitudes where these curves are separated by 10° or less. Thus, for altitudes below 110 km, the value of T_M, without consideration for density uncertainty, appears to be bounded within narrow limits; 40° at 110 km and 3° at 98 km.

A rigorous error analysis based on the Gaussian method indicates that $(\delta T_M)_r$, the uncertainty in $(T_M)_r$, is given by

$$(\delta T_M)_r = \left[\left(\frac{u}{\rho_r}\right)^2 + \left(\frac{\rho_a}{\rho_r}(\delta T_M)_a\right)^2\right]^{1/2} \quad (3)$$

where $(\delta T_M)_a$ is the uncertainty in $(T_M)_a$ and

$$\left(\frac{u}{\rho_r}\right)^2 = \left[(T_M)_a + \frac{GM_0}{R}\left(\frac{h_a - h_{a+1}}{2}\right)\right]^2\left(\frac{\delta\rho_a}{\rho_r}\right)^2 + \left[(T_M)_r - \frac{GM_0}{R}\left(\frac{h_{r-1} - h_r}{2}\right)\right]^2\left(\frac{\delta\rho_r}{\rho_r}\right)^2 + \left(\frac{GM_0}{R}\right)^2\sum_{i=a+1}^{r-1}\left(\frac{\delta\rho_i}{\rho_r}\right)^2\left(\frac{h_{j-1} - h_{j+1}}{2}\right)^2 \quad (4)$$

In this expression, $\delta\rho_a$, $\delta\rho_i$, and $\delta\rho_r$ are the uncertainties in ρ_a, ρ_i, and ρ_r, respectively.

Like equation 1, the expression for the temperature uncertainty, equation 3 cannot be evaluated for altitudes near Z_a owing to lack of information, in this instance, about $(\delta T_M)_a$. The ratio (ρ_a/ρ_r), however, again serves essentially to eliminate the need for the unknown quantity when Z_r is sufficiently below Z_a. This is illustrated

graphically on the basis of the previous assumption that $(T_M)_a$ is within the range 173.7° to 973.7° such that $(\delta T_M)_a$ must be less than 800°, which is the separation of the extreme curves at 132.2 km. Under these conditions, $(\rho_a/\rho_r)(\delta T_M)_a$ must be less than the separation of these two curves at any altitude Z_r. Therefore, it is apparent from the graph that, at $Z_r = 100$ km, $(\rho_a/\rho_r)(\delta T_M)_a$ is considerably less than 5°. Under these conditions, $(\delta T_M)_r$ is approximately equal to $\pm(u/\rho_r)$ alone.

For any of the assumed values of $(T_M)_a$ it is possible to compute values of $\pm(u/\rho_r)$ versus Z_r over the entire altitude range of the data in order to evaluate the influence of density uncertainty alone on the five computed profiles. The positive half of this uncertainty component $\pm(u/\rho_r)$ for curve 5 is indicated by the upward-directed flags on curve 5, while the negative half of this uncertainty component for curve 1 is indicated by the downward-directed flags along this curve. For altitudes of 115 km and below, the values of $\pm(u/\rho_r)$ appear to be reasonably small even for curve 5. Thus, considering both the convergence of the T_M versus Z profiles and the uncertainties $\pm(u/\rho_r)$, T_M is well bounded for altitudes below 110 km.

It is also possible to rewrite (2) so that the reference level is at Z_b, the lowest altitude of available data, and the temperature at altitude Z_s is obtained by the upward integration of density from Z_b to Z_s. Thus,

$$(T_M)_s = \frac{\rho_b}{\rho_s}(T_M)_b - \frac{GM_0}{R\rho_s}\left[\rho_b\left(\frac{h_{b+1} - h_b}{2}\right) + \rho_s\left(\frac{h_s - h_{s-1}}{2}\right) + \sum_{j=b+1}^{s-1}\rho_j\left(\frac{h_{j+1} - h_{j-1}}{2}\right)\right] \quad (5)$$

where

ρ_b and ρ_s are densities at altitudes Z_b and Z_s.
$(T_M)_b$ is an unknown value of T_M at altitude Z_b.
$(T_M)_s$ is the computed temperature at altitude Z_s.

The subscript s implies upward integration from Z_b to Z_s to obtain $(T_M)_s$, and for this equation the data points are numbered consecutively, increasing upward from the point at Z_b which is identically point b or point 1.

Again an infinite number of profiles of T_M versus Z are possible, each associated with one of an infinite number of possible choices of the unknown $(T_M)_b$. In this instance, however, the ratio (ρ_b/ρ_s) is always greater than 1, and the members of any pair of curves of T_M versus Z for different values of $(T_M)_b$ diverge with increasing altitude by the amount of $\Delta T_b(\rho_b/\rho_s)$. Thus, any uncertainty in $(T_M)_b$ is also magnified by that ratio. Furthermore, both the ratio term and the integral term become very large as Z increases; hence the uncertainty in their difference, and also in $(T_M)_s$, increases beyond any useful limits. When the assumed value of $(T_M)_b$ is 180° or 204.0° (the latter being equal to that of the United States standard atmosphere for Z_b), equation 5 yields values of $(T_M)_s$ represented by the dashed lines which diverge rapidly from the United States standard values to unrealistically high values as Z increases above 110 km. When $(T_M)_b$ is taken to be successively 151.4664°, 152.2602°, 153.0540°, 153.8478°, and 154.6416°, equation 5 develops identically the five solid-line curves computed by equation 2. The initial selection of a reference temperature of 153.05 ± 1.59°, however, is most unlikely, and for that part of the atmosphere where the mean molecular weight is high, i.e. where N_2 and O_2 are the predominant gases, it is apparent that equation 5 is useless. For high altitudes, however, where He or H_2 dominates the atmosphere so that the mean molecular weight is small and the logarithm of the density-altitude gradient is proportionately reduced, we can show that it is better to develop the temperature-altitude profile upward from a moderately well-known $(T_M)_b$ by means of equation 5 than to work downward from a completely unknown $(T_M)_a$ by means of equation 2.

This analysis shows the value of T_M at 100 km over Eglin Gulf Test Range to be 157 ± 13°; at 97.8 km, T_M is 152 ± 9°. From the shape of the curve, the second value appears to be essentially the mesopause minimum, although no data exist for lower altitudes during this flight. From the previously cited definition it is apparent that T_M is greater than T by a factor M_0/M, the value of which varies with altitude essentially as shown in Table 1. This table was prepared using the values of M from the *United States standard atmosphere* [1962], and hence these values should be reasonably reliable, at least for altitudes $Z < 130$ km. The related difference in degrees between T_M and T for the

TABLE 1. Values of M_0/M and $(T_M - T)$ versus Altitude Z

Z, km	M_0/M, dimensionless	$T_M - T$, deg K
90	1.000	0.00
100	1.003	0.47
110	1.014	3.6
120	1.032	9.2
130	1.050	25.2

median curve (3) of Figure 1 is also given in this table. It is apparent that the difference between the plotted values of T_M and the related values of T is small compared with the uncertainties in T_M at all altitudes involved in this study. Thus, though the graph is strictly a plot of T_M, it adequately represents kinetic temperature T for all practical purposes, particularly for the altitudes below 110 km.

This mesopause temperature of 152° Kelvin is only 75% of the standard-atmosphere value and is low compared with the mean wintertime mesopause value for that latitude as indicated by *Court et al.* [1962]. Instances of similarly low mesopause temperatures have been observed on several other occasions: (*a*) over Wallops Island, 38° north latitude, on June 20, 1963 (J. W. Peterson, private communication, 1964); (*b*) over the Marshall Islands, 10° south latitude, on January 23, 1964 (Peterson, private communication, 1964); (*c*) over Fort Churchill, 58° north latitude, on July 21, 1957 [*Stroud et al.*, 1960]; and (*d*) over Russia during the summer, year and latitude unspecified [*Mikhnevich et al.*, 1957]. Apparently, such low mesopause temperatures are not too unusual in tropical or semitropical regions at various seasons of the year, in contrast with arctic regions where low mesopause temperatures are generally observed only during the summer months.

Summary and conclusions.

1. In the absence of independent temperature information, a single profile of mass density versus altitude yields a T_M versus altitude profile which does not depart drastically from a T versus altitude profile for altitudes below 130 km.

2. The altitude range of reliable T_M values extends from about 15 to 20 km below the greatest altitude of reliable density data down to the lowest altitude for which data are obtained.

3. A temperature T of 152° ± 10°K which is low in comparison with average mesopause temperature values is reported for 98-km altitude over Eglin Gulf Test Range, Florida.

4. This value is similar to other low values of the mesopause temperature observed at least four different times at different locations.

Acknowledgment. This work was supported in part by the National Aeronautics and Space Administration under contract NASw-976.

REFERENCES

Champion, K. S. W., and R. A. Minzner, Revision of United States standard atmosphere 90 to 700 km, *Rev. Geophys., 1,* 57–84, 1963.

Court, A., A. J. Kantor, and A. E. Cole, Supplementary atmospheres, *AFCRL-62-889,* September 1962.

Elterman, L., A series of stratospheric temperature profiles obtained with the searchlight technique, *J. Geophys. Res., 58,* 519–530, 1953.

Faucher, G. A., R. W. Procunier, and F. S. Sherman, Upper-atmosphere density obtained from measurements of drag on a falling sphere, *J. Geophys. Res., 68,* 3437–3450, 1963.

Harrison, L. P., Relation between geopotential and geometric height, *Smithsonian Meteorological Tables,* 6th edition, edited by R. S. List, pp. 217–218, Washington, D. C., 1951.

Mikhnevich, V. V., and I. A. Khvostikov, Study of the upper layers of the atmosphere, *Izv. Akad. Nauk SSSR, Ser. Geofiz., 1957*(11), 1393–1409, 1957.

Miller, L. E., Molecular weight of air at high altitudes, *J. Geophys. Res., 62,* 351–356, 1957.

Minzner, R. A., and W. S. Ripley, The ARDC model atmosphere 1956, *A. F. Surv. Geophys. 86, ARCRC TN-56-204,* 1956.

Minzner, R. A., W. S. Ripley, and T. F. Condron, U. S. Extension of the ICAO Standard Atmosphere, Washington, D. C., 1958.

Minzner, R. A., K. S. W. Champion, and H. L. Pond, The ARDC model atmosphere 1959, *A. F. Surv. Geophys. 115, AFCRC TR-59-267,* 1959.

Newell, H. E., Jr., *High Altitude Rocket Research,* p. 112, Academic Press, New York, 1953.

Sauermann, G. O., and R. F. K. Herzog, Helium in the earth's atmosphere, *Geophys. Corp. Am. Tech. Rept. 61-6-N,* 1961.

Spencer, N. W., G. P. Newton, C. A. Reber, L. H. Brace, and R. Horowitz, New knowledge of the earth's atmosphere from the aeronomy satellite (Explorer 17), *Goddard Space Flight Center Rept. X-651-64-114,* Greenbelt, Maryland, 1964.

Stroud, W. G., W. Nordberg, W. R. Bandeen, F. L. Bartman, and P. Titus, Rocket-grenade measurements of temperatures and winds in the mesophere over Churchill, Canada, *J. Geophys. Res., 65,* 2307–2323, 1960.

United States Standard Atmosphere, National Aeronautics and Space Administration, U. S. Air Force, and U. S. Weather Bureau, Government Printing Office, Washington, D. C., 1962.

(Received September 7, 1964; revised November 6, 1964.)